UNIVERSITY OF MICHIGAN
APR 15 1952
ENGINEERING LIBRARY

JOURNAL OF THE AERONAUTICAL SCIENCES

VOLUME 19 APRIL, 1952 NUMBER 4

CONTENTS

An Analytical Approach to the Fuel Sloshing and Buffeting Problems of Aircraft.....HAROLD LUSKIN AND ELLIS LAPIN 217
The Compressible Boundary Layer.....GEORGE B. W. YOUNG AND EARL JANSSEN 229
Experiments on Interaction of Shock Waves and Cylindrical Bodies at Supersonic Speeds.....M. V. MORKOVIN, E. MIGOTSKY, H. E. BAILEY AND R. E. PHINNEY 237
Shock-Tube Studies of Transonic Flow over Wedge Profiles....WAYLAND GRIFFITH 249
Remarks on Dynamic Loads in Landing.....ADAM ZAHORSKI 258
A Study of Transonic Gas Dynamics by the Hydraulic Analogy.....E. V. LAITONE 265
Analysis of Nonuniform Columns and Beams by a Simple D.C. Network Analyzer.....GEORGE W. SWENSON, JR. 273
Reply to Discussions of the Wright Brothers Lecture.....P. B. WALKER 276
Readers' Forum: "Secondary Flow in Cascades," by Hsuan Yeh; "Sweptback Wing Stress Analysis," by L. A. Goran; "Slender Body Theory for Supersonic Unsteady Flow," by John W. Miles; "Comments on 'The Evaluation of Theoretical Critical Compression in Sandwich Plates,'" by Bernard Budiansky and Charles Libove; "Three-Dimensional Conformal Transformations," by Keeve M. Siegel; "Erratum," by N. Scholz; "Comments on 'Horizontal Tail Loads in Abrupt Pull-Ups from Level Flight,'" by R. M. Rosenberg and also by Bernard Etkin; "Erratum," by P. P. Bijlaard; "On the Flow Around a Rotating Disc in a Uniform Stream," by Arthur N. Tifford and Sheng To Chu; "Frequency Response of an Airplane from Flight-Test Data," by G. M. Andrew and J. H. Polve; "On the Speed of Sound in Gases," by Irvine I. Glass; "On Interference Factors for Finned Bodies," by John W. Miles; "Comments on 'Uniformly Loaded Semi-Infinite Wedge-Shaped Plates,'" by Eric Reissner.....279–288

Published by the

INSTITUTE OF THE AERONAUTICAL SCIENCES, INC.

JOURNAL OF THE AERONAUTICAL SCIENCES

Editor: HUGH L. DRYDEN, *Director, N.A.C.A.*

Associate Editor: ROBERT R. DEXTER *Managing Editor:* BERNEICE H. JARCK

Editorial Committee

Aerodynamics

Francis Clauser
Howard Emmons
Alexander Flax
R. Paul Harrington
R. T. Jones
Carl Kaplan
H. W. Liepmann
C. C. Lin
H. F. Ludloff
Harold Luskin
John R. Markham
Clark B. Millikan
Shatswell Ober
W. Bailey Oswald
Allen E. Puckett
Elliott G. Reid
H. J. F. Reid
Russell Robinson
G. B. Schubauer
W. R. Sears
John Stack
Theodore von Kármán
Richard von Mises

Flight Testing

W. K. Ebel
R. R. Gilruth
Melvin N. Gough
E. G. Stout

Meteorology

C. F. Brooks
D. M. Little
E. J. Minser
F. W. Reichelderfer
H. C. Willett

Structures and Materials

W. B. Bleakney
E. W. Conlon
L. H. Donnell
E. C. Hartmann
N. J. Hoff
Samuel Levy
E. E. Lundquist
J. S. Newell
Alfred S. Niles
W. Ramberg
E. Reissner
F. R. Shanley
H. W. Sibert
C. R. Strang
S. Timoshenko
H. S. Tsien
Chi-Teh Wang

Rotating Wing Aircraft

F. B. Gustafson
K. H. Hohenemser
Bartram Kelley
R. B. Maloy
Ralph McClarren
R. H. Miller
R. H. Prewitt
Igor I. Sikorsky

Physiologic Problems

H. G. Armstrong
Louis H. Bauer
Eugene Du Bois
W. Randolph Lovelace, II
Ross A. MacFarland
A. D. Tuttle

Flight Propulsion

George W. Brady
Frank W. Caldwell
L. S. Hobbs
E. E. Johnson
Joseph Keenan
R. P. Kroon
Hans Reissner
Abe Silverstein
C. Fayette Taylor
E. S. Taylor
P. Taylor
E. S. Thompson
H. S. Tsien

Aircraft Design

W. E. Beall
W. K. Ebel
Hall L. Hibbard
Richard Hutton
C. L. Johnson
A. A. Kartveli
C. J. McCarthy
Fred E. Weick
Robert J. Woods

Air Transport

Charles Froesch
J. A. Herlihy
R. D. Kelly
Otto E. Kirchner
Jerome Lederer
John C. Leslie
R. Dixon Speas

Instruments

Allan G. Binnie
J. R. Bradburn
Charles H. Colvin
C. S. Draper
S. G. Eskin
O. E. Esval
H. W. Holzapfel
W. L. Howland
George H. Purcell
C. F. Savage
O. Hugo Schuck
C. L. Seward, Jr.
L. D. Statham
R. C. Sylvander
D. K. Warner

Vibration and Flutter

Lee Arnold
M. A. Biot
R. L. Bisplinghoff
William Bollay
Chieh-Chien Chang
I. E. Garrick
Martin Goland
J. P. Den Hartog

Fuels and Oils

D. P. Barnard
J. H. Doolittle
Graham Edgar
R. T. Goodwin
S. D. Heron
A. M. Rothrock

SUBSCRIPTION RATES

JOURNAL OF THE AERONAUTICAL SCIENCES, Published Monthly.—United States and Possessions: 1 Year, $12.00; Single Copies $1.50. Foreign Countries Including Canada (American Currency Rates): 1 Year, $13.00; Single Copies, $1.50.

AERONAUTICAL ENGINEERING REVIEW, Published Monthly.—United States and Possessions: 1 Year, $3.00; Single Copies, $0.50. Foreign Countries Including Canada (American Currency Rates): 1 Year, $3.50; Single Copies, $0.50.

Notices of change of address should be sent to the Institute at least 30 days prior to actual change of address.

Manuscripts for publication, proofs, and all correspondence should be addressed to the Editorial Office of the JOURNAL.

Correspondence regarding subscriptions may be addressed to Publication Office, 20th and Northampton Sts., Easton, Pa., or to the Editorial Office of the JOURNAL OF THE AERONAUTICAL SCIENCES, 2 East 64th Street, New York 21, New York.

Copyright, 1952, by the Institute of the Aeronautical Sciences, Inc.

Entered as Second Class Matter at the Post Office, Easton, Pa., May 1, 1937. Acceptance for mailing at a special rate of Postage provided for in the Act of August 24, 1912. Authorized April 29, 1937.

JOURNAL OF THE AERONAUTICAL SCIENCES

VOLUME 19 APRIL, 1952 NUMBER 4

An Analytical Approach to the Fuel Sloshing and Buffeting Problems of Aircraft*

HAROLD LUSKIN† AND ELLIS LAPIN‡

Douglas Aircraft Company, Inc.

ABSTRACT

Two dynamics problems are discussed: the motion of an aircraft with partially full fuel tanks and airplane buffeting.

In discussing the first problem, it is stated that for small motions the fuel in a tank can be replaced by a fixed mass plus a simple pendulum. A spring-mass system is an alternative that is used in writing the linearized equations of longitudinal motion for an aircraft with a partially full fuel tank. The motion is found to be described by three essentially independent oscillations: the phugoid, the short period, and a fuel oscillation. The fuel oscillation has a frequency essentially the same as that of the fuel in a stationary tank, and significant damping is obtained only by the use of tank baffles.

In connection with airplane buffeting, it is indicated that it appears to be an aeroelastic response problem that should be susceptible to analytic approaches. Some ideas on the nature of the forcing functions are presented. It is suggested that concepts from turbulence and the mechanics of stochastic processes may be useful in developing a rational buffeting theory.

INTRODUCTION

WHILE AERONAUTICAL ENGINEERS must solve many problems without waiting for suitable theories to be developed, it is nevertheless true that theoretical methods may be of considerable assistance. Theory may indicate the correct parameters and some of the relations between them. Analysis may suggest useful experiments and the proper quantities to be measured. Methods for interpreting the experimental data may be found. A successful theory may even result. In such cases certain steps have often been followed.

(1) The physics of the problem has been understood and the problem has been formulated.

(2) The equations (simplified to the point where they can be handled easily but not to the point where the essential character of the problem has been lost) relating the variables have been written.

(3) The solution to the equations have been found and applied.

(4) Experimental results have been obtained to verify the accuracy of the assumptions.

As the engineering art has developed, many problems have passed through these steps. The problems not solved by analysis might have resisted attack for many reasons. Some of them might never have been important. For others, the mathematics may not have been available, or the labor of obtaining the numerical solutions may have been too great. Sometimes the problem was not well defined.

Two aeronautical problems for which complete theories do not exist are considered here. The problem of the motions of an aircraft with partially full fuel tanks has not been sufficiently pressing in the past to attract much analytical attention. The buffeting problem has not yet been completely formulated. It is the intent of this paper to carry these problems through some of the steps toward solution.

The problem of the motion of an aircraft with partially full fuel tanks (also called "fuel sloshing") has been known for many years. Test pilots have been aware of it because it was associated with both lateral and longitudinal oscillations of disturbing magnitude and with unusual fore-and-aft trim changes. It has been eliminated in the few cases where it has occurred by the installation of empirically designed tank baffles. Turbojet and rocket-powered vehicles, however, have generally tended to have higher than usual values of

Presented at the Annual Summer Meeting, I.A.S., Los Angeles, June 27–29, 1951.

* The concepts and results discussed in this paper derive from the work of the members of the Aerodynamics Research Group of the Engineering Department of the Douglas Aircraft Company, Inc., Santa Monica Division. E. W. Graham and Dr. Hans W. Liepmann have provided many valuable ideas. Dr. Paco Lagerstrom, H. Kleckner, C. R. Bauer, and R. Schaufele have also contributed much to this work.

† Assistant Supervisor, Aerodynamics—Research, Santa Monica Division.

‡ Design Specialist. Santa Monica Division.

the ratio of fuel weight to gross weight. Also, the trend to higher wing loadings and thinner wings has removed the tanks from the wings, where structural members acted as baffles, to the body, where large uninterrupted volumes for tanks exist. Recently, the existence of unexplained flight oscillations has served to focus attention on sources of the difficulties. All of these factors have indicated the need for analysis of the problem. Work on this problem at the Santa Monica Division of the Douglas Aircraft Company, Inc., began in 1949. The first published analytical contribution[1] to the literature of sloshing was made in January, 1951.

The beginning stage in the Douglas study of fuel sloshing developed the concept of replacing the oscillating fuel in each tank by a simple pendulum plus a fixed mass. It was shown by Graham[2] that this concept was consistent with the linearized equations for the small motions of a fluid in a stationary rectangular tank. He later extended the analysis to cover a variety of other tank shapes. This work was of primary importance, since the motion of the fuel and the forces it transmitted to the aircraft were the only elements of the problem not previously well known from conventional stability analyses. The aircraft with sloshing fuel was then replaced by one with a simple pendulum and a fixed mass for each tank. Some of the results of this work having to do with the longitudinal motion are taken up here. The case of the lateral motion has been discussed in reference 1.

Aircraft buffeting is a problem that has been little understood. In fact, a recent review of aeroelasticity[3] had only one statement to make concerning buffeting: "The aerodynamics underlying the buffeting phenomena . . . is still fairly obscure." Buffeting first became important when the low-wing monoplane was introduced. Tests[4] of that configuration showed that a generally satisfactory method for reducing the buffeting to tolerable levels was the use of the wing-fuselage fillet. Buffeting research was largely directed, therefore, at development of fillets for each particular aircraft. Such additional work[5] as was done considered the vibrations to occur in the following way: 'A stalled wing produces a wake of considerable extent and intensity. The wake is essentially a Kármán vortex trail and thus has a unique frequency associated with it. The tail structure responds to the fluctuations and is supposed to have its own natural frequencies removed from that of the wake in order to avoid resonance.' Other research into buffeting has been exploratory (or has merely defined the flight buffeting régimes for particular aircraft) and has not resulted in a clear formulation of the problem. This being the case, it has not been possible to proceed with a solution. Furthermore, new types of buffeting have appeared which are not corrected by fillets or described by older theories. At the present time, developments in the fields of dynamic analysis and fluid turbulence may be possibly be of aid in providing a better understanding of the buffeting problem. In the present paper this possibility is briefly explored.

Study of the Literature led to some calculations by Graham[6] on the disturbances created by a vortex trail. Later, Liepmann[7] suggested that some of the ideas of turbulence could be used to provide insight into the aerodynamics of buffeting. He used this to calculate the mean square lift response of an airfoil to the random angle of attack fluctuations of isotropic turbulence, since a turbulent wake is considered to be more realistic than the vortex trail.

Nomenclature in Order of Appearance

W_p	= weight of equivalent simple pendulum, which replaces the fuel in the equivalent dynamical system, lbs.
W_f	= actual fuel weight, lbs.
h/l	= ratio of fuel height to fuel-tank length
L_p/l	= ratio of simple pendulum length to fuel-tank length
Y_p/l	= ratio of pendulum height above undisturbed fluid surface to fuel-tank length
P	= period, sec.
g	= gravitational acceleration constant, ft./sec.^{2}
F	= horizontal force on fuel-tank sides, lbs.
θ	= pendulum displacement angle; also fuel free surface displacement angle, rad.
W_t	= total weight, airplane plus fuel, lbs.
m_t	= total mass, airplane plus fuel, slugs
m_p	= mass of equivalent pendulum, slugs
u, w	= perturbation velocities of the aircraft along the x, z axes, ft. per sec.
q	= angular velocity of the aircraft about the y axis, rad. per sec.
$X_{aero.}, Z_{aero.}, M_{aero.}$	= aerodynamic forces parallel to the x and z axes, and aerodynamic moment about the y axis, lbs. and lb. ft.
θ	= angle between the x axis and the horizon, rad.
ϑ_0	= initial value of θ, rad.
ϑ	= perturbation in θ, rad.
U_0	= air speed in undisturbed flight, ft. per sec.
V	= air speed at any instant, ft. per sec.
x_a, z_a	= coordinates of the airplane plus fixed mass of fuel center of gravity relative to the x, z axes, ft.
ξ_p, z_p	= coordinates of equivalent moving fuel mass center of gravity relative to the x, z axes, ft.
L	= lift, lbs.
s	= x coordinate of the equilibrium position of the moving fuel mass center of gravity in undisturbed flight, ft.
I_t	= moment of inertia of the system, airplane plus all fuel, about the y axis, slug-ft.^{2}
I_a	= moment of inertia of the airplane plus the fixed fuel about an axis through the point (x_a, z_a), slug-ft.^{2}
I_p	= moment of inertia of the moving fuel about an axis through the point (ξ_p, z_p), slug-ft.^{2}

r = radius of gyration, ft.
c = mean aerodynamic chord, ft.
k = spring constant of the equivalent fuel mass-spring system, lbs. per ft.
D_t = airplane rotary damping constant, lb. ft. sec.
D_f = fuel viscous damping constant, lb. sec. per ft.
λ = root of the characteristic equation
$X_u = (\partial X_{aero.}/\partial u)_{u=0}$
$X_w = (\partial X_{aero.}/\partial w)_{w=0}$
$Z_u = (\partial Z_{aero.}/\partial u)_{u=0}$
$Z_w = (\partial Z_{aero.}/\partial w)_{w=0}$
$M_\alpha = (\partial M_{aero.}/\partial w/U_0)_{w=0}$
} = aerodynamic resistance derivatives
$M_q = [\partial M_{aero.}/\partial(qc/U_0)]$ = aerodynamic rotary derivative
D = drag, lbs.
C_D = drag coefficient
C_{D_p} = parasite drag coefficient
C_L = lift coefficient
$C_{L\alpha}$ = lift curve slope
α = angle of attack, rad.
V_y = vertical velocity amplitude, ft. per sec.
Γ = circulation, ft.²/sec.
b = spacing between vortices, ft.
h = spacing of vortex rows, ft.
$\overline{C_L}^2$ = mean square lift coefficient
$\overline{w}^2$ = mean square vertical velocity, ft.²/sec.²
c = airfoil chord, ft.
L = scale of turbulence, ft.

Dynamics of an Aircraft with Partially Full Fuel Tanks

The Dynamics of the Fuel Motion

The one new component occurring in the problem being considered is the fuel, which is free to move. As many new degrees of freedom are thereby added to the ordinary rigid body aircraft dynamic analysis as there are coordinates describing the fuel configuration. For a completely general fuel motion, an infinite number of coordinates are needed. Such a description of the dynamics is complex, and only the configuration for the fuel moving under small disturbances (which is consistent with the assumptions usually made in aircraft dynamic stability analysis) in its fundamental mode will be studied here. With this assumption each tank adds two new degrees of freedom to the dynamical system. Considering longitudinal motions only, a tank adds only one new degree of freedom.

Insight into the dynamics of the fuel motion can be had by observing the motion of water in a container. An arbitrary large disturbance to the container will create a confused motion of the free surface, but soon the smaller waves will die out, leaving only a moderately damped more or less periodic motion. Repeating the experiment with a smaller disturbance along only one axis will show the periodic motion more clearly. Finally, the use of a small container will show heavy damping and thus indicate light damping in large tanks. A similar example of fluid in motion is that of the manometer, which is easily shown to have a simple oscillatory mode.[8]

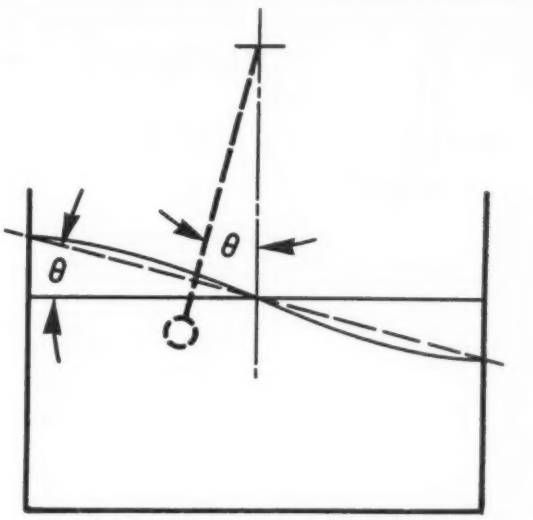

FIG. 1. Definition of fluid surface displacement angle and pendulum displacement angle.

It is indicated that the fuel in a large aircraft tank without baffles will, after a small disturbance, have a lightly damped periodic oscillation, and that it can be approximated by a simple pendulum. This possibility was studied by Graham.[2] His results for the stationary† rectangular tank are based on the linearized expression for the velocity potential given by Lamb. He shows that the fuel in its fundamental mode can be replaced by a simple pendulum plus a fixed mass for pendulum angular displacements, θ, like the fluid surface angular displacement as shown in Fig. 1. Sinusoidal waves are found to exist on the free fluid surface. The expressions for the ratio of pendulum weight to fuel weight, pendulum length to tank length, and height of the pendulum axis above the undisturbed surface to the tank length are found to be functions only of the ratio of undisturbed fluid height to tank length.

$$W_p/W_f = [\tanh(\pi h/l)]/(\pi h/l) \quad (1)$$

$$L_p/l = (1/\pi)\coth(\pi h/l) \quad (2)$$

$$Y_p/l = (1/\pi)[2 - \cosh(\pi h/l)]/\sinh(\pi h/l) \quad (3)$$

These relations are plotted in Fig. 2.

Some intuitive feeling for the equivalent pendulum can be gained by studying the extreme cases of an almost empty tank and a deep tank. For the nearly empty tank, the pendulum has nearly the same weight as the fluid. For the deep tank, on the other hand, the effective mass is small.‡ The geometry of the two pendulums is shown in Fig. 3.

† A study[15] of the nonstationary tank has shown that the stationary tank is an adequate representation for this problem.

‡ A tank that is completely full or nearly so and which has a fixed top may not be described by this analogy.

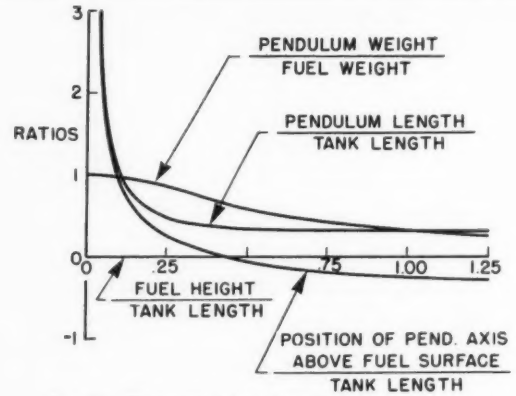

FIG. 2. Characteristics of equivalent pendulum.

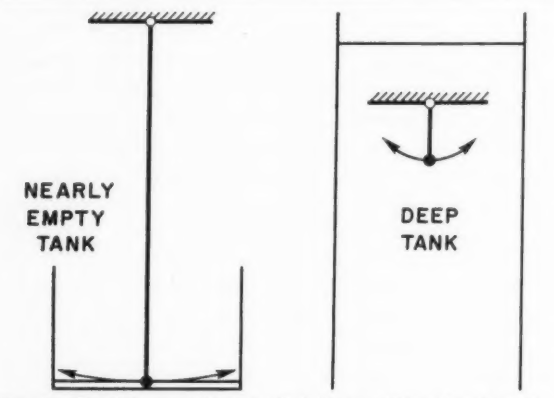

FIG. 3. Pendulum analogy to fuel in two-dimensional tanks. Extreme cases.

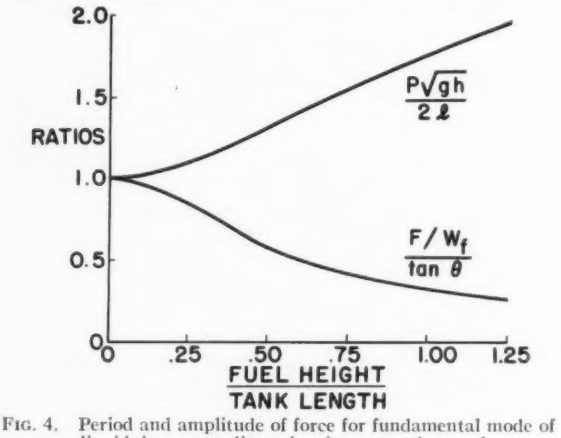

FIG. 4. Period and amplitude of force for fundamental mode of a liquid in a two-dimensional rectangular tank.

The period, P, of the fundamental mode is given by

$$P/(2l/\sqrt{gh}) = [(\pi h/l) \coth (\pi h/l)]^{1/2} \quad (4)$$

while the amplitude of the horizontal force on the tank sides, F, is given by

$$F/W_f = [\tanh (\pi h/l) \tan \theta]/(\pi h/l) \quad (5)$$

Fig. 4 is the plot of these relations. These formulas simplify for cases where the fuel is shallow, $h/l \ll 1/2$, and where the fuel is deep, $h/l \gg 1/2$. For example, for the shallow tank the period is

$$P \doteq 2l/\sqrt{gh} \quad (6)$$

and for a deep tank

$$P \doteq 2\sqrt{\pi l/g} \quad (7)$$

Eq. (6) gives the time for a shallow water wave to make a trip across the tank and back. The velocity of this wave is $\sqrt{gh}$.

The small motion approximation gives a vertical force on the pendulum which is equal to its weight and a side force which is proportional to its displacement. Those considerations show that a mass and a spring are completely equivalent to the pendulum in simulating the small motions of the fuel. The spring stiffness, the force for unit displacement, is equal to the pendulum weight divided by the pendulum length. The mass has the same magnitude as that of the pendulum.

The Longitudinal Motion of an Aircraft with Sloshing Fuel

The motion of an aircraft in its plane of symmetry is to be studied for the case where fuel is in motion in one tank. It is supposed that the fuel is replaced by its equivalent mass and spring system. To eliminate coupling with the lateral motion, the fuel will be assumed to remain symmetrically disposed with respect to the plane of symmetry.

A set of rectangular coordinates fixed relative to the body is selected. The origin is assumed fixed at the position of the center of gravity of the entire system under the initial equilibrium conditions. The longitudinal, x, axis is assumed aligned with the initial relative wind, and, for simplicity, the motion of the fuel equivalent mass is taken as parallel to the aircraft longitudinal axis. Fig. 5 illustrates the coordinate system and its geometrical relation to the aircraft and equivalent fuel mass centers of gravity.

The system contains four degrees of freedom: translation along the two coordinate axes lying in the plane of symmetry, a rotation about the axis perpendicular to the plane of symmetry, and a translation of the fuel parallel to the aircraft longitudinal axis. By application of Newton's laws, the four independent differential relations between these degrees of freedom may be derived in the following form:

$$m_t[\dot{u} + wq] = X_{\text{aero.}} - m_p\ddot{x}_p - W_t \sin\theta + m_p x_p q^2 \quad (8a)$$

$$m_t[\dot{w} - q(U_0 + u)] = Z_{\text{aero.}} - W_t \cos\theta + m_p x_p \dot{q} + 2m_p \dot{x}_p q \quad (8b)$$

$$I_t\dot{q} + m_p z_p \ddot{x}_p - m_p[2(s - x_a - x_p)q\dot{x}_p + x_p\dot{w} + w\dot{x}_p] = M_{\text{aero.}} - W_p x_p \cos\theta \quad (8c)$$

$$-m_p\ddot{x}_p = W_p \sin\theta + kx_p + m_p(s - x_a - x_p)q^2 + m_p z_p\dot{q} + m_p(\dot{u} + wq) \quad (8d)$$

Introducing $\theta = \vartheta_0 + \vartheta$, where the perturbation in attitude, ϑ, is small, and neglecting products and squares of the perturbation variables, the linearized form of the equations of motion result.

$$m_t\dot{u} = X_{\text{aero.}} - m_p\ddot{x}_p - W_t \sin\vartheta_0 - W_t\vartheta\cos\vartheta_0 \quad (9a)$$

$$m_t(\dot{w} - U_0 q) = Z_{\text{aero.}} + W_t\cos\vartheta_0 - W_t\vartheta\sin\vartheta_0 \quad (9b)$$

$$I_t\dot{q} + m_p z_p\ddot{x}_p = M_{\text{aero.}} - W_p x_p\cos\vartheta_0 \quad (9c)$$

$$m_p\ddot{x}_p = W_p(\sin\vartheta_0 + \vartheta\cos\vartheta_0) + kx_p + m_p z_p\dot{q} + m_p\dot{u} \quad (9d)$$

In Eqs. (8c) and (9c) the moment of inertia of the system has been taken as

$$I_t = I_a + I_p + m_a(x_a^2 + z_a^2) + m_p(\xi_p^2 + z_p^2) \quad (10)$$

where I_a is the moment of inertia for a rotation about the point (x_a, z_a) of the aircraft including the "fixed" part of the fuel and I_p is the moment of inertia for a rotation about the point (ξ_p, z_p) of the equivalent mass of moving fuel, both parts of the fuel considered as rigid bodies. The correction to the moment of inertia that accounts for the fact that the fuel is not rigid has not been considered.†

Expansion of the matrix of coefficients of Eqs. (9) yields a sextic for the characteristic equation as contrasted to the quartic that results from the ordinary aircraft stability equations [Eqs. (9a), (9b), and (9c) with equivalent fuel mass terms omitted]. The roots of the quartic equation generally describe the aircraft motion as composed of two oscillations. In the sextic the appearance of two additional roots introduces an additional mode, which may be an oscillation or a combination of subsidences and/or divergences and which also modifies the two original aircraft oscillations.

It is desired that the nature of the new motion and the extent of its influence on the original motions of the aircraft be investigated. Ordinarily, the phugoid and short-period motions of an aircraft may be studied separately because, having widely different frequencies, the coupling between these motions is slight and the dynamic equations may be modified in accordance. Anticipating that the fuel motion natural frequency and the aircraft short-period frequency may be of the same order and thus far removed from the phugoid frequency, investigation of the nature of the additional mode is facilitated by consideration of the special case

† Graham, in an extension of reference 2, has shown the correction is small.

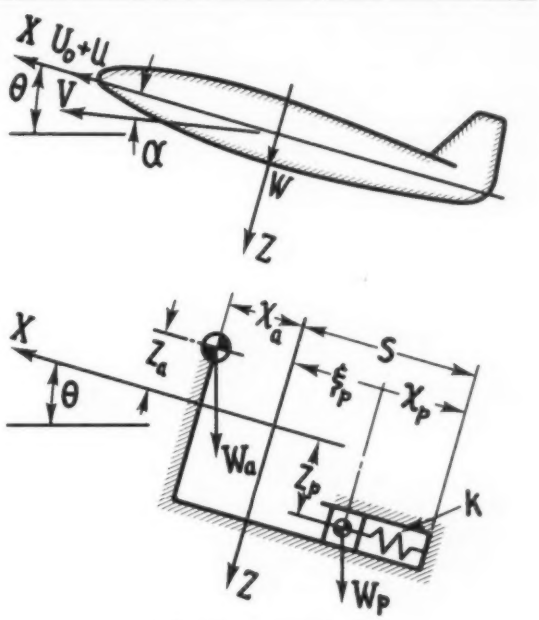

FIG. 5. Geometry.

in which the long-period motion is eliminated. This may be accomplished by assuming a constraint such that $u = 0$ and $w = U_0 \sin\theta$. Taking, for simplicity, $z_p = \vartheta_0 = 0$, Eqs. (9c) and (9d) become

$$(m_t r^2)\dot{q} = (w/U_0)M_\alpha + (qc/2U_0)M_q - W_p x_p \quad (11a)$$

$$-m_p\ddot{x}_p = W_p\vartheta + kx_p \quad (11b)$$

In these equations $-M_\alpha$ and $-M_q$ are the aerodynamic spring and damping constants. Using the fuel and airplane short-period motion natural frequencies

$$\omega_p^2 = k/m_p, \quad \omega_t^2 = -M_\alpha/m_t r^2$$

and taking

$$D_t = -cM_q/2U_0 m_t r^2$$

Eqs. (11) may be written

$$\ddot{\vartheta} + D_t\dot{\vartheta} + \omega_t^2\vartheta + (W_p/W_t)(g/r^2)x_p = 0 \quad (12a)$$

$$\ddot{x}_p + \omega_p^2 x_p + g\vartheta = 0 \quad (12b)$$

To account for the possibility of viscous damping of the fuel motion by baffles, say, Eq. (12b) may be modified by the introduction of a viscous damping term, $D_p\dot{x}_p$,

$$\ddot{x}_p + D_p\dot{x}_p + \omega_p^2 x_p + g\vartheta = 0 \quad (12c)$$

The characteristic equation for the set of simultaneous differential equations, Eqs. (12a) and (12c), is

$$(\lambda^2 + D_t\lambda + \omega_t^2)(\lambda^2 + D_p\lambda + \omega_p^2) - (W_p/W_t)(g/r)^2 = 0 \quad (13)$$

When the ratio of the effective fuel weight to the total weight approaches zero, the meaning of this equation is

simply that the motion that exists is the aircraft short-period oscillation and an uncoupled oscillation determined by the natural period and damping of the fuel. For finite values of the parameter $(W_p/W_t)\,(g/r)^2 = \nu$, the frequency and damping of each of these modes are modified. To determine the extent of this modification it is necessary to extract the roots of the quartic.

For the special case of zero aerodynamic and fuel damping, extraction of the roots is simple,

$$\lambda^4 + (\omega_t^2 + \omega_p^2)\lambda^2 + (\omega_t^2\omega_p^2 - \nu) = 0 \quad (14)$$

$$\lambda = \pm i\sqrt{-\frac{(\omega_t^2 + \omega_p^2)}{2} \pm \sqrt{\left(\frac{\omega_t^2 - \omega_p^2}{2}\right) + \nu}} \quad (15)$$

and, for $\omega_p = \omega_t = \omega$,

$$\lambda = \pm i\sqrt{-\omega^2 \pm \sqrt{\nu}} \quad (16)$$

Only the frequencies of the oscillations are affected.

While for specific cases Eq. (13) may be factored by numerical methods, it is desirable to have at least approximate relations from which the change in damping and frequency from the uncoupled modes may be obtained. This may be done by assuming a power series expansion in orders of ν for the coefficients of the biquadratic equal to the original quartic and then evaluating the coefficients of the power series expansions. Another way is to assume a perturbation in the auxiliary function, $\lambda = \lambda^* + \mu$, where λ^* satisfies the original quartic with $\nu = 0$, and to evaluate μ in terms of the coefficients of the original quartic and λ^*. The first method results in more convenient relations and will be used below.

By power series development of the coefficients of the biquadratic,

$$(\lambda^2 + a\lambda + b)\,(\lambda^2 + \alpha\lambda + \beta) = (\lambda^2 + a_0\lambda + b_0)\,(\lambda^2 + \alpha_0\lambda + \beta_0) - \nu = 0 \quad (17)$$

where

$$a = a_0 + a_1\nu + a_2\nu^2 + \ldots = \sum_0^i a_i\nu^i$$

$$b = \sum_0^i b_i\nu^i$$

$$\alpha = \sum_0^i \alpha_i\nu^i$$

$$\beta = \sum_0^i \beta_i\nu^i$$

Carrying the power series development only to terms of first order in ν,

$$a_1 = -\frac{(a_0 - \alpha_0)}{\beta_0(a_0 - \alpha_0)^2 - \alpha_0(a_0 - \alpha_0)(b_0 - \beta_0) + (b_0 - \beta_0)^2} \quad (18a)$$

$$\alpha_1 = -a_1 \quad (18b)$$

$$\beta_1 = -\frac{a_1[\alpha_0(a_0 - \alpha_0) - (b_0 - \beta_0)]}{(a_0 - \alpha_0)} \quad (18c)$$

$$b_1 = a_1(a_0 - \alpha_0) - \beta_0 \quad (18d)$$

This approximate factorization will fail at the point where two real repeated roots occur. Here, one of the real repeated roots may be obtained from the real root of the cubic resulting from differentiation of the original quartic. Comparison of Eqs. (13) and (17) and application of Eq. (15) lead to

$$\Delta D_t = -\frac{(D_t - D_p)\nu}{\omega_p^2(D_t - D_p)^2 - D_p(D_t - D_p)(\omega_t^2 - \omega_p^2) + (\omega_t^2 - \omega_p^2)^2} \quad (19a)$$

$$\Delta D_p = -\Delta D_t \quad (19b)$$

$$\Omega_t^2 = \left[\omega_t^2 - \left(\frac{D_t}{2}\right)^2\right] - \frac{\Delta D_t}{D_t - D_p}(\omega_t^2 - \omega_p^2) \quad (19c)$$

$$\Omega_p^2 = \left[\omega_p^2 - \left(\frac{D_p}{2}\right)^2\right] + \frac{\Delta D_t}{D_t - D_p}(\omega_t^2 - \omega_p^2) \quad (19d)$$

where Ω_i^2 are the squares of the frequencies of the new motions to first order in ν. $[\omega_i^2 - (D_i/2)^2]$ are the squares of the frequencies of the uncoupled modes, and ω_i^2 are the squares of the natural frequencies of the short period and the fuel motion. For small ν, the approximate roots found from Eq. (19) agree well with those obtained by numerical methods.

The new motion is an oscillation in which the damping and the square of the frequency vary linearly with the coupling quantity ν. For typical values of ν, the coupling between the new mode and the aircraft short-period oscillation is small. This is illustrated by Fig. 6 for a specific case of an aircraft with a short-period natural frequency of 1 cycle per sec. and damping such that the amplitude is diminished to one-half in two cycles. Zero viscous fuel damping was assumed, and a typical value of $(W_p/W_t)\,(g/r)^2 = \nu = 1.0$ was selected. It is seen that even at resonance the damping of the short period mode is only slightly diminished (6 per cent). The frequency was found to be altered by only a fraction of a percent. Fig. 7 shows a similar result for the fuel motion.† At a certain small value

† The actual motion of the airplane and of the fuel are each the sum of two motions. The words "short period" and "fuel motion" are merely used to identify the modes associated with certain roots of the characteristic equation.

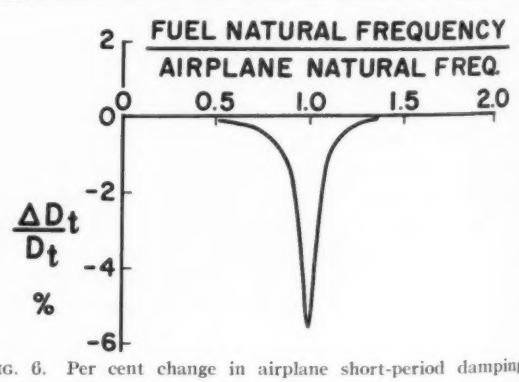

FIG. 6. Per cent change in airplane short-period damping.

of ω_p/ω_t, it is possible to obtain a pair of real roots and a pair of complex roots, and one of the real roots may be positive. Physically, this situation corresponds to the introduction of a weak spring in the equivalent fuel mass-spring system. The restoring force of this spring is insufficient to overcome the weight force component acting on the fuel upon rotation of the airplane and the excursion of the fuel mass increases without limit. Here, the fuel motion oscillation degenerates into a subsidence and divergence. This case arises when the fuel tank is nearly empty (the weak spring implies a long natural period or a long pendulum).

Even though no viscous damping of the fuel motion was assumed, the coupling introduced a small damping, as shown by Fig. 7. For practical purposes this damping is inadequate, however, and diminution of the fuel motion must be secured by some physical apparatus such as baffles. The influence of a baffle that will provide a damping such that the fuel motion amplitude is reduced to one-quarter in one cycle has been calculated. It was found that with fuel frequencies close to that of the airplane short period, the presence of the baffles improves the airplane damping by about 10 per cent.

Returning to Eq. (9), it is recalled that with motionless fuel the phugoid motion of the aircraft may be obtained, approximately, by considering flight at constant angle of attack and with small inertia of the aircraft. For this case, from Eq. (9),

$$m_t\dot{u} = uX_w - W_t\vartheta \tag{20a}$$

$$-m_tU_0\dot{\vartheta} = uZ_u \tag{20b}$$

and the characteristic equation is

$$\lambda^2 - \frac{X_u}{m_t}\lambda - \frac{W_tZ_u}{m_tU_0} = 0 \tag{21}$$

By substituting the usual relations

$$X_u \doteq -\frac{2}{U_0}\left(\frac{1}{2}\rho U_0^2S\right)C_D = -\frac{2D}{U_0}$$

$$Z_u \doteq -\frac{2}{U_0}\left(\frac{1}{2}\rho U_0^2S\right)C_L = -\frac{2W_t}{U_0}$$

into Eq. (21), there results

$$\lambda = \frac{g}{U_0}\left[-\frac{D}{W_t} \pm i\sqrt{2 - \left(\frac{D}{W_t}\right)^2}\right] \tag{22}$$

which gives the customary approximate relation for the damping and frequency of the long-period oscillation.

With sloshing fuel, the angle of attack in the phugoid is no longer constant. From Eq. (9c), for $z_p = 0$, and $\dot{q}$ and q small,

$$(w/U_0)M_\alpha - W_px_p = 0 \tag{23a}$$

while from Eq. (9d), with $\ddot{x}_p$ and $\dot{u}$ small,

$$W_p\vartheta + kx_p = 0 \tag{23b}$$

With small m_p/m_t, Eqs. (9a) and (9b) may be written

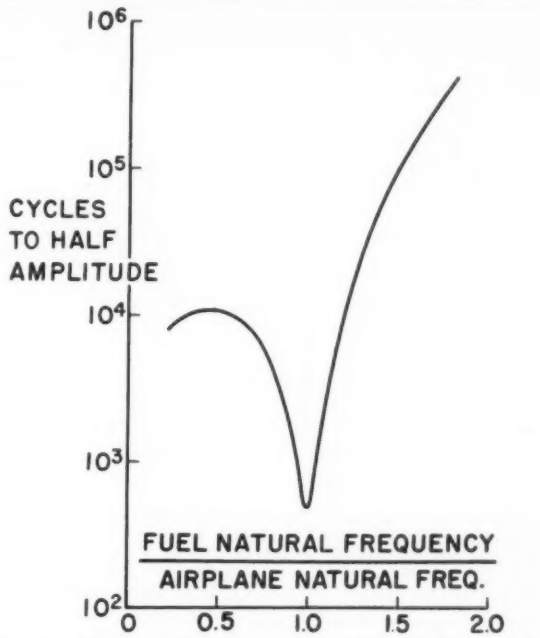

FIG. 7. Damping of the fuel mode. Airplane natural frequency, w_t = 1 cycle per sec. Airplane damping, 2 cycles to $^1/_2$ amplitude. $(W_p/W_t)(g/r)^2 = 1.0$.

$$\dot{u} = u\frac{X_u}{m_t} + w\frac{X_w}{m_t} - g\vartheta$$

or

$$\dot{u} = u\frac{X_u}{m_t} + w\frac{X_w}{m_t} + \frac{\omega_p^2M_\alpha}{U_0W_p}w \tag{24a}$$

since by Eqs. (23a) and (23b)

$$\vartheta = \frac{-k}{W_p}x_p = \frac{-\omega_p^2M_\alpha}{gU_0W_p}w$$

and

$$\left(\dot{w} + \frac{\omega_p^2M_\alpha}{gW_p}\dot{w}\right) = uZ_u + wZ_w \tag{24b}$$

The characteristic equation for the set, Eqs. (24a) and (24b), is

$$\lambda^2 - \left[\frac{X_u}{m_t} + \frac{Z_w}{m_t}\left(\frac{1}{1 + (\omega_p^2M_\alpha/gW_p)}\right)\right]\lambda + \left[\frac{X_u}{m_t}\frac{Z_w}{m_t}\left(\frac{1}{1 + (\omega_p^2M_\alpha/gW_p)}\right) - \frac{Z_u}{m_t} \times \left(\frac{1}{1 + (\omega_p^2M_\alpha/gW_p)}\right)\left(\frac{X_w}{m_t} + \frac{\omega_p^2M_\alpha}{U_0W_p}\right)\right] = 0 \tag{25}$$

and, with

$$\omega_p^2M_\alpha/gW_p = \omega_p^2\omega_t^2/\nu$$

$$X_u \doteq -2D/U_0$$

$$Z_u \doteq -2W_t/U_0$$

$$K = 1 + (\omega_p^2\omega_t^2/\nu)$$

$X_w \doteq (W_t/U_0) - [(\partial D/\partial \alpha)/U_0]$ $\quad C_D = C_{D_p} + (C_L^2/\pi \text{A.R.})$

$Z_w \doteq -(D/U_0) - [(\partial L/\partial \alpha)/U_0]$ it is found that

$$\lambda = \frac{g}{U_0}\left\{-\left[\frac{D}{W_t}\left(\frac{2K+1}{2K}\right)+\frac{C_{L\alpha}/C_L}{2K}\right]\pm i\sqrt{2-\left[\frac{D}{W_t}\left(\frac{2K+1}{2K}\right)+\frac{C_{L\alpha}/C_L}{2K}\right]^2+\frac{2}{K}\left[\left(\frac{D}{W_t}\right)^2\left(1+\frac{C_{L\alpha}}{C_L}\right)+\left(1-\frac{2C_{L\alpha}}{\pi \text{A.R.}}\right)\right]}\right\} \quad (26)$$

For typical values of airplane short-period natural frequency, ω_t, fuel natural frequency, ω_p, and the ratio, ν, the difference between the dampings and frequencies given by Eqs. (26) and (22) is negligible.

In the rather unlikely case that the fuel natural frequencies and long-period frequencies are nearly in resonance, the fuel and phugoid motions must be considered simultaneously. A quartic characteristic equation will be obtained which must then be analyzed by methods similar to those already described.

Thus it is seen that the longitudinal motion of an aircraft with sloshing fuel is composed of three essentially independent oscillations: the phugoid, the airplane short period, and the fuel oscillation. The coupling between these motions is, for practical purposes, negligible. Satisfactory damping of the fuel oscillation must be obtained by the use of a damping device, such as baffles, within the fuel tank. These results are in agreement with less approximate analyses in which factorization of the characteristic sextic was performed by numerical methods. All the variables in this problem, u, w, ϑ, and x_p, will have solutions of the same mathematical form. Flight experience has shown that the new oscillatory mode is apparent to an observer within the airplane as a pulsing in the acceleration $\dot{u}$. This may, perhaps, be more readily comprehended by visualizing the motion of a cart containing a mass attached to it by a spring, as shown in Fig. 8. Both the cart and the mass oscillate longitudinally about the system center of gravity while that point is transported (with phugoid and short-period motions) in space.

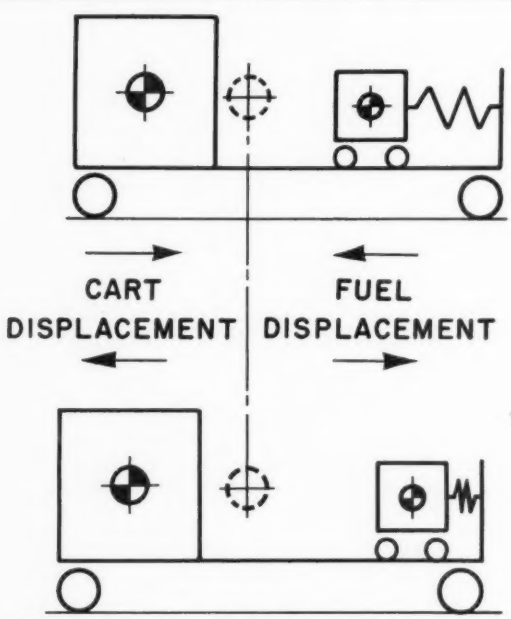

FIG. 8. Analogy to the longitudinal pulsing motion.

BUFFETING

A General Description of the Aircraft Buffeting Problem

Buffeting is a forced vibration in which the external forces are generated by eddying flows.† Fluctuating forces may act on the component producing the eddying flow, or they may be induced on some other part of the aircraft which is in or near the eddies. The eddying flow can be produced by wing or tail shock-stall at high subsonic speeds; by separation on the wing at the low speed stall; by separation from dive flaps, bomb-bay doors, landing-gear doors, wing flaps, canopies, radomes and guns; by the mixing region created by a jet or by a propeller slipstream; and by numerous other things. The most important cases of low-speed buffeting resulted from separation at the wing-fuselage juncture of some low-wing monoplanes. At higher speeds the principal buffet problem is concerned with transonic wing and/or tail shock-stall.

At the present time, the problem of buffeting has not been solved. No design methods are available whereby stall warning or buffet loads can be predicted. It is not possible to estimate the effect of wing or tail geometry, tail position, Mach Number, and other variables on buffeting. No completely satisfactory methods for investigating buffeting during routine wind-tunnel tests have been developed. Aircraft designers have only experience on generally similar designs (where such are available) for guidance, and the buffeting char-

† Flutter is a self-excited vibration not generated by external forces. Buffeting is a response problem; flutter, a stability problem.

acteristics therefore remain unknown until the flight-test period. This situation has made it necessary for some aircraft to undergo long development programs in flight and even then to be limited in performance by placards. What is needed is: (1) a procedure for designing aircraft with the desired degree of stall warning and for predicting buffet loads; (2) a procedure for checking those calculations in the wind tunnel; and (3) a procedure for investigating buffeting in flight and for correcting such troubles as may arise.

An analytical solution to a problem requires as its starting point a suitable description of the phenomenon under investigation. For vibration problems it is necessary to be able to specify inertias, dampings, restoring forces, (or their analogies) and external forces. It is necessary to understand the kinematics of the problem and to visualize the constraints and couplings relating the variables.

The masses (inertias) of the buffeting problem are those of the aircraft itself. The dampings are both structural and aerodynamic in origin, as are the restoring forces. The external forces result from the fluctuating loads acting on the stalled body or from the induced loads created by its wake. It may be of interest to discuss how some of these forces may enter into the problem. First, suppose a rigid body like a wing is supported in a steady stream. The flow configuration will depend on the Mach Number, M, the Reynolds Number, R, and the attitude of the body relative to the stream, α. The magnitude of the forces will depend, in addition, on the static pressure, p. These variables determine the external force that is the input. Since the body is rigid and stationary, there is no damping and no inertia. The restoring force supplied by the support is then equal and opposite to the aerodynamic force. The essentials of this description are shown in Fig. 9. The outputs of this system are the force on the support and the flow variables in the wake. For certain values of the input parameters, the wake becomes large, both the wake and the force fluctuate, and buffeting occurs. For the nonrigid case, the displacements, velocities, and accelerations must also be considered.

Before discussing more complicated cases, it is noted that it is not presently possible to estimate the fluctuations of force and wake in the buffet régime for the simple case just discussed, even for elementary configurations like a two-dimensional cylinder.

A more realistic case is one in which the wing is attached to a fuselage and the wake passes near a tail. The output we should like to calculate (for example) is the vertical acceleration at the pilot's compartment. The relations between the inputs and outputs acting on the aircraft components are shown in Fig. 10. It is these things that must be calculated in a buffeting theory. Items (1), (2), and (3) (numbers correspond to those in Fig. 10) have already been discussed. Item (4) is the load in the fuselage-tail attachment. Item

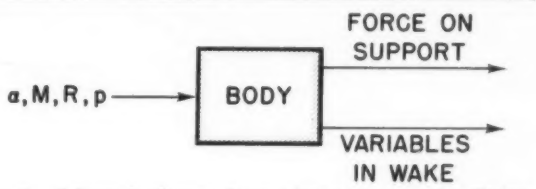

FIG. 9. Schematic diagram for an elementary case of buffeting.

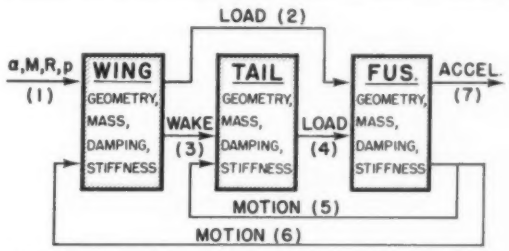

FIG. 10. Possible schematic diagram for buffeting.

(5) is the motion of the tail resulting from fuselage motion, while item (6) is the motion of the wing resulting from fuselage motion. Whether this representation of buffeting due to wing stalling is incomplete or overly complicated could be investigated in a wind tunnel (with suitable attention to the constraint and dynamic effects of the model support) using a flutter-type model. Tests of a complete configuration compared with those with the tail off would indicate whether the wing or the tail is the principal contributor to the fuselage vibrations. Tests with the wing in place to provide a wake, but supported separately, would also help answer that question.

The matrix of differential equations that are the analog of the schematic diagrams just discussed cannot be completely written with presently available knowledge. To do so might require an analytical representation of some of the following items:

(1) The fluctuations of force and moment on rigid stalled bodies as a function of body geometry, α, M, R, and p.

(2) The aerodynamic damping of an oscillating stalled wing.

(3) The vertical velocity fluctuations in the wake of a stalled body as a function of location relative to the wake; body geometry; body α, M, R, and p; and the body's oscillations.

(4) The response of a tail to the disturbances in the wake.

(5) The effect of oscillations on the wake of a stalled wing. These questions relate mostly to the aerodynamic data of buffeting. The use of such data in the theory of the vibrations of aircraft will provide a theory of buffeting. The last section of this paper discusses several attempts to calculate some of these aerodynamic variations.

Words and Phrases

von Kármán and Biot,[9] under the title "Words and Phrases," have a collection of definitions of concepts and operations in common use by physicists and engineers. They also note the existence of a collection of legal terms with the same title which includes especially the legal interpretation of commonly used expressions. A number of words, phrases, concepts, and operations have been associated with buffeting. Eberle[10] has made an interesting survey of some of these concepts. An informal review of these is in order here to see if they convey any precise information concerning this phenomenon; also, one new phrase will be introduced.

(*1*) *The Vortex Trail and the Strouhal Number.*—To obtain the frequency properties, a large part of the buffeting literature assumes that the wake of a stalled wing is a Kármán vortex street (or trail). A single characteristic frequency, given nondimensionally by the Strouhal Number, carries all the energy of the trail. Severe buffeting is supposed to be avoided by keeping the empennage natural frequencies far from that of the trail, thus avoiding resonance. These ideas are mainly based on data from model tests of cylinders and airfoils at low Reynolds Numbers and probably cannot be carried over to full scale. This was pointed out by von Kármán[11] himself: "Even for two-dimensional flows, the vortex street pattern only appears for Reynolds Numbers below a definite limit of the order of 10^5. Above this value, the regular character of the wake disappears and is replaced by a completely turbulent one." The upper limit to the Reynolds Number at which the trail exists is also discussed by Den Hartog.[12] It would seem that a more realistic concept is that the full-scale wake has a continuous frequency spectrum. This implies that resonance with the structure *cannot* be avoided. The solution to buffeting must therefore depend largely on reducing the magnitude of the fluctuations arising from flow separation and/or keeping the turbulent wake away from the structure.

(*2*) *The Total Head Wake*—Measurements of total head loss in the wake of a stalled wing are often made in buffeting investigations. A considerable amount of evidence has accumulated which shows that such measurements are of limited value. Duncan[5] measured a "buffeting" wake with a detector, which was essentially a flexible tail, and found that heavy buffeting can occur even outside the total head wake. Eberle mentions a case where, in flight, buffeting occurred with the tail outside the wing wake. In tests of a low-wing monoplane, White and Hood[13] used a fillet to reduce the tail buffeting vibrations to one-seventh their original magnitude. This, however, was accomplished without moving the tail from the center of the total head wake. In view of these facts, it appears that something more meaningful than the total head wake should be found. It is suggested that the "vertical velocity fluctuations" wake may serve that purpose.

(*3*) *Experiments.*—Wind-tunnel tests on buffeting have often been made at low Reynolds Numbers. Duncan's tests, for example, were made at a Reynolds Number in the order of 10^5. It would seem worth while to discover the effect of Reynolds Number on wake and force fluctuations and then to test only at sufficiently large scales. Low-speed buffeting might best be studied on actual aircraft in full-scale wind tunnels. Other questions of testing technique might well be discussed here. It has already been suggested that vertical velocity fluctuations may be the important quantity to measure in the wake. This may be more useful than total head loss measurements or fluctuating wake pressure measurements. Finally, it is suggested that optical methods, such as motion pictures of smoke flow, may be useful but must be accompanied by measurements of fluctuations of force and moment on the stalled body and by measurements of fluctuating vertical velocities (angles of attack) in the wake to provide magnitudes of the forcing functions.

(*4*) *Dynamics of Buffeting.*—Attempts to bring the vibration characteristics of the airplane into the analysis of buffeting have generally considered only the dynamics of the tail (reference 14, for example). This is obviously important if the buffet loads on the tail are to be studied. Estimates of the magnitude of the loads produced by the tail vibrations, however, show that they are small compared to the weight of the aircraft and cannot be the source of the large c.g. accelerations often measured in buffeting. It would seem instead that these accelerations must come from the fluctuations of wing lift or from the large amplitude motions of fuselage resonance. The wind-tunnel tests suggested previously in connection with the schematic diagram of buffeting would aid in choosing between the two possibilities, although it is felt that the fuselage resonance possibility is more likely. If this supposition is correct, it will be necessary to include the fuselage dynamics in analyses of buffeting.

(*5*) *Stochastic Process.*—A stochastic process is one in which randomness plays a large part. Games of chance are stochastic. In physics, Brownian motion and molecular diffusion are examples. Flight through a turbulent atmosphere or taxiing over rough ground are examples in aeronautics. Generally, only certain mean values of the important quantities enter the analysis of stochastic processes, while the concept of phase is completely lost. For example, in coin tossing, it is possible to calculate whether or not a head or tail will turn up only on the average and never for a specific toss. Liepmann[7] has suggested that the flow in the wake is stochastic and that statistical methods are therefore appropriate for the analysis of buffeting.

Thus, while vortex trail, Strouhal Number, total head wake, and dynamics of only certain portions of an aircraft structure may be meaningful concepts in them-

selves, they are of dubious significance as related to the buffeting problem. It is believed that buffeting is dependent fundamentally upon fluctuations of a random nature and that consequently analytical and experimental studies must recognize this by application of appropriate mathematics and the measurement of more directly relevant quantities.

Some Calculations on Buffeting

It might be helpful to have a way to estimate the decay of the disturbances as a tail is raised above a wake. This was studied by Graham[6] by considering the Kármán vortex trail to represent the wake behind a two-dimensional wing on which flow separation had occurred.† While it was realized that the vortex trail concept did not lead to a correct prediction of the frequency characteristics of the wake, it was hoped that it might serve here as a rough approximation to help study the spread of the fluctuations. It was found that, at some distance from the trail, the maximum induced vertical velocities occurred on a vertical line midway between two adjacent alternate vortices. On that line, the amplitude of the velocity was given by

$$V_y = (\Gamma/2b)\,\{\operatorname{sech}\,[(2\pi y/b) - 0.28\pi] + \operatorname{sech}\,[(2\pi y/b) + 0.28\pi]\} \quad (27)$$

The distribution of the vertical velocity amplitude given by this relation is shown on Fig. 11. If the dimension b, the distance between vortex rows, is taken to be the width of the total head wake, then this fluctuation distribution curve agrees moderately well with the low Reynolds Number "detector" data of Duncan. It is seen that a large disturbance can still exist a half total head wake width from the edge of the wake. It was noticed by Graham that the lateral decay of the vertical velocity in the flow field of a sine-wave-shaped wall approached that given by Eq. (27) for lateral positions not too close to the wake. This suggested the use of a wave-shaped wall in simulating the field outside the wake. Since the flow about the wave-shaped wall is known as a function of Mach Number, a compressibility effect is thereby indicated. Graham showed that the effect of compressibility was to spread the disturbances even farther laterally. The effect was small, since the Mach Number involved is that of the vortex trail, which is considerably lower than the airplane Mach Number.

†Eberle[10] suggested the same approach.

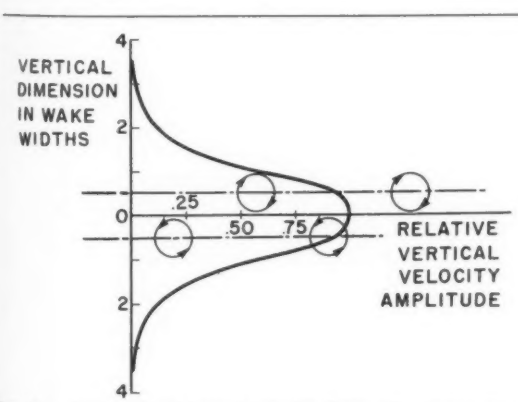

FIG. 11. Amplitude of lateral velocity fluctuation transverse to Kármán vortex trail.

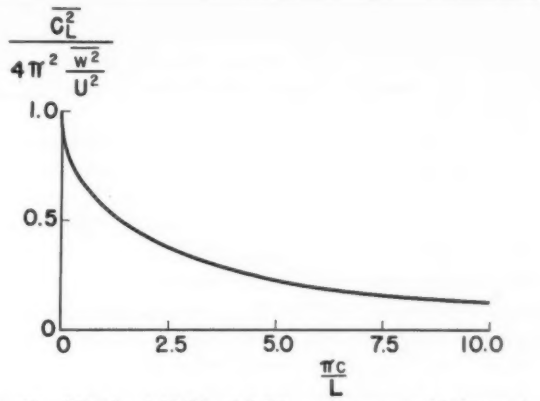

FIG. 12. Lift of a rigid thin airfoil in an incompressible isotropically turbulent flow.

Some new ideas on buffeting were recently reported by Liepmann.[7] He suggests that some well-established concepts of turbulence and statistics may be usefully carried over to this problem. The wake is considered to be turbulent and is described by a continuous power spectrum. The energy of the wake's fluctuations is distributed over a wide frequency range. Hence, resonance with the tail and fuselage is unavoidable. Flight measurements taken during buffeting show that the structure does, in fact, vibrate at its natural frequencies. Since the fluctuations in the wake are random, buffeting is a stochastic process. The central points in Liepmann's suggestions are that (1) the wake of a stalled body is turbulent and is described mathematically by mean values and by power spectra, and (2) the buffeting vibrations of an airplane are a stochastic process. To illustrate some of the concepts and methods involved in this description of buffeting, Liepmann calculates the lift of a rigid two-dimensional thin airfoil in a wake which is approximated by isotropic turbulence. Since only statistical data are known about the wake, only the mean square lift can be calculated. No concept of phase even enters the calculation, since the randomness of the fluctuations in the wake means no information on phase is available. The mean square lift coefficient is found to be

$$\overline{C_L{}^2} = 4\pi^2(\overline{w^2}/U^2)fcn(\pi c/L) \quad (28)$$

Thus, the mean square response of the airfoil of chord c in an isotropically turbulent stream of velocity U depends on the mean square value of the vertical velocity fluctuations, $\overline{w^2}$, and the scale of the turbulence, L. This relation is plotted in Fig. 12. It is seen that the

response to large eddies (L large) approaches the steady-state value given by the lift curve slope 2π, while the response to small eddies approaches zero. Eq. (28) also furnishes useful information concerning experiments.

It is necessary that the spectral distribution of the fluctuations and the relation between the scale of turbulence and the quantity that controls it be established. This calculation is a simple example of the procedure needed to calculate response from a fluctuating wake input. It represents, on Fig. 10, wake (3) going into the tail geometry and producing a load. The motion of the tail, which brings in the inertia, damping, and stiffness forces, also has to be considered. This consideration will show that the amplitude of the motion will be controlled by the damping, since the vibrations will be resonant.

Conclusions

Analytical approaches to two aircraft dynamics problems have been discussed. A scheme for representing oscillations of fuel in a tank was developed and used in studying the longitudinal motion of an aircraft with one partially full fuel tank. The motion of the aircraft was found to be composed of three loosely coupled oscillations: the phugoid, the airplane short period, and the fuel natural mode. The fuel oscillation has a frequency essentially the same as that of the fuel in a stationary tank, and significant damping was obtained only by the use of tank baffles. Arguments were advanced for a rational approach to buffeting on the basis of an aeroelastic response problem. It was suggested that ideas from turbulence and the mechanics of stochastic processes may be useful in setting up a buffeting theory.

References

[1] Schy, A. A., *A Theoretical Analysis of the Effects of Fuel Motion on Airplane Dynamics*, N.A.C.A. T.N. No. 2280, January, 1951.

[2] Graham, E. W., *The Forces Produced by Fuel Oscillation in a Rectangular Tank*, Report No. SM-13748, Douglas Aircraft Company, Inc., Santa Monica, Calif., April 13, 1950 (revised April 16, 1951).

[3] Greidanus, J. H., *A Review of Aeroelasticity*, Applied Mechanics Reviews, Vol. 4, No. 3, p. 139, March, 1951.

[4] Klein, A. L., *Effect of Fillets on Wing-Fuselage Interference*, A.S.M.E. Transactions, January, 1934.

[5] Duncan, W. J., *Tail Buffeting*, Journal of The Royal Aeronautical Society, Vol. XXXVIII, No. 278, pp. 108–137, February, 1934.

[6] Graham, E. W., *Notes on Some Aspects of Tail Buffeting*, Report No. SM-13664, Douglas Aircraft Company, Inc., Santa Monica, Calif., November 22, 1949.

[7] Liepmann, H. W., *An Approach to the Buffeting Problem from Turbulence Considerations*, Report No. SM-13940, Douglas Aircraft Company, Inc., Santa Monica, Calif., March 13, 1951.

[8] Den Hartog, J. P., *Mechanical Vibrations*, 3rd Ed., p. 48; McGraw-Hill Book Company, Inc., New York, 1947.

[9] von Kármán, T., and Biot, M. A., *Mathematical Methods in Engineering*, 1st Ed., pp. 469–476; McGraw-Hill Book Company, Inc., New York, 1940.

[10] Eberle, R. B., *Notes on Periodic Wake Disturbances, Strouhal Number and Tail Buffeting*, Report No. 7985, Chance Vought Aircraft, Dallas, Tex., October 7, 1949.

[11] von Kármán, T., *Hydrodynamics; Lecture Notes Used in the Hydrodynamics Course at C.I.T.*, Quoted in reference 10, p. 9.

[12] Den Hartog, J. P., *Recent Developments in Dynamics and Vibration*, Applied Mechanics Reviews, Vol. 4, No. 1, p. 3, January, 1951.

[13] White, J. A., and Hood, M. J., *Wing-Fuselage Interference, Tail Buffeting, and Air Flow About the Tail of a Low-Wing Monoplane*, N.A.C.A. T.R. No. 482, p. 18, 1934.

[14] Abdrashitov, G., *Tail Buffeting*, Report No. 395, Central Aero-Hydrodynamical Institute, Moscow, 1939 (Translated as N.A.C.A. T.M. No. 1041).

[15] Graham, E. W., and Rodriguez, A. M., *The Characteristics of Fuel Motion Which Affect Airplane Dynamics*, Report No. SM-14212, Douglas Aircraft Company, Inc., Santa Monica, Calif., November 27, 1951.

The Compressible Boundary Layer*

GEORGE B. W. YOUNG† AND EARL JANSSEN‡

The Rand Corporation and University of California at Los Angeles

SUMMARY

The laminar boundary-layer equations in integral form as obtained by Moore[1] are solved on the mechanical differential analyzer. The method of analysis permits the use of the best known variation of the air properties with temperature. Solutions are obtained for Mach Numbers ranging from incompressible speeds to the hypersonic régime at ambient temperatures of 100°, 400°, and 800°R. for both insulated-plate and heat-transfer cases. From these results, an approximate design procedure for the calculation of the characteristics of both the laminar and turbulent boundary layers is obtained and presented as an aid to missile designers.

INTRODUCTION

WITH THE EXCEPTION OF MOORE'S SOLUTION,[1] all existing solutions[2–5] of the laminar boundary-layer equations employe either a power law for the viscosity variation with temperature or a constant Prandtl Number or both. These assumptions limit their usages to the range of Mach Number and ambient temperature to which the assumptions are valid. Although these restrictions are generally not severe (some solutions being valid to $M \sim 5$), the present analysis removes these limitations and shows the trends of the characteristics of the boundary layer at high Mach Number and low ambient temperature. The thermodynamic and physical properties of air, pertinent to the boundary-layer solution, employed herein are given in the Appendix.

The laminar boundary-layer equations in integral form as obtained by Moore are solved on the mechanical differential analyzer. The variation of the flow properties through the boundary layer are obtained for ambient temperatures of 100°, 400°, and 800°R. by a converging procedure at several wall shear stress conditions to yield Mach Number variation and at several heat-transfer conditions including the insulated plate. The ambient temperatures of 100°, 400°, and 800°R. are chosen in anticipation that the present results will be helpful to investigators attempting to correlate results from hypersonic tunnels (where the temperatures are low) with flight-test data (where the ambient temperatures are high).

Received August 20, 1951.

* The authors wish to record their appreciation to Miss Barbara Dodge, of The RAND Corporation, for her excellent computational assistance and also to the differential analyzer staff of the University of California for their able assistance.

† Research Engineer, Missiles Division.

‡ Staff Engineer, Department of Engineering.

EQUATIONS OF THE LAMINAR BOUNDARY LAYER AND THEIR DIFFERENTIAL ANALYZER SOLUTIONS

The laminar boundary layer over a flat plate in two-dimensional compressible flow, with steady-state and zero pressure gradient conditions, is described by three equations:

Conservation of Momentum

$$\rho u \frac{\partial u}{\partial x} + \rho v \frac{\partial u}{\partial y} = \frac{\partial}{\partial y}\left(\mu \frac{\partial u}{\partial y}\right)$$

Conservation of Mass

$$[\partial(\rho u)/\partial x] + [\partial(\rho v)/\partial y] = 0$$

Conservation of Energy

$$\rho u \frac{\partial h}{\partial x} + \rho v \frac{\partial h}{\partial y} = \frac{\partial}{\partial y}\left(k \frac{\partial T}{\partial y}\right) + \mu\left(\frac{\partial u}{\partial y}\right)^2$$

The following steps and transformations have been made by Hantzsche and Wendt and Moore[1] and are simply summarized here:

(a) Transform the equations to total differentia, equations, with z as the single independent variablel by letting

$$z = y/\sqrt{x}; \qquad \partial z/\partial x = -z/2x$$

$$\partial z/\partial y = 1/\sqrt{x}; \qquad \tilde{v} = v\sqrt{x}$$

(*b*) Transform to u as the independent variable by introducing $G(u) = \mu\,(du/dz)$ and reduce the system to two equations

$$\frac{dG}{du}\frac{dh}{du} = \frac{d}{du}\left(\frac{k}{\mu c_p} G \frac{dh}{du}\right) + G$$

$$G(d^2G/du^2) = -(1/2)\rho\mu u$$

by combining the momentum and energy equations and the momentum and mass equations.

(c) Put into dimensionless form by letting

$$\eta = \frac{u}{\sqrt{h_B}}; \qquad g = \frac{G}{\sqrt{(1/2)\rho_B \mu_B (h_B)^{3/2}}}$$

$$j = h/h_B; \qquad Pr = \mu c_p/k$$

where the subscript B refers to a base temperature (taken as 400°R. for this investigation).

(d) Transform to a new independent variable, t, to avoid a singularity which appears in the equations rearranged for differential analyzer solution by letting

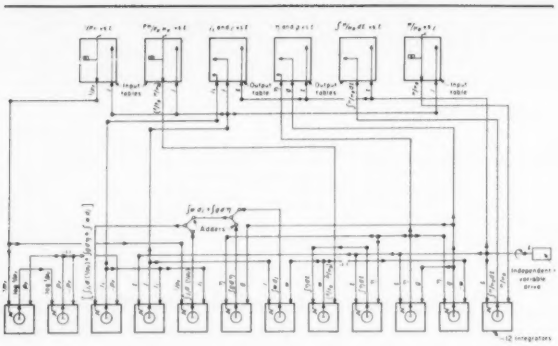

FIG. 1. Schematic diagram for the differential analyzer solution of the laminar boundary-layer equations.

$$g = \frac{d\eta}{dt}\,; \qquad \frac{dw}{dt} = \frac{\rho u}{\rho_B \mu_B}\,\eta$$

The two resulting equations are

$$\frac{d^2 j}{dt^2} = -Pr\left[w\frac{dj}{dt} + \left(\frac{dj}{dt}\right)\frac{d(1/Pr)}{dt} + g^2\right]$$

$$dg/d\eta = -w$$

since $w = 0$ when y or t is zero. The equations, along with certain associated transformation equations, are solved by integrating through the boundary layer from the plate ($t = 0$) to the free stream ($t = t_\delta$). The solution consists of j, dj/dt, η, g, and $\int \mu/\mu_B\, dt$ as functions of t.

The complete set of five equations rearranged for analyzer solution are

$$\frac{dj}{dt} = -\int Pr\, d\left[\int w\, dj + \int \frac{dj}{dt}\, d\left(\frac{1}{Pr}\right) + \int g d\eta\right]$$

$$g = -\int w\, d\eta$$

$$\eta = \int g\, dt$$

$$w = \int \frac{\rho\mu}{\rho_B\mu_B}\, d \int \eta\, dt$$

$$j = \int (dj/dt)\, dt$$

The equation that relates the original independent variables x and y to the independent variable t is

$$\sqrt{\frac{\rho_B \sqrt{h_B}}{2\mu_B}}\,\frac{y}{\sqrt{x}} = \int \frac{\mu}{\mu_B}\, dt$$

The reciprocal of $1/Pr$ is obtained by two integrations,

$$\log (1/Pr) = \int Pr\, d(1/Pr)$$

$$Pr = -\int Pr\, d[\log (1/Pr)]$$

The schematic diagram for the machine solution is shown in Fig. 1. The air properties ($1/Pr$, $\rho\mu/\rho_B\mu_B$, and μ/μ_B), as given in the Appendix are supplied from input tables during the course of the solution. Further details concerning the differential analyzer are given in references 6, 7, and 8.

This is a two-point boundary problem requiring six boundary values to determine a solution uniquely. The four values at the plate are: $\eta = \eta_w = 0$; $w = w_w = 0$; $j = j_w$, assigned for desired plate temperature; and $(dj/dt) = (dj/dt)_w = 0$, for the insulated plate case; or $g = g_w$, assigned arbitrary values for the heat-transfer case to give a range of Mach Number.

The two values in the free stream are: $j = j_\delta$, determined by the free-stream temperature; and $g = g_\delta = 0$. Note that t_δ itself is not known but is determined when g goes to zero.

The solution* of this two-point boundary problem on the differential analyzer involves guessing a value for g_w [or for $(dj/dt)_w$ in the heat-transfer case], setting it in the machine (along with the known values at $t = 0$), and running the machine to $g = 0$. If the value of j as g approaches zero is the desired one, then the solution is considered complete. If not, a new value for g_w or $(dj/dt)_w$ must be guessed and the procedure repeated. This converging procedure is aided by plotting j_δ vs. g_w [or j_δ vs. $(dj/dt)_w$ for the heat-transfer case]. The rapidity of this convergency depends on the approximation of the first guess, the linearity of j_δ with g_w or $(dj/dt)_w$, and the sensitivity of the machine in the particular region of the parameters. The parameter combinations employed are tabulated in Table 1.

* In certain regions of the parameters the value of j_δ obtained from the machine was subject to some dispersion—i.e., repeating runs with the same initial values gave different values for j_δ. This happened at large values of j_w and small values of j_δ, for which there were corresponding large values of g_w. The integrator generating $\int g\, d\eta$ [contributing to one of the terms in (dj/dt)] was observed to be "jumpy." When the machine was run faster, the "jumpiness" increased. Correspondingly, the dispersion in j_δ increased. By running the machine slowly, the dispersion decreased to zero. The trouble was believed to be due to the slipping of the integrator wheel of this one integrator when the acceleration of its moving parts reached a certain threshold value. By keeping the speed down, this threshold value was never reached. No runs that could not be repeated or which did not give values of j_δ and g_w or $(dj/dt)_w$ which lay on a smooth curve were considered valid.

TABLE 1
Parameter Combinations

Insulated Plate		Heat Transfer		
Assigned	Desired	Assigned	Assigned	Desired
j_w	j_δ	j_w	g_w	j_δ
1	0.25, 1	1	2.06	0.25
2	0.25, 1, 2	1	3.27	0.25
3	0.25, 1, 2	1	5.82	0.25
4	0.25, 1, 2	1	9.94	0.25
6	0.25, 1, 2	3	2.06	0.25, 1, 2
10	0.25, 1, 2	3	3.27	0.25, 1, 2
15	0.25, 1, 2	3	5.82	0.25, 1, 2
25	1, 2	3	9.94	0.25, 1, 2
40	1, 2	3	12.95	1, 2
		6	2.06	1, 2
		6	3.27	0.25, 1, 2
		6	5.82	0.25, 1, 2
		6	9.94	0.25, 1, 2
		6	12.95	1, 2

TABLE 2

The Characteristics of the Laminar Boundary Layer at the Nominal Ambient Temperature of 100°R. (Insulated Plate)

Run No.	M	T_δ (°R.)	$(C_f\sqrt{Re})_\delta$	$(C_f\sqrt{Re})_w$	Γ	T_i (°R.)	T' (°R.)	$\frac{\delta}{x}\sqrt{Re_\delta}$	$\frac{\delta^*}{x}\sqrt{Re_\delta}$	$\frac{\delta^{**}}{x}\sqrt{Re_\delta}$
3c	4.23	99	0.690	0.677	0.851	400	380	13.49	9.86	0.68
4j	6.42	101	0.651	0.693	0.841	800	642	22.87	19.19	0.64
2d	8.17	99	0.620	0.702	0.820	1,182	911	31.34	28.20	0.63
5a	9.57	100	0.593	0.709	0.791	1,550	1,200	37.22	34.24	0.58
1d	11.67	104	0.555	0.714	0.756	2,246	1,680	49.61	46.30	0.55
6a	15.45	102	0.501	0.721	0.711	3,565	2,570	...	...	...
7a	20.45	90	0.462	0.721	0.670	5,135	3,820	97.09	94.59	0.46

TABLE 3

The Characteristics of the Laminar Boundary Layer at the Nominal Ambient Temperature of 400°R. (Insulated Plate)

Run No.	M	T_δ (°R.)	$(C_f\sqrt{Re})_\delta$	$(C_f\sqrt{Re})_w$	Γ	T_i (°R.)	T' (°R.)	$\frac{\delta}{x}\sqrt{Re_\delta}$	$\frac{\delta^*}{x}\sqrt{Re_\delta}$	$\frac{\delta^{**}}{x}\sqrt{Re_\delta}$
3e	0.22	400	0.674	0.674	...	400	400	5.02	1.69	0.64
4i	2.43	402	0.629	0.681	0.842	800	738	7.51	3.94	0.64
2e	3.47	400	0.601	0.692	0.812	1,182	1,000	10.05	6.10	0.60
5b	4.28	401	0.575	0.699	0.783	1,550	1,313	11.03	7.83	0.56
1e	5.52	405	0.541	0.705	0.745	2,246	1,782	14.26	11.15	0.53
6d	7.49	401	0.499	0.714	0.703	3,565	2,700	19.96	16.81	0.48
7b	9.59	388	0.458	0.716	0.664	5,135	3,970	26.71	24.07	0.45
8c	12.44	398	0.417	0.724	0.630	8,160	6,000	36.11	34.08	0.40
9e	15.95	396	0.383	0.734	0.608	12,645	8,880	50.92	48.81	0.38

TABLE 4

The Characteristics of the Laminar Boundary Layer at the Nominal Ambient Temperature of 800°R. (Insulated Plate)

Run No.	M	T_δ (°R.)	$(C_f\sqrt{Re})_\delta$	$(C_f\sqrt{Re})_w$	Γ	T_i (°R.)	T' (°R.)	$\frac{\delta}{x}\sqrt{Re_\delta}$	$\frac{\delta^*}{x}\sqrt{Re_\delta}$	$\frac{\delta^{**}}{x}\sqrt{Re_\delta}$
4e	0.26	794	0.671	0.672	...	800	800	4.94	1.67	0.64
2f	1.74	800	0.638	0.680	0.792	1,182	1,120	6.14	2.80	0.63
5c	2.45	808	0.612	0.687	0.767	1,550	1,416	7.34	3.77	0.61
1f	3.52	797	0.576	0.696	0.733	2,246	1,900	9.02	5.62	0.57
6f	4.95	810	0.533	0.710	0.693	3,565	2,736	11.88	8.55	0.52
7f	6.45	792	0.490	0.712	0.659	5,135	4,040	15.54	12.24	0.49
8e	8.54	805	0.448	0.723	0.626	8,160	6,000	20.30	17.82	0.43
9f	11.33	765	0.405	0.729	0.605	12,645	8,950	28.40	26.57	0.39

TABLE 5

The Characteristics of the Laminar Boundary Layer at the Nominal Ambient Temperature of 100°R. (Heat Transfer Plate)

Run No.	M	T_δ (°R.)	T_w (°R.)	$(C_f\sqrt{Re})_\delta$	$(C_f\sqrt{Re})_w$	T' (°R.)	$\frac{Nu_\delta}{\sqrt[3]{Pr_\delta}\sqrt{Re_\delta}}$	$\frac{\delta}{x}\sqrt{Re_\delta}$	$\frac{\delta^*}{x}\sqrt{Re_\delta}$	$\frac{\delta^{**}}{x}\sqrt{Re_\delta}$
14d	8.63	97	400	0.667	0.655	530	0.312	19.62	16.14	0.65
15d	11.84	101	400	0.639	0.629	720	0.318	26.79	23.35	0.63
20f	19.19	94	400	0.584	0.572	1,350	0.331	45.59	42.61	0.56
21c	29.64	95	400	0.514	0.504	2,500	0.323	77.27	76.06	0.49
10f	8.93	101	1,182	0.615	0.696	957	0.307	32.28	28.74	0.62
11f	12.37	102	1,182	0.594	0.673	1,195	0.329	38.15	34.43	0.59
16f	18.74	105	1,182	0.553	0.629	1,695	0.339	51.46	48.20	0.53
17i	32.20	85	1,182	0.500	0.561	2,925	0.315	104.9	102.9	0.48
13f	13.39	96	2,246	0.553	0.708	1,750	0.313	55.99	52.97	0.54
18f	22.40	80	2,246	0.524	0.668	2,313	0.332	...	...	...
19d	31.88	92	2,246	0.468	0.605	4,100	0.312	...	...	...

TABLE 6

The Characteristics of the Laminar Boundary Layer at the Nominal Ambient Temperature of 400°R. (Heat Transfer Plate)

Run No.	M	T_δ (°R.)	T_w (°R.)	$(C_f\sqrt{Re})_\delta$	$(C_f\sqrt{Re})_w$	T' (°R.)	$\left(\frac{Nu}{\sqrt[3]{Pr}\sqrt{Re}}\right)_\delta$	$\frac{\delta}{x}\sqrt{Re_\delta}$	$\frac{\delta^*}{x}\sqrt{Re_\delta}$	$\frac{\delta^{**}}{x}\sqrt{Re_\delta}$
10e	4.55	402	1,182	0.591	0.680	1,120	0.345	10.11	6.77	0.58
11e	6.31	405	1,182	0.572	0.657	1,350	0.354	11.61	8.28	0.56
16e*	9.70	401	1,182	0.538	0.619	1,834	0.361	15.38	12.33	0.52
17g (rep.)	14.83	404	1,182	0.481	0.554	3,012	0.348	22.49	19.76	0.45
22e	18.44	410	1,182	0.450	0.516	4,300	0.333	...	...	...
13e	6.68	398	2,246	0.531	0.692	1,975	0.347	15.49	12.35	0.53
18e	10.20	394	2,246	0.503	0.657	2,520	0.354	19.52	16.31	0.50
19e	15.50	394	2,246	0.461	0.599	3,880	0.339	26.33	23.43	0.45
23c	18.70	416	2,246	0.437	0.566	4,920	0.327	...	...	...

TABLE 7
The Characteristics of the Laminar Boundary Layer at the Nominal Ambient Temperature of 800°R. (Heat Transfer Plate)

Run No.	M	T_δ (°R.)	T_w (°R.)	$(C_f\sqrt{Re})_\delta$	$(C_f\sqrt{Re})_w$	T' (°R.)	$\left(\frac{Nu}{\sqrt[3]{Pr}\sqrt{Re}}\right)_\delta$	$\frac{\delta}{x}\sqrt{Re_\delta}$	$\frac{\delta^*}{x}\sqrt{Re_\delta}$	$\frac{\delta^{**}}{x}\sqrt{Re_\delta}$
10d	3.29	798	1,182	0.621	0.661	1,325	0.349	7.29	3.53	0.62
11d	4.55	805	1,182	0.602	0.640	1,550	0.353	7.94	4.37	0.60
16d	6.99	792	1,182	0.568	0.605	2,250	0.356	9.94	6.58	0.56
17h	10.57	812	1,182	0.513	0.546	3,340	0.344	13.18	10.30	0.50
22d	13.43	784	1,182	0.476	0.510	4,500	0.339	16.67	14.21	0.46
13d	4.77	801	2,246	0.574	0.678	2,145	0.352	9.78	6.43	0.56
18d	7.22	804	2,246	0.536	0.647	2,684	0.348	11.33	8.40	0.52
19g	10.98	800	2,246	0.488	0.591	4,100	0.337	15.30	12.31	0.49
23e	13.63	792	2,246	0.462	0.561	5,100	0.329	18.45	15.62	0.46

THE CHARACTERISTICS OF THE LAMINAR BOUNDARY LAYER

The characteristics of the laminar boundary layer are determined for both the insulated-plate case and the heat-transfer case at nominal ambient temperatures of 100°, 400°, and 800°R. The results are tabulated in Tables 2 to 7. The methods employed in the transformation of the mathematical parameters into the physical parameters are as follows:

(a) Mach Number

$$M_\delta = \left(\frac{u}{a}\right)_\delta = \frac{\eta_\delta\sqrt{h_B}}{\sqrt{32.2R\gamma j_\delta T_B}}$$

(b) Skin-Friction Parameters

$$(C_f\sqrt{Re})_\delta \equiv \frac{\tau_w}{(1/2)\rho_\delta u_\delta^2}\sqrt{\frac{\rho_\delta u_\delta x}{\mu_\delta}} \equiv \frac{\sqrt{2}g_w}{\eta_\delta^{3/2}\sqrt{\rho_B\mu_B}}$$

$$(C_f\sqrt{Re})_w = \frac{\tau}{(1/2)\rho_w u_\delta^2}\sqrt{\frac{\rho_w u_\delta x}{\mu_w}} \equiv \frac{\sqrt{2}g_w}{\eta_\delta^{3/2}}\sqrt{\frac{\rho_w\mu_w}{\rho_B\mu_B}}$$

(c) Heat-Transfer Parameter

$$\frac{Nu_\delta}{\sqrt[3]{Pr_\delta}\sqrt{Re_\delta}} = \frac{1}{(T_t - T_w)}\frac{(Pr_\delta)^{2/3}}{(Pr_w)}\left(\frac{dj}{dt}\right)_w T_B\left(\frac{c_{pB}}{c_{p\delta}}\right)\frac{1}{\sqrt{2}}\frac{1}{\sqrt{\eta_\delta}}\sqrt{\frac{\rho_B\mu_B}{\rho_\delta\mu_\delta}}$$

(d) Temperature Recovery Factor

$$\Gamma \equiv \frac{2}{(\gamma-1)}\frac{1}{M_\delta^2}\left(\frac{T_t}{T_\delta} - 1\right) \equiv \frac{5}{M_\delta^2}\left(\frac{T_t}{T_\delta} - 1\right)$$

(e) Film Temperature or Reference Temperature for Fluid Properties.—The film temperature, T', is obtained from the relation of $\rho\mu/\rho_B\mu_B$ with T and the following equation for $\rho'\mu'/\rho_B\mu_B$:

$$\rho'\mu'/\rho_B\mu_B = \sqrt{2}g_w/\eta_\delta^{3/2}(C_f\sqrt{Re})_{M=0}$$

The value of 0.673 is used for $(C_f\sqrt{Re})_{M=0}$ in Tables 3 to 7 in order to be consistent with the incompressible solutions as obtained presently with the differential analyzer.

(f) Various Boundary-Layer Thicknesses

From the variations of η, j, and $\int(\mu/\mu_B)\,dt$ with t, the variations of u/u_δ and T/T_δ with $(y/x)\sqrt{Re_\delta}$ are obtained; also the thickness of $u/u_\delta = 0.995$, the displacement thickness, and the momentum thickness are determined. The relation between $(y/x)\sqrt{Re_\delta}$ and t is

$$\frac{y}{x}\sqrt{Re_\delta} \equiv \frac{y}{x}\sqrt{\frac{\rho_\delta u x}{\mu_\delta}} \equiv \sqrt{2\frac{u}{\sqrt{h_B}}\frac{\mu_B}{\mu_\delta}\frac{T_B}{T_\delta}}\int_0\frac{\mu}{\mu_B}\,dt$$

The displacement and momentum thicknesses are obtained by the numerical integration, using the trapezoidal rule, of the following integrals:

$$\frac{\delta^*}{x}\sqrt{Re_\delta} = \int_0^\infty\left(1 - \frac{T_\delta u}{T u_\delta}\right)d\left(\frac{y}{x}\sqrt{Re_\delta}\right)$$

$$\frac{\delta^{**}}{x}\sqrt{Re_\delta} = \int_0^\infty\frac{T_\delta u}{T u_\delta}\left(1 - \frac{u}{u_\delta}\right)d\left(\frac{y}{x}\sqrt{Re_\delta}\right)$$

The solutions for the nominal ambient temperature of 400° and 800°R. for the insulated-plate case are compared with the results of von Kármán and Tsien in Fig. 2. They used the assumptions that $Pr = 1$ and $\mu/\mu_\delta = (T/T_\delta)^{0.76}$, which should give good results for moderate Mach Numbers. The comparison is good for $T_\delta = 400$°R. up to $M \sim 4$ and for $T_\delta = 800$°R. up to $M \sim 2$. Included in this figure is the solution of Moore for air at dissociation equilibrium, considering variable air properties, at the nominal ambient temperature of 400°R. The close agreement of the results for $T_\delta = 400$°R. indicates that the effect of air dissociation is small.

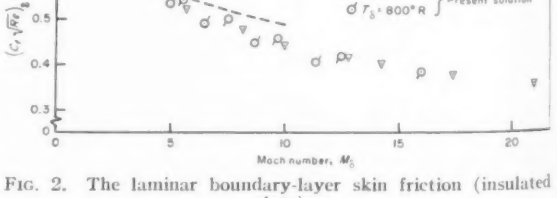

FIG. 2. The laminar boundary-layer skin friction (insulated plate).

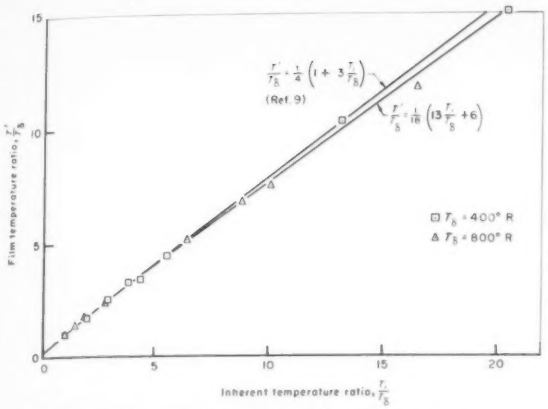
Film temperature ratio, $\frac{T'}{T_\delta}$
Inherent temperature ratio, $\frac{T_r}{T_\delta}$
$\frac{T'}{T_\delta} = \frac{1}{4}\left(1 + 3\frac{T_r}{T_\delta}\right)$
(Ref. 9)
$\frac{T'}{T_\delta} = \frac{1}{18}\left(13\frac{T_r}{T_\delta} + 6\right)$
□ T_δ = 400° R
△ T_δ = 800° R

FIG. 3. The film temperature for the insulated-plate case.

A comparison of the film temperatures with the results of Rubesin and Johnson[9] are shown in Figs. 3 and 4. The agreements are excellent at moderate Mach Numbers. For Mach Number greater than approximately 5, the following equations are recommended:

(*a*) *Insulated-Plate Case*

$$T'/T_\delta = (1/18)\,[13(T_r/T_\delta) + 6]$$

(*b*) *Heat-Transfer Case*

$$T'/T_\delta = 0.70 + 0.023\,M_\delta^2 + 0.58\,(T_w/T_\delta)$$

The results for the nominal ambient temperature of 100°R. indicate higher values of the skin-friction parameter, $(C_f\sqrt{Re})_\delta$. This is due to the existence of the maximum in the variation of the density-viscosity ratio with the enthalpy parameter (see Appendix) at low air temperatures. Higher values are also indicated for the temperature recovery factor, inherent temperature, and film temperature ratio. However, the heat-transfer parameter is little affected. This peculiarity would serve as a warning that comparisons of hypersonic wind-tunnel data with flight-test data should be made with caution.

Since the flow characteristics for T_δ = 400°R. command the most interest and the trends are similar to those for T_δ of 100° and 800°R., the variations of u/u_δ, T/T_δ, g, and dj/dt for T_δ = 400°R. are plotted versus $(y/x)\sqrt{Re_\delta}$ in Figs. 5 to 16, with Mach Number as the parameter.

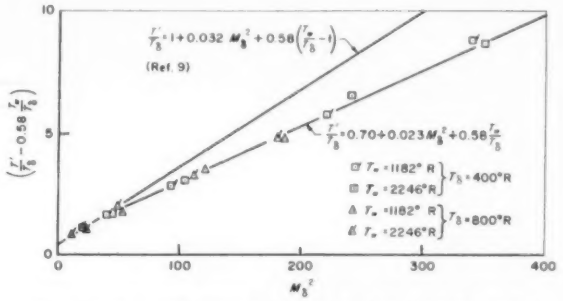
$\frac{T'}{T_\delta} = 1 + 0.032\,M_\delta^2 + 0.58\left(\frac{T_w}{T_\delta} - 1\right)$
(Ref. 9)
$\frac{T'}{T_\delta} = 0.70 + 0.023\,M_\delta^2 + 0.58\frac{T_w}{T_\delta}$
□ T_w = 1182° R
■ T_w = 2246° R
} T_δ = 400° R
△ T_w = 1182° R
▲ T_w = 2246° R
} T_δ = 800° R
$\left(\frac{T'}{T_\delta} - 0.58\frac{T_w}{T_\delta}\right)$
M_δ^2

FIG. 4. The film temperature for the heat-transfer case.

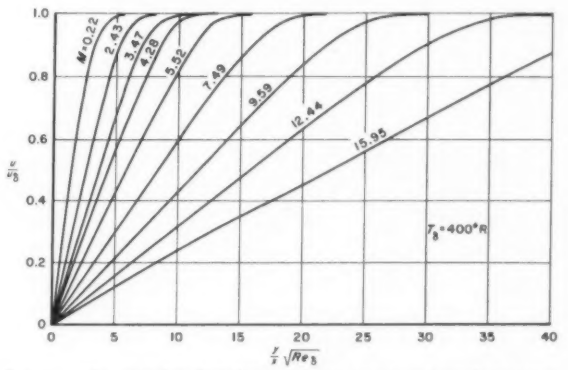

FIG. 5. The velocity distribution in the laminar boundary layer (insulated plate).

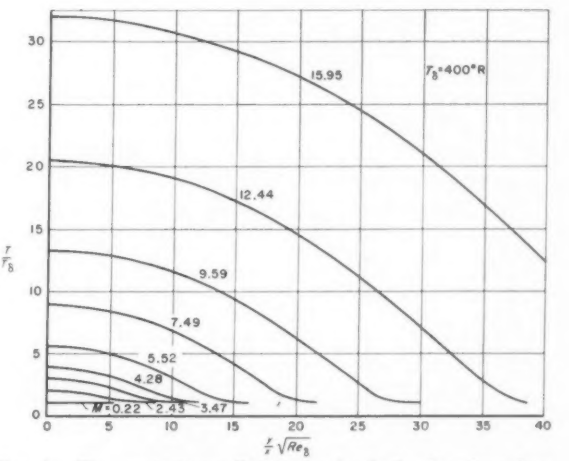

FIG. 6. The temperature distribution in the laminar boundary layer (insulated plate).

CONCLUDING REMARKS

It is almost self-evident from the correlation of T'/T_δ with M_δ, as shown in Fig. 4 for T_δ of 400° and 800°R., that the approximate design procedure of using the incompressible relations for the laminar skin friction and evaluating the air properties at the film temperature, T', should give good results at hypersonic, as well as supersonic, speeds in the ambient temperature range of missile flights. More important, there are indications that this procedure can be applied approximately to the turbulent boundary layer. That is, use the incompressible relations for the turbulent heat-transfer and skin-friction coefficients and the following relations for T':

$$\frac{T'}{T_\delta} = 1 + 0.032M_\delta^2 + 0.58\left(\frac{T_w}{T_\delta} - 1\right) \quad \text{(for } M < 5.6\text{)}$$

$$\frac{T'}{T_\delta} = 0.70 + 0.023M_\delta^2 + 0.58\left(\frac{T_w}{T_\delta}\right) \quad \text{(for } M > 5.6\text{)}$$

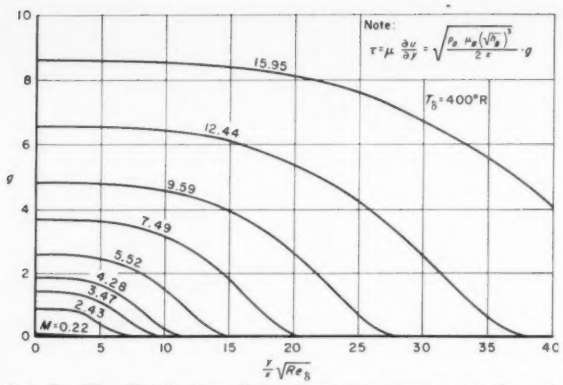

FIG. 7. The distribution of the shear stress parameter through the laminar boundary layer (insulated plate).

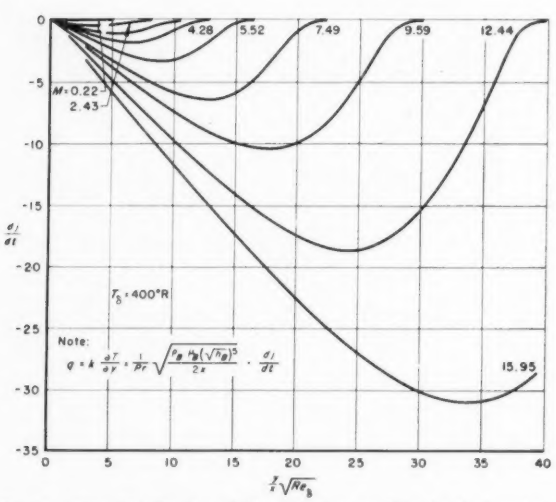

FIG. 8. The distribution of the enthalpy gradient in the laminar boundary layer (insulated plate).

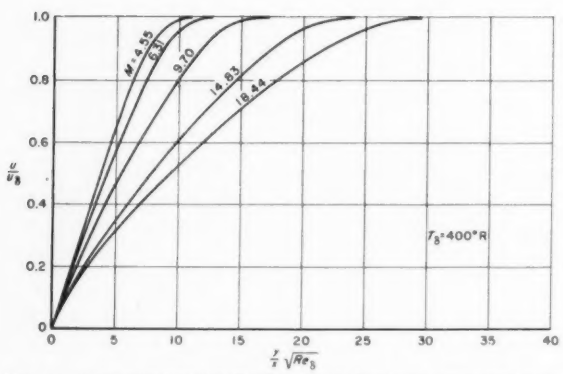

FIG. 9. The velocity distribution in the laminar boundary layer (T_w = 1,182°R.).

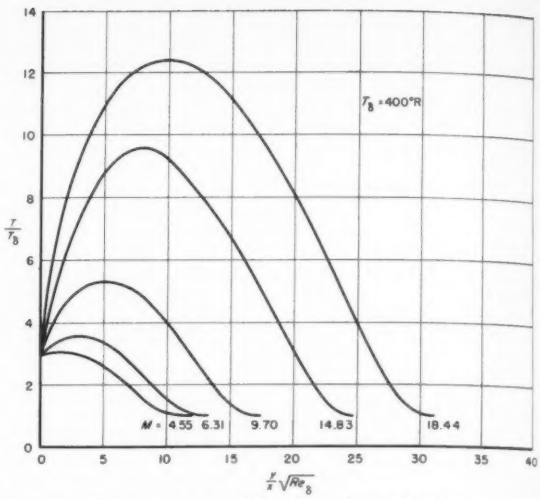

FIG. 10. The temperature distribution in the laminar boundary layer (T_w = 1,182°R.).

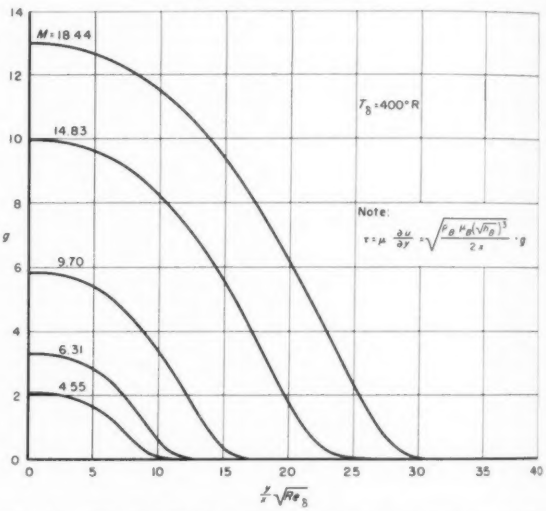

FIG. 11. The distribution of the shear stress parameter in the laminar boundary layer (T_w = 1,182°R.).

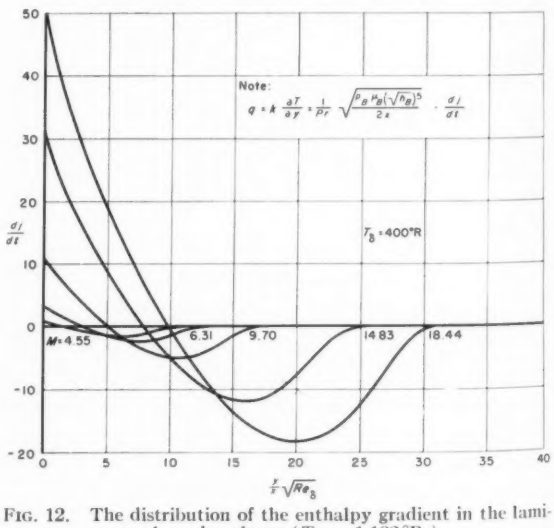

FIG. 12. The distribution of the enthalpy gradient in the laminar boundary layer (T_w = 1,182°R.).

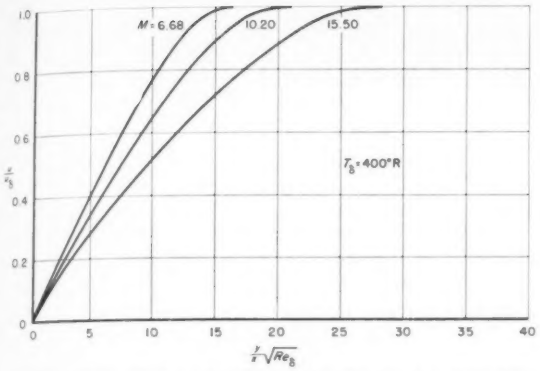

FIG. 13. The velocity distribution in the laminar boundary layer (T_w = 2,246°R.).

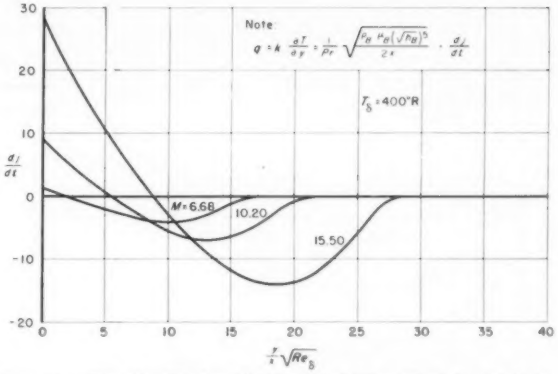

FIG. 16. The distribution of the enthalpy gradient in the laminar boundary layer (T_w = 2,246°R.).

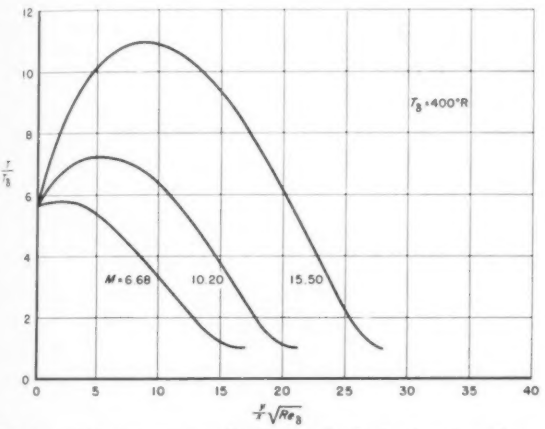

FIG. 14. The temperature distribution in the laminar boundary layer (T_w = 2,246°R.).

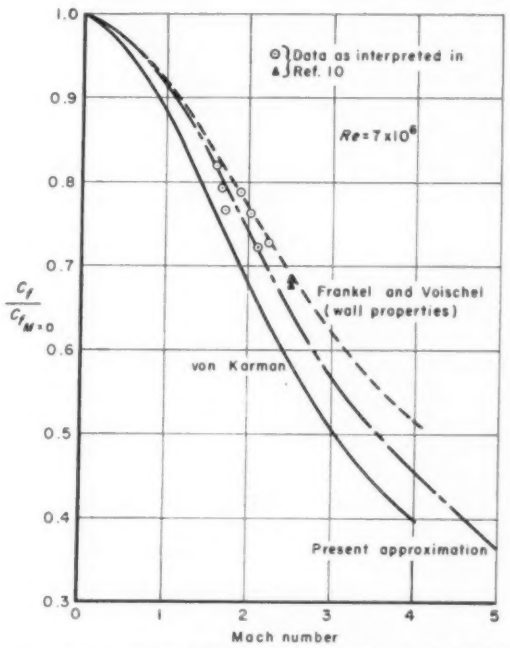

FIG. 17. The average turbulent boundary-layer skin friction (insulated plate).

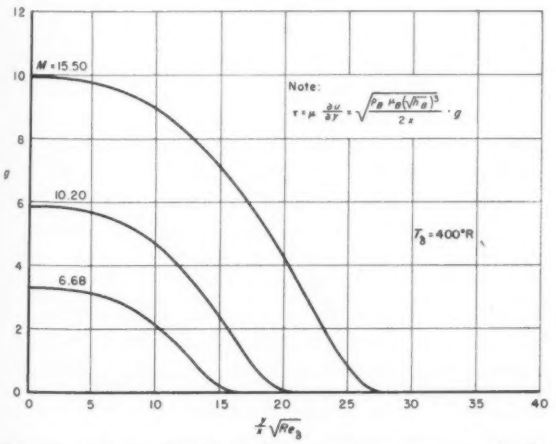

FIG. 15. The distribution of the shear stress parameter in the laminar boundary layer (T_w = 2,246°R.).

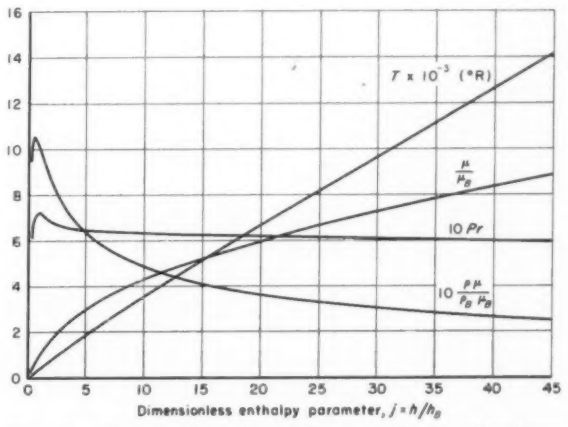

FIG. 18. The air properties pertinent to the boundary-layer solution.

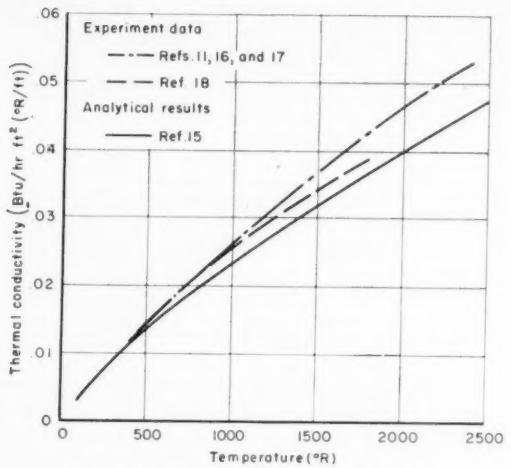

FIG. 19. The thermal conductivity of air.

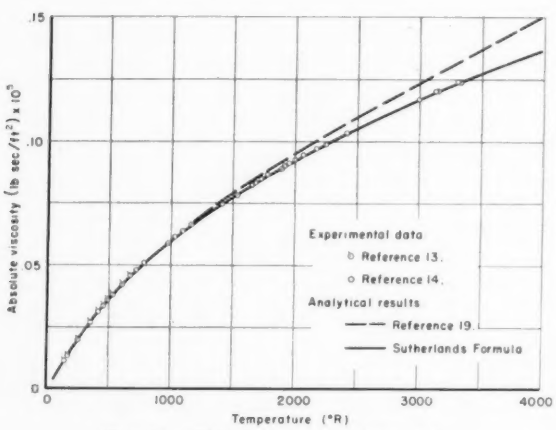

FIG. 20. The absolute viscosity of air.

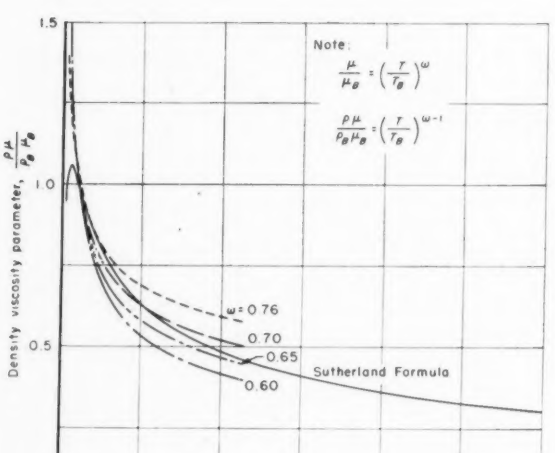

FIG. 21. The comparison of various viscosity laws.

In Fig. 17 the application of this approximate method to the turbulent skin friction over an insulated plate is compared with some data as interpreted by Rubesin, Maydew, and Varga.[10]

APPENDIX—AIR PROPERTIES AS A FUNCTION OF TEMPERATURE

The air properties, μ, c_p, k, ρ, and h must be known as a function of temperature. The beauty of the present method of analysis lies in the fact that the best known variation of the air properties can be utilized without recourse to approximate expressions, relating the air properties to the temperature. This is possible because the numerical solutions, employing the mechanical differential analyzer, can absorb graphical data. The air properties in dimensionless parameters as used herein are given in Fig. 18.

The enthalpy information is obtained from Keenan and Kaye[11] and Krieger and White.[12] The viscosity variation is calculated from Sutherland formula—that is,

$$\frac{\rho\mu}{\rho_B\mu_B} = \frac{1+\theta}{\sqrt{T/T_B} + (\theta/\sqrt{T/T_B})}$$

or

$$\frac{\mu}{\mu_B} = \left(\frac{T}{T_B}\right)\frac{1+\theta}{\sqrt{T/T_B} + (\theta/\sqrt{T/T_B})}$$

where $\theta = 0.522$. This variation agrees excellently with the experimental data of Fortier[13] and Vasilesco[14] which cover a temperature range from 146.7° to 3,321.2°R. The variation of the Prandtl Number with temperature possesses a degree of uncertainty because of insufficient information on the thermal conductivity of air. However, fortunately, the effect of this variation plays a minor role in the analysis. The Prandtl Number values as used are obtained with values of the thermal conductivity calculated by Hirschfelder and Curtis[15] for temperatures up to 500°R. In the temperature region between 600° to 2,400°R., the values of Keenan and Kaye[11] and Tribus and Boelter[16] are used. At the higher temperatures, the Prandtl Number variation is extrapolated using the variations of the air components, as calculated with kinetic theory, as a guide. The present state of the art on thermal conductivity and viscosity is presented in Figs. 19 and 20. In Fig. 21, the results of using power laws for the viscosity variation are compared with the Sutherland formula.

REFERENCES

[1] Moore, L. L., *A Solution of the Laminar Boundary Layer Equations for a Compressible Fluid with Variable Properties, Including Dissociation*, Project RAND, The RAND Corporation, P-50, January 12, 1949. (Also available as Master's Thesis, Department of Engineering, University of California at Los Angeles, February, 1949.)

(*Continued on page 288*)

Experiments on Interaction of Shock Waves and Cylindrical Bodies at Supersonic Speeds*

M. V. MORKOVIN,† E. MIGOTSKY,‡ H. E. BAILEY,** AND R. E. PHINNEY**
University of Michigan

ABSTRACT

While two-dimensional shock-wave reflections have received much attention, in most applications either the shock surface or the reflecting surface is curved. Elements of nonviscous theory for three-dimensional shock reflections by two of the present authors indicated the likelihood of anomalous reflection for configurations such as that of a plane shock impinging on a cylinder aligned with the free stream. This paper presents the highlights of the experimental investigation of this three-dimensional shock-cylinder configuration conducted in the University of Michigan Supersonic Wind Tunnel at a Mach Number of 1.90.

One general result is the striking boundary-layer cross flow induced by the sharp pressure gradients across the reflection line on body surfaces. For the present configuration, the cross flow, in and outside of the boundary layer, results in a separated region on the lee side of the body. The effects of boundary-layer character and thickness and of shock strength on the overall flow and pressure fields are studied by means of body-pressure distributions and several visualization techniques. Implications of the present findings for practical applications are discussed.

SYMBOLS

- δ = flow deflection angle across incident shock in the vicinity of the cylindrical body
- ω = meridian angle
- θ = shock-wave inclination angle
- M = free-stream Mach Number
- p = static pressure on surface of cylindrical body
- p_0 = free-stream stagnation pressure
- Δp = pressure rise on cylindrical body due to presence of shock wave
- II' = trace of shock plane
- e = subscript, indicating that the variable is in the plane normal to the local direction of shock-cylinder intersection
- (r_1) = boundary layer artificially roughened by paint line
- (r_2) = boundary layer artificially roughened by two roughness rings

Presented at The Aerodynamics Session, Annual Summer Meeting, I.A.S., Los Angeles, June 27–28, 1951.

* This work was sponsored partly by the U.S. Air Force and partly by the Engineering Research Institute, University of Michigan. The staff of the University of Michigan Supersonic Wind Tunnel have contributed to this report in discussions, in constructing and operating the equipment, and in reducing the data. Their help is acknowledged with thanks.

† Associate Professor; now Research Scientist, The Johns Hopkins University, Baltimore.

‡ Research Associate; now Aeronautical Research Scientist, Ames Aeronautical Laboratory, N.A.C.A. Part of this report is based on Migotsky's Ph.D. thesis at the University of Michigan, 1951.

** Research Associate, Engineering Research Institute.

INTRODUCTION

DURING THE LAST 5 YEARS much attention has been given to the study of the two-dimensional problem of supersonic shock wave reflections from a flat surface with boundary layer both analytically[1–4] and experimentally.[5–11] Although the problem is far from solved, some understanding of the basic variables influencing the phenomenon has been achieved, notably through references 1, 9, and 10.

It is generally accepted that the nonviscous theory of so-called regular two-dimensional shock reflection[12] yields the correct values of the pressure jump and the shock-wave direction at distances sufficiently far from the point of impingment of the shock on the wall. Near this point, both upstream and downstream, the boundary layer is strongly affected by the shock wave. When the boundary layer is laminar, the resulting adverse pressure gradient is felt far upstream (as much as 100 times the undisturbed boundary-layer thickness,[9,10]) and the layer is believed to separate for all but the weakest shock waves. The incoming shock reflects as an expansion wave from the free separated surface and turns it back to the wall, forming a bubble. The outgoing compression waves generated by the thickening and separation, as well as by the reattachment of the boundary layer, tend to coalesce with the expansion wave and to form a single sharp compression wave (the reflected shock) far enough from the wall. For a given Mach Number, the interaction between the laminar boundary layer and the shock increases as the shock strength increases and the boundary layer thickness decreases.[1, 10]

Reflection from a wall with a turbulent boundary layer is less well understood. For weaker shocks,[9–11] the boundary layer appears to thicken more or less rapidly just upstream of the impingment point, and the wall pressure measurements indicate a sharp rise with a relatively small upstream influence. For stronger shocks,[11] local separation and, finally, bifurcation may occur with the corresponding shock-expansion-shock pattern and increasing upstream influence. The ranges in which these régimes occur seem to depend also on the Mach Number and the boundary-layer thickness. It is believed that the basic difference lies in the fact that a given adverse pressure gradient produces a much smaller rate of growth when the boundary layer

is turbulent than when it is laminar. Reference 9 demonstrated that the observed difference between the laminar and turbulent cases cannot be ascribed to the relative thickness of the subsonic portion of the layers. In absence of published data, however, it is believed that the effect of an increase in thickness of a turbulent boundary layer could be explained by the role of the increased thickness of the subsonic layer as an avenue for upstream influence.

In practice, the configurations in which a shock wave falls upon a solid boundary are generally three-dimensional—i.e., either the shock wave or the reflecting (interfering) surface is curved in such a manner that the line of their intersection is not everywhere normal to the oncoming stream lines. It follows that there are at least two effects not present in the two-dimensional problem heretofore analyzed: (a) The flow field downstream of the reflecting wave is not uniform and generally involves a postreflection cross flow (relative to preshock stream-line direction) even in the nonviscous case; (b) the (vector) pressure gradient affecting the boundary layer may have an appreciable component normal to the preshock stream lines; where the velocities inside the boundary layer are small, one may expect a boundary-layer cross flow considerably stronger than the outer postreflection cross flow (a).

Two of the present authors established[13] the link between the two-dimensional and the three-dimensional nonviscous reflection theory, the so-called local sweepback principle. Since in both cases the reflection is governed by the condition of no velocity normal to the body and since locally the flow changes (singularity type) across incident and reflected shocks literally dwarf any flow changes due to continuous curvature of stream lines or shock waves, one needs merely to consider the local two-dimensional reflection problem in the effective plane, defined as the plane normal to the intersection of the incident shock with the body. The result of such point-by-point solutions along the intersection line would yield initial values of velocity on the surface of the body; since these initial values of velocity are not constant because of the three-dimensional nature of the problem, a rather complex three-dimensional flow behind the shock waves would ensue. To solve completely the problem of nonviscous three-dimensional shock reflection, one would have to compute this postreflection flow, which in the two-dimensional case was merely a uniform parallel flow.

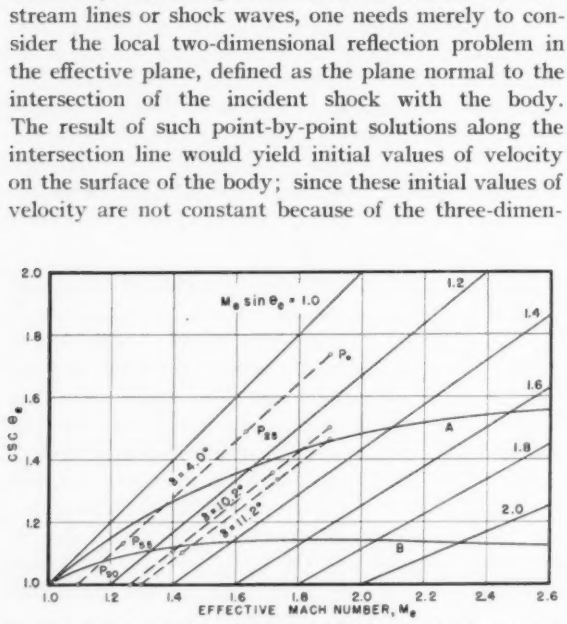

FIG. 1. Representation of the possible shock reflections based upon nonviscous theory.

One of the cases studied analytically in reference 13 was that of a plane shock wave impinging on an infinite cylinder, which is aligned with the steady free stream. It was found that at all supersonic Mach Numbers and at all shock orientations there are regions on the reflecting cylinder where a regular (nonviscous) shock reflection cannot occur. If the shock did not warp near these irregular regions, there would also be regions on the body where no reflection at all is possible. Clearly, according to the nonviscous theory, the three-dimensional nature of the body or shock must induce some changes, such as warping, in the incident shock wave *before it reaches the surface.* Such a behavior is again basically different from that in the two-dimensional case. Should the warping be in the form of Mach Y type of reflection, pockets of subsonic flow would be created so that the reflection phenomenon would become more directly dependent on the conditions downstream. Also, any warping whatsoever would make the analytical solution of the postreflection flow nearly impossible.

It appeared likely that the shock interference with the boundary layer, in particular the boundary-layer cross flow already mentioned, could modify the conditions of reflection appreciably and possibly mask the anomalous reflection predicted by the nonviscous theory. Since the plane-shock cylinder configuration also represents the simplest case of the important wing-body interference problem (wing influencing body without reciprocal influence of body on wing), it was decided to explore this case of three-dimensional shock reflection experimentally.

Experimental Objectives and Techniques

The experiments were conducted in the 1.90 Mach Number channel of the University of Michigan Supersonic Wind Tunnel. This tunnel, which is intermittent and has an 8- by 13-in. test section, is described in reference 14, and its detailed calibration is reported in reference 15. The model configuration can be seen in Figs. 2 and 8; problems connected with model design and instrumentation are discussed in detail in references 16 and 17.

Broadly speaking, the objectives of the experiments were, by various visualization techniques and pressure measurements: (1) to explore the regions on the cylinder where anomalous reflection is indicated by the nonviscous theory;[13] (2) to obtain the main characteristics of the boundary-layer and postreflection cross flows; (3) to assess various effects on (1) and (2) due to changes of the boundary layer and of the shock strength.

In pursuing objective (1), a special technique was designed to check optically a point in the region of anomalous reflection which otherwise cannot be seen. This was accomplished by simultaneously rotating the shock system by 25° around the axis of the cylinder and yawing the schlieren beam by 25° from its normal position (see Fig. 9a). The choice of these angles can be understood in the light of the results of the nonviscous theory of reference 13 which are summarized in Fig. 1. The abscissa, M_e, represents the projection of the free-stream Mach Number, M, on the plane normal to the line of intersection between the shock plane and the cylinder. The angle θ_e is the effective shock wave angle in this normal plane. Thus, at the $\omega = 90°$ meridian, $M_e = M \sin \theta$ and $\theta_e = 90°$—i.e., the ordinate $\csc \theta_e = 1$; as free-stream Mach Number M varies or as the strength of the incident shock varies due to change of wedge angle δ, the points P_{90} corresponding to the 90° meridian are represented on the horizontal axis. In the same sense, shock conditions at any point on the incident side of the cylinder will be represented by a point in the sector between the straight line $M_e \sin \theta_e = 1$ and the horizontal axis for all Mach Numbers and shock strengths.

According to the nonviscous theory, any region on the cylinder corresponding to points above the curve A is a region where regular reflection is possible. Points below curve A correspond to regions where regular reflection of a truly plane incident shock becomes impossible. Finally, points between curve B and the axis $\csc \theta_e = 1$ refer to the region on the cylinder where, if the shock could remain plane, no reflection at all would be possible.

For a given Mach Number and shock strength, the projection of the M vector normally to the shock plane is the same at all points and is equal to $M_e \sin \theta_e = M \sin \theta$. Thus, as one proceeds along the shock-cylinder intersection, one covers a segment of one of the family of inclined straight lines $M_e \sin \theta_e =$ constant in Fig. 1. The starting point of the segment corresponding to $\omega = 0$ may be anywhere, say above curve A where regular reflection is possible; the segment must then always cross curves A and B and end on the horizontal axis, which corresponds to $\omega = 90°$.

The segments corresponding to three of the cases studied by pressure measurements at $M = 1.90$—namely, $\theta = 35.2°$, 41.8°, and 42.9° (effective wedge angles 4.0°, 10.2°, and 11.2°)—are shown dotted in Fig. 1. In the case $\delta = 10.2°$, one sees from points corresponding to 0° and 25° meridian, P_0 and P_{25}, that the shock can have regular reflection at the normally observed meridian $\omega = 0°$ but that the nonviscous theory indicates anomalous reflection at the meridian $\omega = 25°$, which was made visible by the yawed-schlieren system.

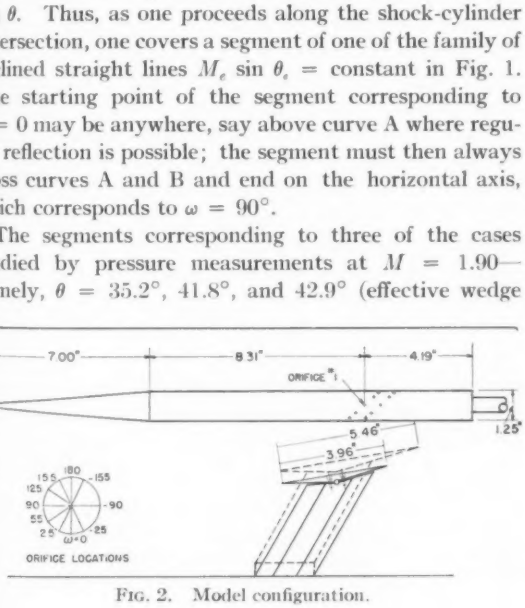

FIG. 2. Model configuration.

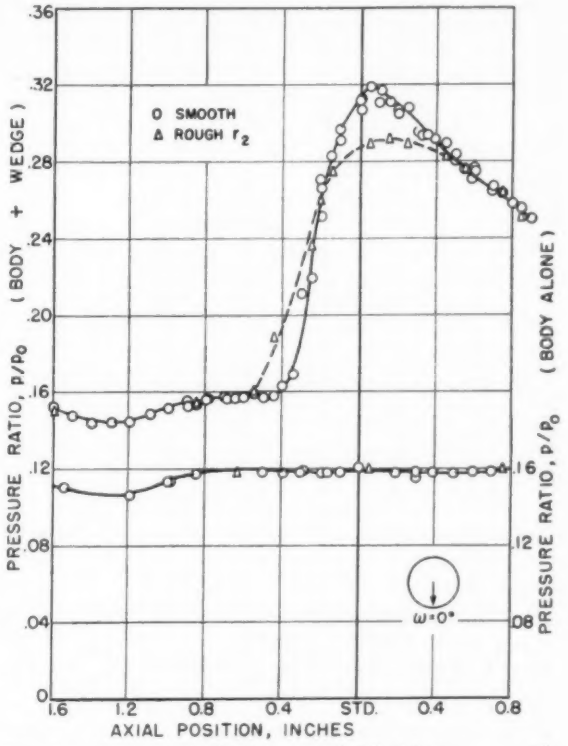

FIG. 3a. Pressure distribution on cylindrical body. $\omega = 0°$; $\delta = 10.2°$.

Ordinary schlieren photographs with different knife-edge positions were taken regularly. In addition, the flow was studied by shadowgraphs and the light-scattering technique recently used by N.A.C.A. (so-called vapor technique). In pursuing objective (2) a special mixture of china-clay, oil of wintergreen, and iso-safrole was developed by Murphy,[1] of the tunnel staff. A thin film of this colorless mixture applied to the body evaporates at the proper rate during the 20-sec. tunnel runs so that the flow lines in the inner portion of the boundary layer become visible (Figs. 11b, 12b, 13b, 15b, and 16). The tuft technique was also used for indication of average flow directions near the surface.

The location of static pressure orifices (0.025 in. in diameter) is shown in Fig. 2. The cylinder was moved fore and aft and was rotated about its axis in the cases $\delta = 4.0°$ and 11.2° in order to obtain as complete a coverage of the shock neighborhood as desired. The model axial position for which orifice No. 1. fell 0.29 in. forward of the centerline of the tunnel window was arbitrarily designated as *standard axial position*, and all

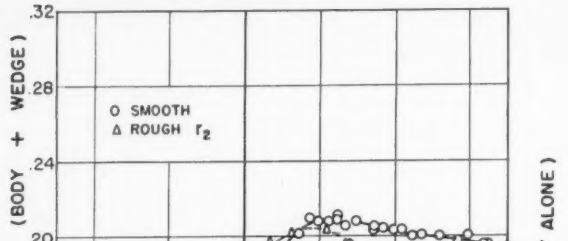

FIG. 3b. Pressure distribution on cylindrical body. $\omega = 90°$; $\delta = 10.2°$.

axial displacements were measured and recorded with respect to this standard. At first, a rotatable wedge, W_1, 3.50 in. wide and 3.96 in. long, was used as the shock generating unit. As the blocking characteristics of this particular configuration in the tunnel became clearer, a second wedge, W_2 (5.50 in. wide, 5.46 in. long, and 0.40 in. closer to the body), furnished a larger testing region in the vicinity of the shock not appreciably affected by the outside interference such as that due to wedge tips, model nose and shoulder, etc. The tunnel and cylinder interference effects are essentially eliminated by considering the pressure increments, Δp, of body in presence of wedge over the body alone configuration (see, for instance, Fig. 3a).

In order to bring out the overall effects of large changes in body cross section, some experimental investigations of interaction between the identical plane shock wave and a long square body were made. The length of the body, shoulder to base, was 12.50 in., and the depth and width were 1 in. The pyramidal nose was 7 in. long and had a half angle of 4°5′. Fig. 15a shows the square body and a typical interaction pattern.

The Reynolds Number at the standard plane on the body was 5.43×10^6. Laminar boundary layer was not obtainable at this station. By shifting the cylinder 3 to 5 in. aft of the standard position, optical studies (without pressure distributions) of the shock-wave interference with a laminar boundary layer were made (Figs. 9a and 9b). The condition of turbulent boundary layer near the pressure orifices was designated as "smooth" when the transition point was not controlled artificially, rough (r_1) when a narrow line was painted on the body 1 in. downstream of the cone-cylinder shoulder, and rough (r_2) when two rings (wire diameter 0.022 in.) were slipped on the cone (Fig. 8). For runs in the smooth condition there was an unpredictable* variation of the transition point (as much as $3\frac{1}{2}$ in.) and a consequent variation in the boundary-layer thickness which in turn was responsible for a larger scatter of pressure measurements in the vicinity of shock impingement (Fig. 3a). The paint line in the rough (r_1) condition appeared to bring about a uniform boundary layer judging by the elimination of scatter in the total head measurements on the body surface. The total head pressure probes were made by flattening 0.065-in. outside diameter stainless-steel tubes to give an opening having an inside dimension of 0.007 in. The probes were soldered to the rear side of the body (Fig. 11b) so that they would not influence the static pressure measurements on the front side.

In order to obtain the effective shock deflection angles δ, the negatives of the various schlieren photographs were projected onto a ground glass, and the shock inclination near the cylinder relative to the trace $\omega = 0°$ was read several times by different people on a special protractor. From the average value of θ, the deflection angle δ was deduced by using graphs from reference 19. Such a procedure may lead to errors of as much as $\pm 0.30°$ in the present case.

In the preceding description of the experimental techniques, the likely sources of errors were brought out. It is believed that the errors actually present do not influence the understanding of the basic effects that were selected for study in objectives (1), (2), and (3).

The Three-Dimensional Flow Field

The problem of shock-wave diffraction around the cylinder can also be visualized as a pressure and flow field response to a sudden (step) application of a constant angle of attack to the portion of the cylinder downstream from the inclined shock plane. According to the linearized view of the problem, there would be local distortions of the flow and pressure fields in the vicinity of the "loading" line on the body; these distortions would disappear with increasing distance downstream, until ultimately the flow would settle down to the (doublet) flow around an infinite circular cylinder at the given angle of attack. In the nonlinear view, the distortions of the field near the loading line may well be greater and may include the effects of Mach Y formation and warping of the shock wave out of the incident plane. Viscosity is likely to modify the field distortion by allowing distortion of the effective flow boundary by virtue of boundary-layer changes. It is likely that

* It is likely that the phenomenon is connected with variable heat transfer from the body caused by differences in the temperature of the tunnel air supply and the body at the beginning of the run. Despite much effort, no conclusive correlation has as yet been obtained.

even in the nonlinear viscous case the local field distortions will die down with increasing distance downstream and the flow will settle down to the *viscous* flow around an infinite cylinder at the same angle of attack (yaw).

The distortions of the field due to the boundary layer are twofold. First, there is the essentially two-dimensional effect of the upstream propagation of the pressure rise associated with the shock as discussed in the Introduction. This effect, of course, modifies basically the boundary layer as a whole (see for instance the boundary-layer edge in Fig. 9b). Second, a boundary-layer flow across meridional planes is generated, thus further modifying the effective boundary surface. The inclination (relative to the free stream) of the flow lines in the boundary layer (Figs. 11b, 12b, and 13b) on the side of the body appears to be always somewhat less than the corresponding shock-wave angle but is several times as large as the angle of deflection across the shock outside the boundary layer. This flow-line inclination decreases with distance downstream from the shock but the boundary-layer cross flow persists. The corresponding partial disappearance of the boundary layer from the $\omega = 0°$ meridian and its accumulation on the $\omega = 180°$ meridian are clearly visible in all schlieren photographs with horizontal knife edge.

It is notable that the overall features of the field just described are all present in the case of shock diffraction around a square body (Fig. 15) and are therefore likely to occur for most convex elongated bodies. Fig. 15b of the flow lines on the side of the square body shows that while these are inclined at slightly over 40° (corresponding to a shock angle of 42.9°), the line along which the flow lines start sharply curving is inclined nearly 60° to the free stream. This illustrates the effect of the cross flow as an "increasing obstacle" to the oncoming flow as one proceeds along the shock-body intersection line and of the observable forward warping of the shock wave (Fig. 15a). Both of these effects can be observed on schlieren photographs of the cylindrical body such as Fig. 12a. The shock continuation beyond the body on the lee side indicates some forward warping; the continuous compressive wave, which coalesces into a shock upstream of the main shock continuation on the lee side, indicates the boundary-layer effect. This forward effect at an angle greater than the shock angle is naturally evidenced by the higher inclination of the line along which the pressure rise begins on the composite pressure distributions of Figs. 4 and 5.

Lee-Side Effects

The phenomenon of shock reflection on the lee side ($90° < \omega < 270°$) is fundamentally different from that on the incident side ($|\omega| < 90°$) even in the nonviscous case. Thus, on the incident side, the oncoming shock wave induces velocities that are directed into the surface of the body, and it can be considered that their

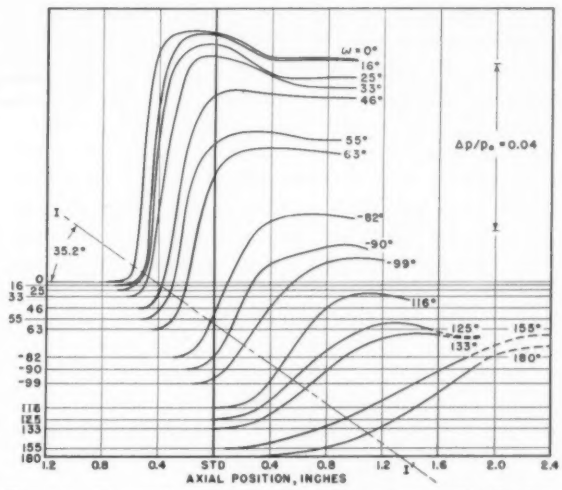

FIG. 4. Composite arrangement of pressure distribution. $\delta = 4.0°$.

required cancellation brings about the reflected shock wave. As the shock wave spreads toward the lee side after passing the $\omega = \pm 90°$ meridians, the shock-induced velocities have a component away from the body. Even if one knew the line along which the shock intersects the body on the lee side, it is not clear physically that these outward radial velocity components need be completely canceled and that the flow must continue to follow the surface, especially in the viscous case. The cancellation of the outward component or any part of it would have to be effected by an expansion wave originating along the intersection line. The expansion wave would tend to weaken the shock wave which generated it and form a "shadow" region (partly or completely shielded from the oncoming shock).

Shadowgraphs (Figs. 9b and 10), schlieren photographs (Figs. 8, 12a, and 14), and irreproducible pictures obtained by the vapor technique show that the

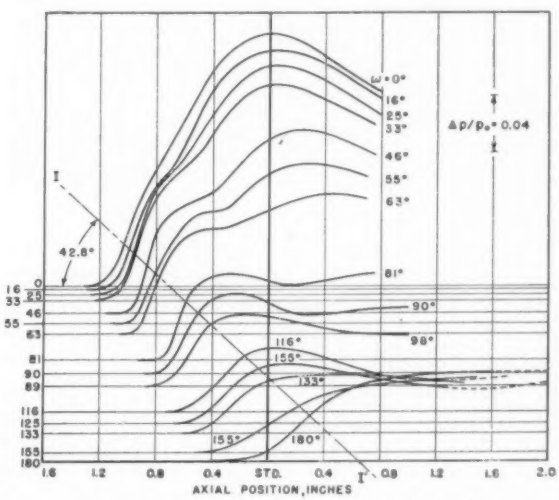

FIG. 5. Composite arrangement of pressure distribution. $\delta = 11.2°$.

incident shock is indeed broken up and does not reform in the $\omega = 180°$ plane for a distance of one to three diameters from the body. The regeneration of the shock on the lee side is undoubtedly connected with the thickening and accumulation of the boundary layer. In the laminar case the boundary layer can be clearly seen to curve away from the body at some distance upstream from the plane of the shock in Fig. 9b. Similarly, in the turbulent case, schlieren photographs (Figs. 8, 11a, 12a, and 13a) indicate that the outside flow in the vertical plane $\omega = 180°$ deflects away from the cylinder surface at an angle somewhat less than the deflection angle across the oncoming shock (but nearly proportional to it). The wedgelike space thus created is apparently occupied by slower moving air made up of the original boundary layer on the lee side and from air swept in from the bottom and sides of the cylinder by the previously mentioned cross flow of the boundary layer.

The separation on the lee side thus seems to be akin to that which may occur on bodies with sweepback.[20] Since the shock wave induces a crosswise component of flow, this similarity is not surprising. As a matter of fact, the flow resembles that over bodies of revolution at moderate angles of attack (except in the immediate vicinity of the shock wave), and there is some evidence of corresponding vortex formation discovered by Allen.[21] Fig. 13b exhibits a typical formation of boundary-layer flow lines on the lee side of the cylinder ($\delta = 14.3°$), and Fig. 15b shows a similar pattern on top of the square body ($\delta = 11.2°$). The flow lines neck in where the shock influence is felt first and then diverge from the $\omega = 180°$ meridian again. It is not clear whether the two regularly appearing flow lines, which seem to absorb others and become rather strong, mark the line of separation on the side of the body or not.

Once the lee-side separation appears it seems to persist, even when an expansion wave with the opposite pressure gradient affects it (Fig. 8). In general, an expansion wave falling upon the body produces practically no boundary-layer cross flow in the opposite direction. Since the local cross component of the pressure gradient in an expansion wave some distance from the expansion corner is a mere fraction of the corresponding conrponent due to a shock wave, this is readily understandable.

From the preceding observations it appears likely that there will be a tendency toward lee-side separation on bodies of revolution (and elongated convex bodies in general), even when the oblique shock is generated by a wedge abutting on the side of the body. Whether the strength of the boundary-layer cross flow is materially changed when the ratio of the body diameter to the boundary-layer thickness is increased as on full-scale prototypes remains to be seen. The design of winged models for tunnel investigation of those aspects of supersonic wing-body interference associated with the boundary-layer build-up and its effect in the region of tail surfaces is now in progress at the University of Michigan.

Pressure Field

Figs. 3a and 3b exemplify the effects of boundary-layer thickness on pressure distributions at $\omega = 0°$ and 90° meridional stations for a moderate shock strength ($\delta = 10.2°$). For the thicker boundary layer, the net pressure rise in Fig. 3a is smaller, but the shock is felt farther upstream. This latter behavior is in qualitative agreement with the concept of the subsonic sublayer (which also thickens) as avenue of upstream propagation. On the side of the body ($\omega = 90°$), the smooth and rough (r_2) boundary-layer conditions unexpectedly lead to different pressure levels (Fig. 3b); this effect is probably caused by the difference in the boundary-layer cross flow in the two cases. Since it is known that the pressure distributions at $\omega = 90°$ rise again farther downstream (Fig. 5), the pressure may ultimately reach the same level in the two cases.

The considerations concerning the pressures at $\omega = 90°$ have implications for pressure measurements by long-needle probes and static pitot tubes. It has been generally agreed that near shock waves the pressure orifices on the probes should be located at $\omega = 90°$ rather than $\omega = 0°$ or 180°. Reference 9 reports a strong influence of the nature of the probe boundary layer on the pressure measurements near shock waves and recommends (with caution) making the boundary layer turbulent. If the present larger scale results can be extended to the small probe scale, even these latter measurements are subject to a considerable degree of distortion. Fig. 14 exhibits the similarity between the shock-interaction patterns for a probe and the present model. In particular, the reflected wave at $\omega = 0°$ and the lee-side separation are indicated.

The pressure field around the cylinder at $\delta = 4.0°$ and 11.2°, together with the shock trace II', is represented in the spatial composite pressure distributions of Figs. 4 and 5. The reader can interpret most of the features of these distributions in terms of the concepts of the boundary-layer cross flow and the postreflection outer flow. The latter flow tends to relieve the overpressure on the incident side rather rapidly. As already discussed, details of these pressure distributions depend on the nature and thickness of the boundary layer and on shock strength. The maximal values of $\Delta p/p_0$ are shown irrespective of their longitudinal position, in Fig. 7, as a function of ω. For comparison, pressure jumps based on nonlinear nonviscous theory[12] are shown in Fig. 7 for $0 \leq \omega \leq \omega_A$ and for $\omega = 90°$ (point C). In the case of relatively strong shocks, as well as weak shocks, the maximum pressure jumps recorded fall short of the values predicted by the theory even at $\omega = 0°$. The pressure jump on the $\omega = 90°$ meridian is also much smaller than the single jump

across the oncoming shock wave (point C). This smallness of the wall pressure jumps can probably be ascribed to the effect of a relatively thick boundary layer that could accommodate sizable radial pressure gradients and to the three-dimensional relieving effect of the cross flow. The latter effect is probably responsible for shifting the smallest values of pressure jumps to the vicinity of $\omega = 120°$ meridian. Two aspects of the overall pressure variation deserve closer attention.

(1) The forward bump in the pressure distributions on the incident side of Fig. 5 is associated with the boundary-layer cross flow and has some characteristics of a dead-air bubble.* In Fig. 6, the static pressure variations at $\omega = 55°$ and $63°$ are matched with the surface total-head variations at $\omega = -50°$ and $-59°$. It would appear that at the location of the bump the component of flow velocity against the total-head probe opening has vanished so that the static and total pressure values are essentially the same. For the relatively thick boundary layer and relatively strong shock of $\delta = 11.2°$, the same behavior seems to take place over most of the incident side; for thinner boundary layers and weaker shocks, the static pressure bump and the total-head dip develop only for higher ω's on the incident side of the body. For instance, at $\delta = 10.2°$ with smooth turbulent boundary layer (Fig. 3a), the bump is absent and develops only somewhere between $\omega = 25°$ and $\omega = 55°$. For the smooth turbulent boundary layer at $\delta = 4.0°$ the effect is not discernible. It is interesting to note (Fig. 5) how this bump, associated with the boundary-layer cross flow, gradually becomes the main pressure peak as ω increases past 80°—i.e., while the lee side is partly shielded from the direct shock, a relatively forward pressure rise occurs there due to the boundary-layer cross flow.

(2) Comparison of pressure variations on the lee side shows that, irrespective of the boundary-layer

* See also next section.

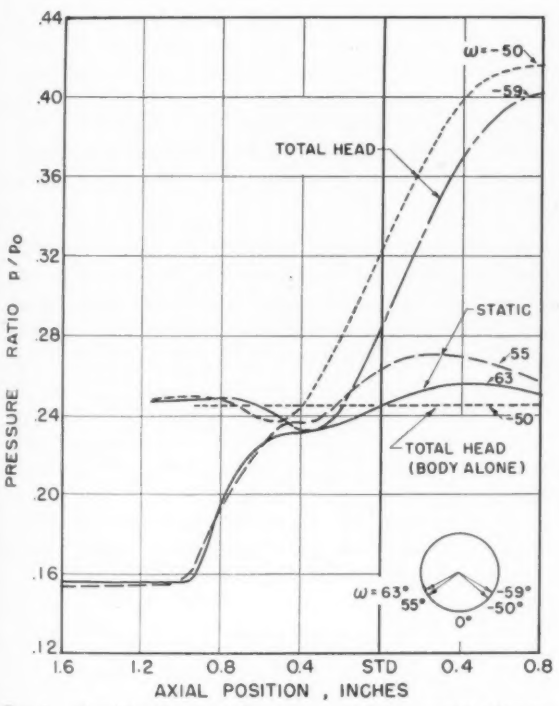

FIG. 6. Total head and static pressure variation on side of body.

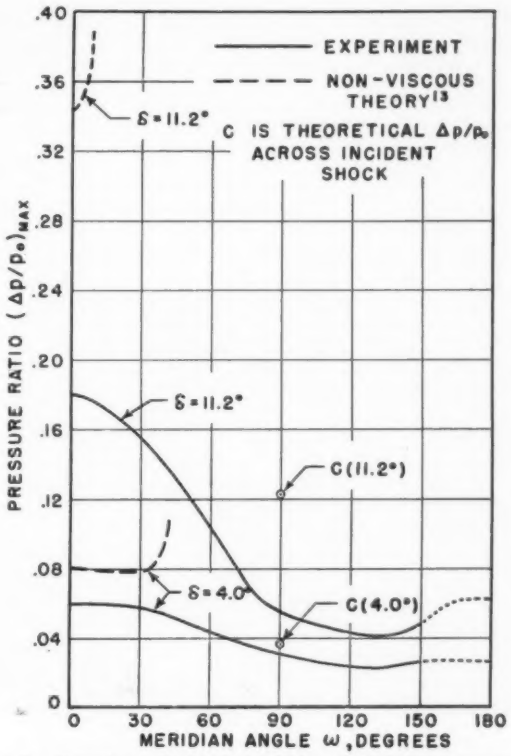

FIG. 7. Experimental and theoretical variation of pressure ratio $(\Delta p/p_0)_{max.}$ with meridian angle ω.

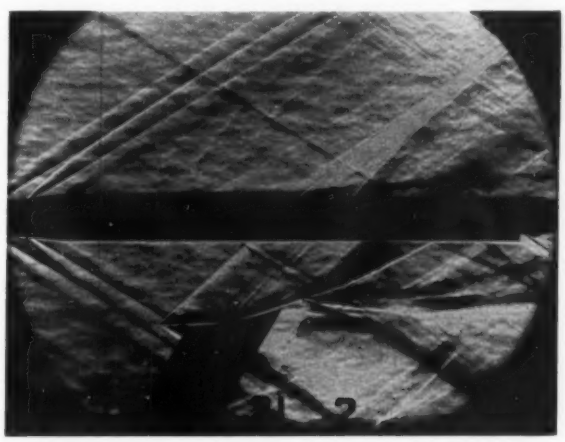

FIG. 8. Overall view of shock reflection pattern from circular body. Horizontal knife edge; $\delta = 10.2°$; rough (r_2) condition.

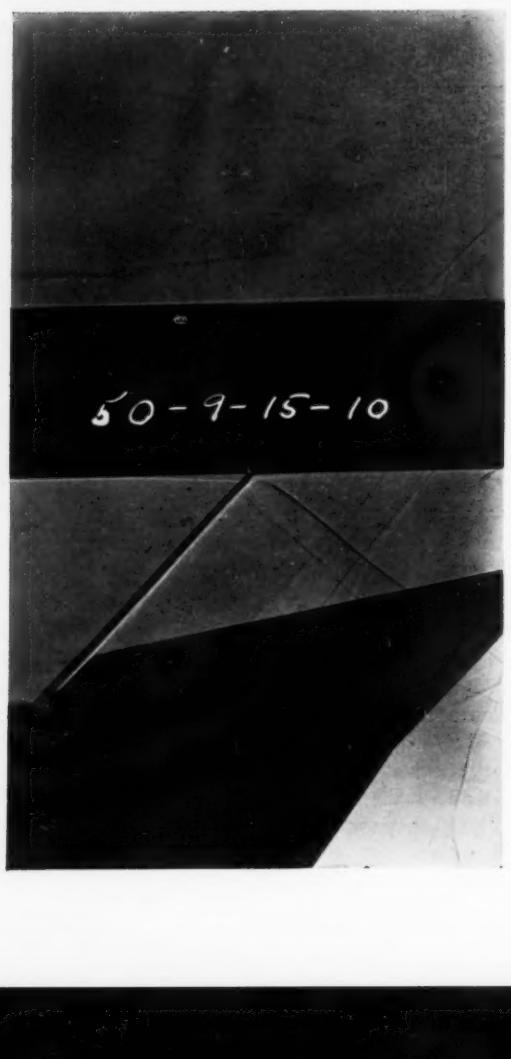

FIG. 9. Typical shock reflection pattern from circular body with laminar boundary layer viewed in $\omega = 25°$ plane; $\delta = 10.2°$. *Top* (a) Vertical knife-edge schlieren. *Bottom* (b) Shadowgraph.

thickness and shock strength, the pressure starts rising again slowly as one crosses the meridional planes toward $\omega = 180°$. This is consistent with the settling down of the flow to that around the cylinder at an angle of attack. This latter flow exhibits a similar adverse pressure gradient in both the potential and viscous case.[21]

Comparison with Theory and with Two-Dimensional Experiments

The optical data obtained in this investigation show that the anomalous effects predicted by the nonviscous theory[13] are masked by the boundary layer so far as can be observed at $\omega = 25°$ for the critical case $\delta = 10.2°$ (see Fig. 1), irrespective of the laminar or turbulent nature of the boundary layer. In the laminar case no evidence of a Mach Y type of reflection was obtained (Figs. 9a and 9b). This is not surprising inasmuch as the protuberance-type geometry of the laminar boundary layer in the neighborhood of the intersection changes the local requirements on the deflection angles which were the critical conditions for the existence of a regular reflection in the nonviscous theory. In the turbulent case there was also no significant difference in the basic shock reflection pattern between $\omega = 0°$ and $\omega = 25°$. It had been conjectured[13] that a Mach Y type of reflection might occur in the predicted region of anomalous reflection; however, for a given boundary layer, no Mach Y configuration could be ascribed to the change from $\omega = 0°$ to $\omega = 25°$ location.* As a matter of fact, for a given shock strength any observable Mach Y shocks appear to be related primarily to increase in thickness of the boundary layer. [There seems to be no clear-cut criteria for distinguishing between bifurcated regular reflections and Mach Y reflections from either schlieren photographs or wall pressure measurements probably because the transition is rather gradual (see Figs. 13c, 13d, 23, and 32 of reference 9)].

It is interesting to note that, while there is boundary-layer cross flow and therefore a modification of the effective boundary of the three-dimensional body at all shock strengths, the pressure bump associated with the cross flow does develop only at higher ω's on the incident side when the shocks are weaker. It is difficult to determine the demarcation line between the peak type (Fig. 3a) and the bump-plateau type of pressure distributions, especially since it is likely to depend on bound-

* The schlieren system could not be yawed more than 25° because of tunnel window buckets, and thus, unfortunately, no meridians beyond $\omega = 25°$ could be observed.

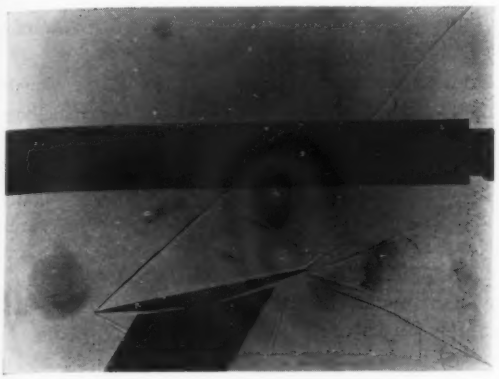

FIG. 10. Typical shadowgraph of shock reflection pattern from circular body.

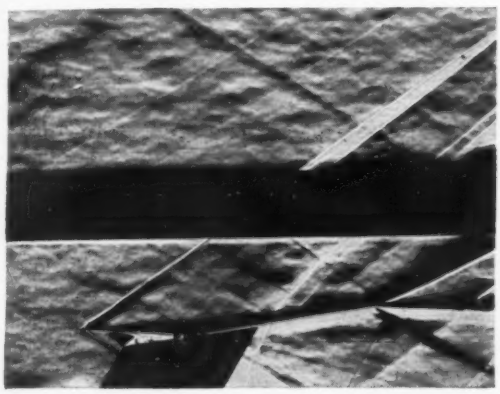

FIG. 11a. Typical shock reflection pattern from circular body with turbulent boundary layer; smooth condition; horizontal knife-edge schlieren; $\delta = 4.0°$.

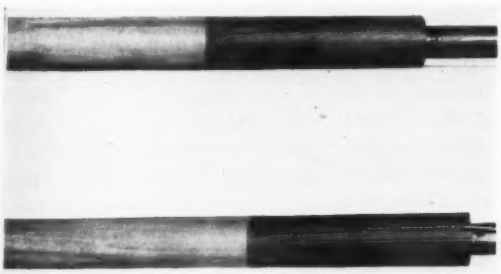

FIG. 11b. Surface stream-line patterns on circular body; $\delta = 4.0°$.

ary-layer thickness. From the present experiments it would appear to lie in the region of anomalous reflection[13] between the curves A and B of Fig. 1. Whether the development of the bump is actually associated with the impossibility of regular shock reflection (in presence of the boundary layer) on the side of the body or not will remain for speculation.

The reflection pattern of the shock wave ($\delta = 10.2°$) from the incident side of the body (both $\omega = 0°$ and $\omega = 25°$) in the case of the laminar boundary layer (Figs. 9a and 9b) is similar to that obtained for the two-dimensional case[8–10] as described in the "Introduction." However, in the present case, the edge of the boundary layer has a greater curvature corresponding to a stronger envelope-type reflected shock upstream of the impingement line. Whether the explanation is to be sought in the three-dimensionality of the configuration or in the greater shock strength is not clear.

In the case of the turbulent boundary layer, the reflection patterns obtained are in fair agreement with those of reference 11. For weak shocks (Fig. 11a) the reflected shock seems to be followed by a weak expansion wave and another faint compression wave. This behavior, as well as the sharpness in the corresponding pressure rise (Fig. 4, $\omega = 0°$), agrees also with the results of references 9 and 10. As shock strength is increased, the upstream influence (which also increases with boundary-layer thickness) grows and a configuration of an evelope-type shock, an expansion fan, and a second envelope-type compression results (Figs. 8, 12a, 13a, 14). In reference 11 (where the optical resolution was unimpaired by the finite width of the reflecting body) this configuration was associated with

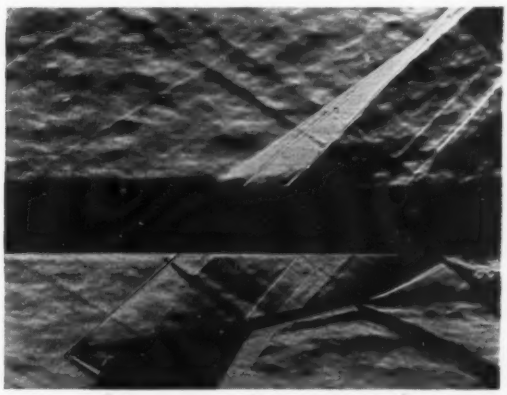

FIG. 12a. Typical shock reflection pattern from circular body with turbulent boundary layer; rough (r_1) condition; horizontal knife-edge schlieren; $\delta = 11.2°$.

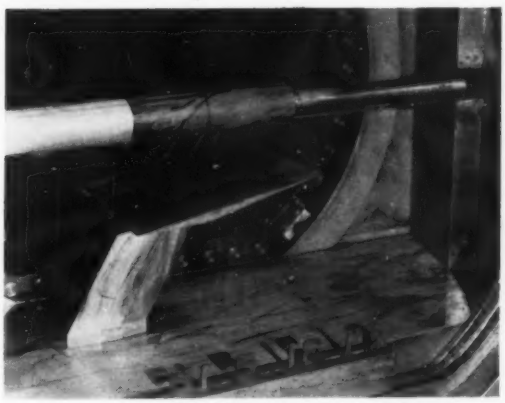

FIG. 12b. Surface stream-line patterns; $\delta = 11.2°$.

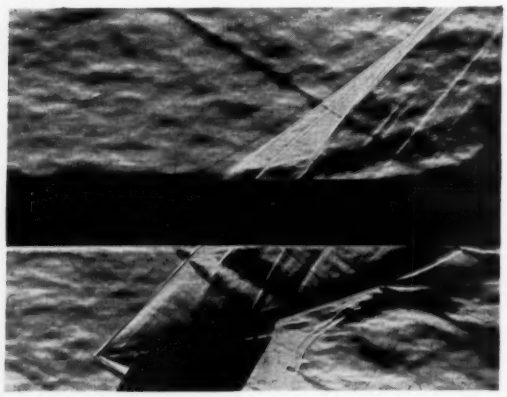

FIG. 13a. Typical shock reflection pattern from circular body with turbulent boundary layer; rough (r_1) condition; horizontal knife-edge schlieren; $\delta = 14.5°$.

FIG. 13b. Surface stream-line pattern on lee side of circular body; $\delta = 14.5°$.

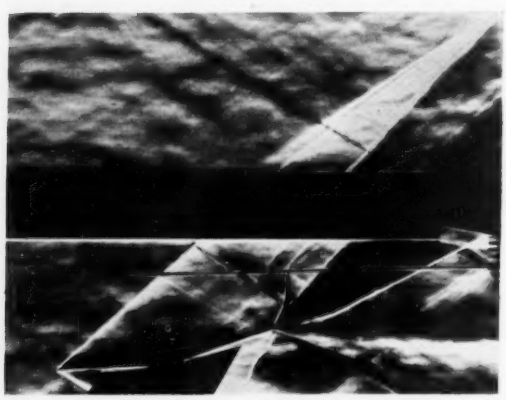

FIG. 14. Shock reflection patterns from circular body and probe; smooth condition; horizontal knife-edge schlieren; $\delta = 10.2°$.

local separation (bubble) of the turbulent boundary layer. In the case of the square body ($\delta = 11.2°$) this bubble can also be seen (Fig. 15a); the corresponding boundary-layer flow lines (irreproducible in print) corroborate its existence.

There is a suggestion of a turbulent boundary-layer bubble on the cylinder in most schlieren photographs with horizontal knife edge (Figs. 8, 12a, 13a, 14, etc.) for $\delta = 10°.2$. The evidence of the flow lines relative to the presence of a bubble at $\omega = 0°$ or $\omega = 25°$ on the cylinder is inconclusive at all δ's observed.

Shadowgraphs such as Fig. 10 indicate that the second reflected compressive wave is rather gradual. A similar conclusion can be reached from the second reflection of the reflected shocks from the rear of the wedge (Fig. 12b).

It must be remembered that three-dimensional effects, in particular, the cross flow that thins the boundary layer downstream from the point of incidence at $\omega = 0°$ may influence the comparison (including the two-shock configurations) with other investigations. The fact that a clear-cut bifurcation causing separation without reattachment[11] was not obtained at the strongest shocks ($\delta = 14.3°$) may be thereby explained. (On the other hand, bifurcated reflections in two-dimensional passages are strongly influenced by the downstream characteristics of the diffusion process and may be no more representative of the local shock-boundary-layer conditions.)

Applications to Wind-Tunnel Testing

In Fig. 11a one can discern several weak shocks (practically Mach lines) which appear to issue from the surface of the cylinder upstream of the shock incidence. Three pairs of these shocklets appear more or less distinctly in all the schlieren photographs in the same relative position with respect to the tunnel, irrespective of body axial position. [A fourth pair of Mach lines, which move with the body, is at times observable (Fig. 13a); these are caused by the occasionally loosened juncture between parts of the model.] The stationary Mach lines are connected with the very problem of reflection of (weak) plane shocks from a cylinder studied in this report. A simple, "ray-by-ray" construction of the reflected wave reveals that the reflected rays form a three-dimensional (nearly conical) surface; the shape of stronger reflected waves observed by the vapor technique and from their interception on wedge (Fig. 12b) confirms the construction. The three pairs of stationary Mach lines are really profiles of three-dimensional reflected Mach surface brought out by the schlieren light beam normal to the sidewalls. The plane incident waves and their reflections from the square body travel in vertical planes from sidewall to sidewall and cannot therefore be picked up directly by the schlieren system (Fig. 15a).

The fact that weak nonobservable sidewall disturbances can be located by their visible reflections from cylindrical surfaces can be used as an effective tool in tunnel calibration and tunnel-flow improvement. The actual waves whose reflections are observed in Fig. 8 are extremely weak; they have not been identified during the original calibration of the wind-tunnel. (Incidentally, as in most calibrations, much use was made of static pressure probing, which is subject to additional error near the weak waves, as previously discussed, and may mask the presence of the disturbances.)

The visualization technique used here to establish the cross-flow characteristics can be employed effectively for qualitative studies of most test configurations. As an example, it simultaneously gives typical

information about the flow around the tips of a finite wedge, the interaction of a 7° expansion wave with a circular cylinder, and tunnel blocking characteristics in Fig. 16. With the aid of corresponding schlieren photograph, one can conjecture that (1) the high pressure ($\delta = 16°$) from the lower surface affected the upper surface at angles from tips slightly higher than the free-stream Mach angle; (2) there was some flow separation at the squarely cut tips of the wedge (which raises the question of proper tip design at supersonic speeds); (3) the expansion wave produced an insignificant boundary-layer cross flow on the body as expected from the weak pressure gradients; (4) it was primarily the trailing-edge shock that (unexpectedly) caused separation on the body and contributed to tunnel blocking (in conjunction with similar separation on the floor and sidewalls), see vortex formation at aft stations of body and floor; (5) the juncture between the floor, covered by relatively thick boundary layer, and the swept-forward support strut exhibited undesirable characteristics (probably a λ shock on floor and a detached shock on wedge near the floor) judging by the boundary-layer outflow near wedge and the local vortex bubble at juncture of floor with sidewall.

The preceding example is intended to draw attention to the known but often neglected truism in wind-tunnel testing that qualitative techniques may lead to better understanding of the flow than quantitative force and pressure measurements and may save much time (and money) especially in exploratory investigations. The strong boundary-layer effects due to oblique pressure gradients demonstrated in this report (and the fact that the resolution of probes and pressure orifices is decreased because of the smaller scale of models and flow fields) suggest a more frequent coupling of visualization techniques with the standard pressure and force measurements in supersonic wind-tunnel testing.

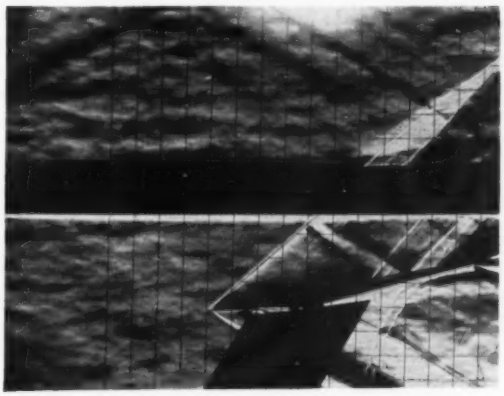

FIG. 15a. Shock reflection pattern from square body.

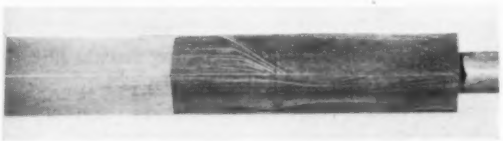

FIG. 15b. Surface stream lines on side and top of square body.

FIG. 16. Surface stream lines on body wedge and tunnel floor for interaction of expansion wave and circular body.

CONCLUDING REMARKS

From reference 13 and the present study it is clear that to the previously recognized basic parameters governing the reflection of shock waves from solid boundaries (boundary-layer character and thickness; shock strength and nature-step or impulse) should be added the factor of the geometry of the three-dimensional shock-body configuration. Three complicating factors arise for truly three-dimensional shock-wave reflections. First, in the cases considered, the extension of the nonviscous singularity type of theory leads to an impasse: either the nonviscous reflection is highly anomalous and even impossible in some regions of the reflecting body, or the body in some manner warps the oncoming plane shock wave toward the upstream direction. Second, a complicated post reflection flow occurs even in the nonviscous case, the initial values for which should come from the nonviscous singularity theory. In the two-dimensional case gratifying progress in understanding the reflection of shock waves from laminar boundary layer on a wall has been achieved by studying simplified models of the viscous flow which approach asymptotically the nonviscous solution. In the three-dimensional cases studied, even the nonviscous solution appears to be elusive, if it exists. Third, pressure gradients across stream lines due to the shock generate a boundary-layer cross flow that further modifies the effective boundary surface.

These three factors appear to give rise to a general interaction pattern (flow and pressure fields) between plane shocks and elongated bodies with widely different cross sections. Its main feature is a strong boundary-layer cross flow and accumulation (separation) on the lee side roughly proportional to the shock strength (yaw

velocity component) and a rapid relieving of pressures on the incident side. The flow field gives indications of settling down to an asymptotic flow at shorter downstream distances from the shock plane than expected from nonviscous considerations. In contrast with the two-dimensional case, this apparent asymptotic flow is intrinsically viscous, since the lee-side separation basically modifies the effective boundary of the body. Thus, even if a quantitative understanding of two-dimensional shock reflection were achieved, only a qualitative appreciation of the three-dimensional case based on experiments is likely.

Inasmuch as the boundary-layer cross flow generated by oblique shock waves is likely to be important in many practical applications, it may be worth while to conjecture on how the findings of this report are likely to be affected by size. Increasing the size of a body or wing will generally not alter the strength or inclination of the shock relative to the oncoming stream lines, but the boundary layer will thicken. In accordance with the present results (Fig. 3a), the thicker boundary layer should accommodate larger pressure gradients normal to the surface so that the pressure gradients across stream lines *near the wall* should be decreased. On the other hand, the actual mass of low-velocity fluid in the inner portion of the boundary layer which responds to the pressure gradient will be increased by the thickening of the boundary layer. It is therefore unlikely that the cross-flow effects will be less important on full-scale prototypes than on wind-tunnel models.

References

[1] Lees, L., *Interaction Between the Laminar Boundary Layer Over a Plane Surface and an Incident Oblique Shock Wave*, Princeton University, Aero. Engrg. Lab., Report No. 143, January, 1949.

[2] Tsien, H. S., and Finston, M., *Interaction Between Parallel Streams of Subsonic and Supersonic Velocities*, Journal of the Aeronautical Sciences, Vol. 16, No. 9, pp. 515–528, September, 1949.

[3] Robinson, A., *Wave Reflection Near a Wall*, Cranfield College of Aeronautics, Report No. 37, May, 1950.

[4] Lighthill, M. J., *Reflection at a Laminar Boundary Layer of Weak Steady Disturbance to a Supersonic Stream Neglecting Viscosity and Heat Conduction*, Quart. Jour. Mech. & Appl. Math. Vol. II, Pt. 3, pp. 303–325, September, 1950.

[5] Fage, A., and Sargent, R. F., *Shock Wave and Boundary Layer Phenomena Near a Flat Surface*, Proceedings Royal Society A., Vol. 190, 1947.

[6] Ashkenas, H., Dhawan, S., Liepmann, H. W., Marble, F., and Roshko, A., *Problems in Shock Reflection*, GALCIT Report to A.A.F., 1948.

[7] Shapiro, A. H., Neumann, E. P., and Barry, F. W., *Some Experiments on the Interaction of Shock Waves with Boundary Layers on a Flat Plate*, M.I.T. Gas Turbine Laboratory, Meteor Report No. 29, October, 1948; also, Jour. Appl. Mech., Vol. 17, No. 2, pp. 126–131, June, 1950.

[8] Liepmann, H. W., *Boundary-Layer Shock-Wave Interaction*, pp. 39–66, Symposium on Experimental Compressible Flow, U.S. Naval Ordnance Lab. Memorandum, No. 1133, June, 1949.

[9] Liepmann, H. W., Roshko, A., and Dhawan, S., *On the Reflection of Shock Waves from Boundary Layers*, GALCIT Report, 1950; N.A.C.A. T.N. No. 2334, April, 1951.

[10] Barry, F. W., Shapiro, A. H., and Neumann, E. P., *The Interaction of Shock Waves with Boundary Layers on a Flat Surface*, M.I.T. Gas Turbine Laboratory, Meteor Report No. 52, March, 1950; also Journal of the Aeronautical Sciences, Vol. 18, No. 4, pp. 229–238, April, 1951.

[11] Bardsley, O., and Mair, W. A., *The Interaction between an Oblique Shock-wave and a Turbulent Boundary-layer*, Phil. Mag., Ser. 7., Vol. 42, pp. 29–36, January, 1951.

[12] Courant, R., and Friedrichs, K. O., *Supersonic Flow and Shock Waves*, pp. 318–350; Interscience Publishers, New York, 1948.

[13] Migotsky, E., and Morkovin, M. V., *Three-Dimensional Shock-Wave Reflection*, University of Michigan Supersonic Wind Tunnel Memorandum No. 118, August, 1949; also, Journal of the Aeronautical Sciences, Vol. 18, No. 7, p. 484, July, 1951.

[14] Garby, L. C., and Nelson, W. C., *University of Michigan 8 × 13 inch Intermittent-flow Supersonic Wind Tunnel*, University of Michigan Memorandum No. 59, Engineering Research Institute, June, 1950.

[15] Culbertson, P., *Calibration Report on the University of Michigan Supersonic Wind Tunnel*, University of Michigan Memorandum No. 36, Engineering Research Institute.

[16] Morkovin, M. V., Migotsky, E., and Bailey, H. E., *On Three-Dimensional Shock-Wave Reflection*, University of Michigan Supersonic Wind Tunnel Memorandum No. 191, January, 1951.

[17] Migotsky, E., *On the Reflection of Shock Waves in Three Dimensions*, Ph.D. Thesis, University of Michigan, April, 1951.

[18] Murphy, J. S., and Phinney, R. E., *Visualization of Boundary-Layer Flow*, Readers' Forum, Journal of the Aeronautical Sciences, Vol. 18, No. 11, p. 771, November, 1951.

[19] Dailey, C. L., and Wood, F. C., *Computation Curves for Compressible Fluid Problems;* John Wiley & Sons, Inc., New York, 1949.

[20] Jones, R. T., *Effects of Sweepback on Boundary Layer and Separation*, N.A.C.A. T.N. No. 1402, July, 1947.

[21] Allen, H. J., *Pressure Distribution and Some Effects of Viscosity on Slender Inclined Bodies of Revolution*, N.A.C A. T.N. No. 2044, March, 1950.

Shock-Tube Studies of Transonic Flow over Wedge Profiles†

WAYLAND GRIFFITH‡
Princeton University

SUMMARY

Steady flow fields around two-dimensional wedges have been studied for Mach Numbers between 0.85 and 1.80 using the shock tube. It has been found that the location and shape of detached shock waves are independent of the wedge angle as long as the shock is not near to attachment.

The position of the sonic line and the pressure distribution over the wedge have been calculated from the density fields measured with a Mach-Zehnder interferometer. For a given wedge, identical pressure distributions are found over a considerable range of supersonic flows. These results suggest simple formulas giving the drag coefficient for each wedge angle which are expected to hold in most of the transonic speed range.

Experimental data on the drag of a thin wedge through the entire transonic range are available for the first time and are in excellent agreement with recent theoretical calculations based on transonic small-disturbance theory.

SYMBOLS

a	= velocity of sound
c	= wedge chord
C_d	= drag coefficient based on D and c
$C_d(t/2)$	= drag coefficient based on D and $t/2$
C_p	= pressure coefficient $= (p - p_1)/(1/2)\rho_1 V_1^2$
D	= pressure drag of half wedge
K	= transonic similarity parameter $= (1 - M)/[\delta(\gamma + 1)]^{2/3}$
L	= slant length of wedge
M	= Mach Number
p	= pressure
s	= detached shock distance measured from shoulder of wedge
t	= wedge thickness
u', v'	= perturbation velocities in x and y directions, respectively
V_1	= free-stream velocity
X	= fractional distance along incline of wedge from tip to shoulder
γ	= specific heat ratio
δ	= wedge half angle
ρ	= density

Superscript

$( )^*$	= critical condition, state where local flow velocity = local velocity of sound

Subscript

$( )_0$	= stagnation value
$( )_1$	= free-stream value
$( )_2$	= refers to region behind detached bow shock

(1) INTRODUCTION

THE PROBLEM OF determining flow patterns in the transonic range presents considerably greater difficulty than cases when the flow is purely subsonic or supersonic. From the theoretical standpoint special troubles arise first because the differential equations of flow are nonlinear and second because the regions of subsonic flow where the equations are elliptic are separated by an unknown boundary from supersonic regions having equations of hyperbolic type. Wind-tunnel data on flows near the speed of sound have so far been unobtainable because tunnel wall interference results in blocking of the flow.

This paper will describe a method by which the shock tube has been used as a sort of intermittent wind tunnel in which flow patterns over the entire transonic range are determined using a Mach-Zehnder interferometer. The results may then be compared with theoretical predictions and wind-tunnel measurements where these are available.

Two rather distinct methods of approaching problems involving mixed flows have been followed: one that deals primarily with the shape and location of detached shock waves in supersonic streams and the other that makes use of the extremely powerful transonic small disturbance theory[1] for treating flows in which the velocity is never far from the speed of sound.

Maccoll and Codd[2] and Drebinger[3] have carried out numerical solutions for the flow around two-dimensional wedges at particular Mach Numbers, while some experimental data on detached shocks have been obtained in a wind tunnel by Pack and Groth[4] and with the hydraulic analogy by Laitone.[5] Approximate methods for predicting the position of detached shocks have been developed by Laitone and Pardee[6] and Moeckel[7] and for axially symmetric flows by Dugundji[8] and Laitone.[9] Experiments on axially symmetric flows have been carried out by Ladenburg, van Voorhis, and Winkler[10] and Heberle, Wood, and Gooderum.[11] Lin and Rubinov[12] and Busemann[13] have discussed some general features of the problem.

The transonic similarity approximation gives an equation that is linear in the hodograph plane. From

Received September 14, 1951.

† This work was supported by an A.E.C. Postdoctoral Fellowship and O.N.R. contract. For suggesting this problem and providing many stimulating discussions, the author would like to give his special thanks to Prof. Walker Bleakney. Assistance in performing the experiments and analyzing data was given by D. K. Weimer, D. E. Brickl, H. H. Bingham, and others of the Princeton Shock Wave Laboratory.

‡ Assistant Professor of Physics, Palmer Physical Laboratory.

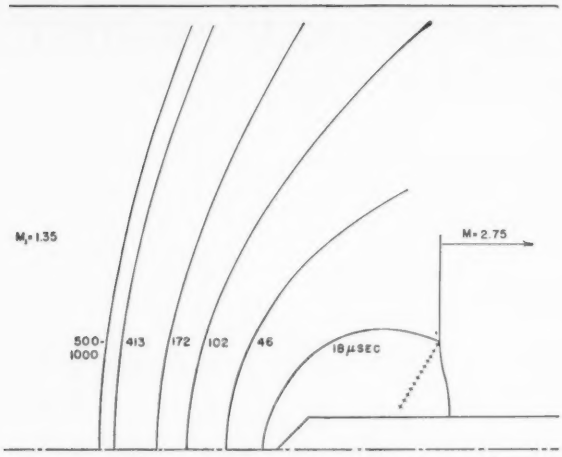

FIG. 1. The location of the shock reflected from a 90° wedge as a function of time after impact showing how a steady position is reached.

this, properties of flows near sonic velocity having theoretical interest are discussed by Guderley.[14] Tsien and Baron[15] have expanded the oblique shock and Prandtl-Meyer relations in terms of the similarity parameter to find lift and drag coefficients for flat plates and asymmetric wedge airfoils in pure supersonic flows. Vincenti and Wagoner,[16] Cole,[17] and Guderley and Yoshihara[18] have obtained solutions giving the pressure distribution over thin wedges. Recent wind-tunnel experiments of Liepmann and Bryson[19] have extended experimental data up to $M = 0.860$ and down to $M = 1.174$.

(2) Supersonic Flow in the Shock Tube

Since the theory and operation of the shock tube have been well described already,[20] we shall include only a few special considerations relevant to the range of strong shocks used in these experiments. The Princeton shock tube is 4 by 18 in. in cross section and 38 ft. long. The tube is divided into regions of high and low pressures by a partition that shatters quickly when it is punctured. A shock whose strength depends on the original pressure ratio then advances through the low-pressure region accelerating the air to a certain Mach Number. The region of air flowing along behind the shock moves at uniform velocity and has the special features that no boundary layers or turbulence exist at the start. Following this region of uniform flow comes the "cold front," the boundary originally occupied by the diaphragm that now separates the compressed gas from the gas originally in the high-pressure end which has expanded and cooled. To accelerate air to a Mach Number of 1, a shock wave having a pressure ratio of very nearly 5:1 must pass through it. To generate a shock of this strength, an initial pressure ratio of 50:1 is needed. If helium is substituted as the high-pressure gas, the higher velocity of sound in helium makes possible the more favorable ratio of 12:1.[21] Stronger shocks will produce flows of Mach Number up to 1.89. All of the wedges were $^1/_4$ in. thick except for the 15° wedge which was 0.080 in. thick. As a result of the small size of the models and low density used in these experiments the Reynolds Number is small, the order of 10^5.

The fact that steady supersonic flow can be observed in the shock tube is shown by results similar to those given in Fig. 1. When a shock wave strikes an obstacle, a reflected wave travels out into the stream telling the oncoming particles of the objects presence. This wave grows for a time (about 500 microsec. for a model $^1/_4$ in. thick) and then reaches a steady position. It has thus become the detached bow wave of the wedge in a supersonic stream. The steady flow is ended when any one of several things occur: (a) reflections from the tube walls return, (b) the incident shock comes back up from the end of the tube, (c) the rarefaction that started into the high-pressure gas when the diaphragm burst reaches the bow wave, or (d) the "cold" gas that was originally behind the diaphragm arrives. In the last case, a steady flow may again be set up before anything else happens, and no theoretical limit is placed on the Mach Number attainable. The highest in this tube to date is 3.7. A special advantage of studies made immediately behind the incident shock lies in the complete absence of a boundary layer prior to the passage of the shock. It is therefore possible to observe nonviscous aerodynamic effects at the start and then

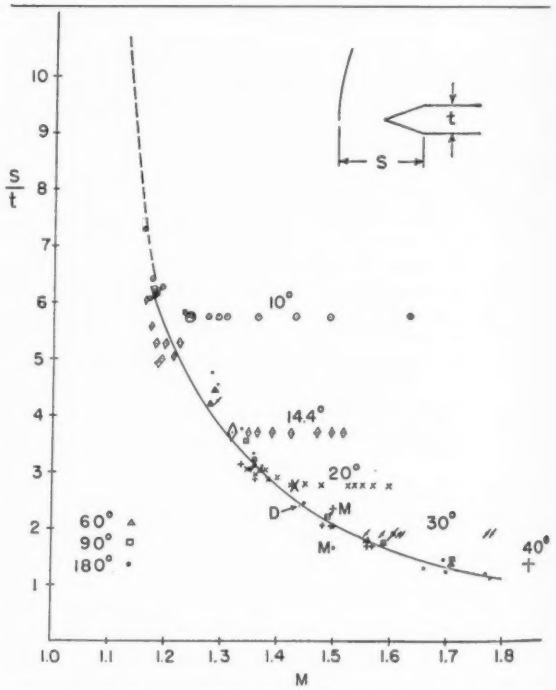

FIG. 2. Bow-wave distance as a function of Mach Number. The two calculated values of Maccoll are marked *M*, and Drebinger's result is marked *D*. The solid line is the experimental curve, and the dashed line is the assumed transonic approximation for the detachment Mach Number.

see what modifications take place as steady-state boundary layers are formed on the models.

All of the experiments reported in this paper were made in the "hot" gas behind the incident shock. With the existing arrangement alternatives (b) or (c) of the previous paragraph were always observed to spoil the flow. The reappearance of the incident shock reflected from the end of the tube was clearly visible, the catchup of the rarefaction being somewhat obscure. No mechanism like the Mach reflection for shocks acts to straighten up a rarefaction wave, so it usually arrived with a considerable slant and changed the flow pattern unsymmetrically. In another investigation, Weimer[22] has shown that the "cold front" has a thickness about twice the tube width, or 8 in., and is clearly observable. The only remaining means whereby the flow could be disturbed without detection is from top and bottom wall interference. Pictures taken with an artificial wall placed near the model show that this too would be unmistakable, so the region of possible steady flow is reasonably clearly known.

(3) Detached Shocks

First, a set of experiments were made to determine the location and shape of detached bow waves on wedges of 10°, 15°, 20°, 30°, 40°, 60°, 90°, and 180° total angle. The bow-wave distance from the shoulder of the wedge, measured in terms of wedge thickness, is plotted as a function of Mach Number in Fig. 2. As has been suggested by several workers,[6, 7, 11] the bow-wave position is practically independent of the wedge angle as long as the bow wave is not near to attachment. Under these conditions the approximate method for predicting bow-wave locations[7] is in fair agreement with experiment. Data from the Michigan shock tube taken by Geiger and Mautz[23] are found to be taken mainly at times before equilibrium is established. With increasing Mach Number, bow waves for blunter wedges successively leave the family and reach a constant distance when attachment occurs. These points are indicated on the graph. As the flow Mach Number approaches 1, the time required for the reflected wave to move out to an equilibrium position increases rapidly so that no data were obtained in this investigation on bow-wave positions for $M < 1.16$. In a later section a method will be described whereby this difficulty is sidestepped. In view of the fact that the experimental curve passes nearly through the detachment points it seems reasonable to assume tentatively that the locus of attachment points gives a good approximation to the bow-wave distance curve in the interval $1 < M < 1.2$. From transonic similarity, the formula for this is

$$s/t = 1.558/(M^2 - 1)^{3/2} \qquad (1)$$

Bow-wave shapes for Mach Numbers near 1.37 are shown for various wedges in Fig. 3. Those for wedge angles above 40° are the same within the accuracy of observation, the 20° case is seen to have a different shape even though the foremost point is the same, and and the bow shock is attached and straight for a 14.4° diamond. According to the shock polar theory, there is a narrow range of Mach Numbers in which a shock is attached but the flow behind it subsonic. A few preliminary experiments bear out Guderley's conclusion that the shock is curved under these conditions.[14] A detailed survey of the attachment process was not made because viscous forces near the surface introduce additional unknown effects, but some conclusions may be drawn with the information available. For a Mach Number well below that at which the bow wave will become attached to a wedge, the shape matches the "standard" shape, Fig. 4. As the Mach Number increases, the shock curvature increases, but its center position still follows the standard formula. When the shock just attaches, it is curved, and the subsonic field between it and the shoulder is nonuniform. According to theory, the Mach Number range for transition from a detached shock to an attached shock with uniform supersonic flow along the incline is only about 0.01, but experiments indicate that the interval of nonuniform flow is much greater than this because of the boundary layer. Hence, the decrease in drag upon shock attachment in a real flow is probably not nearly so abrupt as potential flow theory predicts.

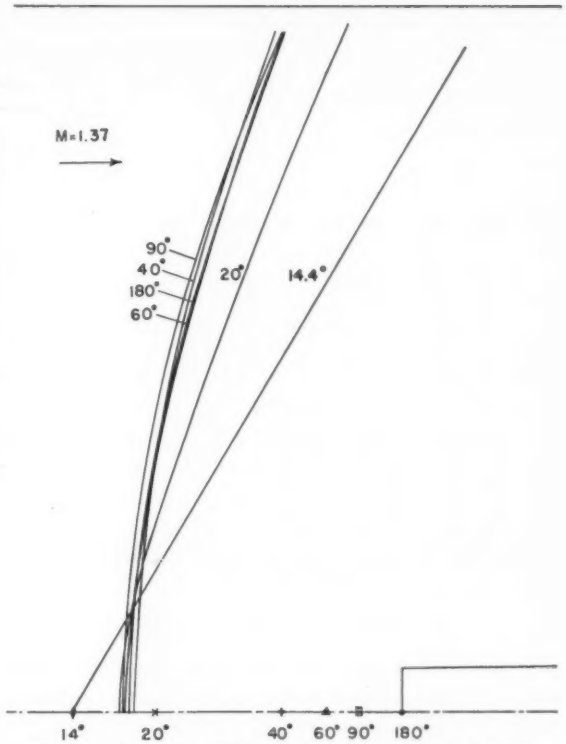

Fig. 3. The bow shocks for various wedges at Mach Numbers near 1.37. When the shock is far from attachment the wave assumes a "standard" form. The symbols on the horizontal axis locate the tips of the various wedges according to the notation in Fig. 2.

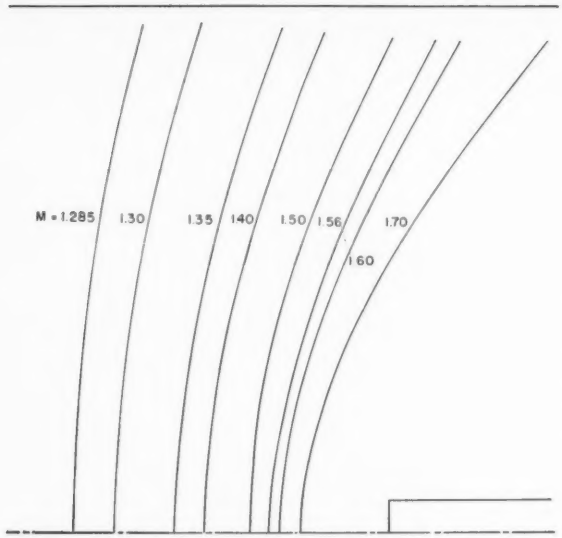

FIG. 4. The "standard" shape of detached shocks for various Mach Numbers.

(4) METHODS OF MEASUREMENT

In previous studies with the shock tube, two methods have been available for computing the incident shock strength: measurement of its velocity and observation of the density change across it with the interferometer. For shocks weaker than 6:1, these differ by less than 1 per cent, and it has always been assumed that the flow Mach Number may be found from the computed density ratio. In the supersonic range, wave angles for attached shocks may be measured after steady flow has been established. Mach Numbers computed from these values are larger than those determined from measurement of the incident shock velocity, while the fringe shifts observed across steady-state bow waves lead to agreement with the wave angle measurements. A number of special experiments were conducted to determine wave angles and shock attachment points for wedges of 10°, 14.4°, 20°, and 30° (M = 1.24, 1.32, 1.43, and 1.60, respectively). When the Mach Number so computed was plotted against the Mach Number determined from the shock velocity, a straight line made a satisfactory fit, extrapolating to no correction of the velocity Mach Number at M = 1.07 and a correction of +10.5 per cent at M = 1.6, the upper limit in these experiments.

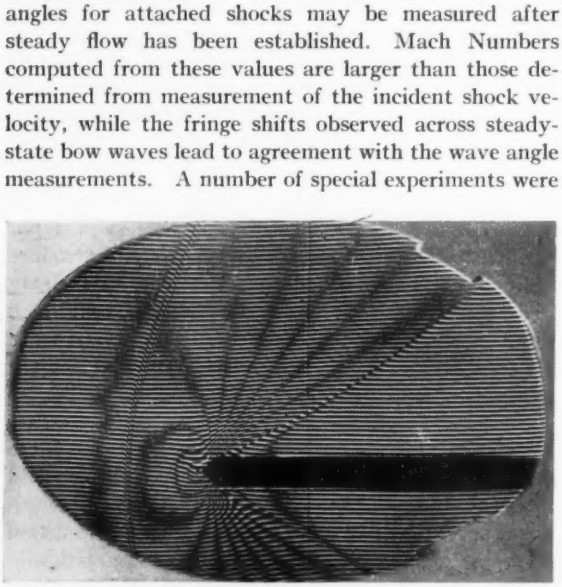

FIG. 5. Superposition of the undisturbed fringe pattern and a steady flow picture reveal the lines of constant fringe shift and therefore lines of constant density as distinct gray bands. Since the fringes are exactly matched ahead of the bow wave, the lines observed represent half-integral fringe shifts. The upstream influence of the shock-boundary-layer interaction on the observation windows is clearly visible.

No tests have been devised as yet to enable one to choose between various conceivable explanations for this shift in flow Mach Number, but careful consideration points to the most likely cause as a change in specific heat ratio γ at the high temperatures produced by these strong shocks or the effective narrowing of the channel due to wall friction.

The theory of the Mach-Zehnder interferometer relates a density change $\rho_2 - \rho_1$ in two-dimensional flow to the fringe shift n_{12} by a proportionality constant that may be evaluated for any particular experimental arrangement.

When an interferometer is adjusted to have equal optical paths everywhere, a uniform field is observed. If a disturbance is introduced, any fringes that appear will then be lines of constant density, but one will be unable to determine the order of a fringe and cannot compute the corresponding densities. For quantitative work, it is therefore necessary to observe the shift of finely spaced fringes. When a "blank" (the undisturbed fringe pattern) is superimposed on that showing the fringes in a disturbed condition, those regions where fringes are just 180° out of phase become readily visible as gray strips, and these are lines of constant density (see Fig. 5). By moving the blank normal to its fringes, the density contours may be followed over the entire field. The surprising feature of this method is the clarity of the gray region, its width appearing to be only about one-tenth of that between successive fringe crossings. Thus under good conditions, lines of constant shift may be located with an accuracy of about $\pm 1/20$ fringe. This method is, in general, as precise as that using direct measurement but becomes less satisfactory in regions where fringes on the blank and the picture are nearly parallel or have widely different spacing. Numbers can be attached to the curves by taking some undisturbed region as the zero condition or by making absolute measurements of fringe location from marking pins placed in the field of view.

When discontinuities in density are present, as is the case with shock waves, two special techniques are available: setting the light source off axis and using the white light fringes. With the first method, the effect of the discontinuity is distributed over adjacent rays so that one can follow individual fringes across it. If white light is used and the interferometer is in good adjustment, only about three fringes will be clear, because different wave lengths quickly get out of step. The central fringe is easily located throughout the field and

its fringe shift computed in terms of the original fringe spacing.

(5) The Sonic Line

The subsonic region immersed in supersonic flow is bounded on the rear by the sonic line, so the location of this line is of considerable theoretical interest. Since the density field is known, it is only necessary to compute the density ratio appropriate to sonic velocity. This will vary for each stream line, depending on the inclination of the shock wave. Two points may be found immediately. The air near the body has gone through a normal shock so its state is known exactly, and the point where the sonic line reaches the wedge may be computed. Also the point where the sonic line meets the shock is easily found. Since the density ratios for these points differ only slightly, the entire curve may be filled in fairly accurately. Representative examples are shown in Figs. 6–9. In cases where bow waves are the same, sonic lines are the same.

Theoretical considerations regarding the intersection of the sonic line with the wedge due largely to Busemann[13] and Guderley[14] may be outlined as follows. In a supersonic region bordering subsonic flow downstream characteristics approaching the sonic line are shown to represent rarefactions, while the other family of characteristics represent compression waves reflected from the sonic line. If these are to be reflected from a boundary as expansion waves, again so that the flow remains smooth—i.e., without shocks—the boundary must be convex. A supersonic region embedded in subsonic potential flow therefore has to be adjacent to a solid body, since there is no other way a suitable boundary can exist. A second important conclusion may be reached from an extension of the incompressible potential flow theory result that the velocity at a convex corner must be infinite. In compressible flow then, the velocity at a convex corner will certainly become supersonic.

These two results—i.e., that flow over a convex corner has to be supersonic and that the entrance to a supersonic region must be adjacent to a convex body—lead to the conclusion that the sonic line must be attached

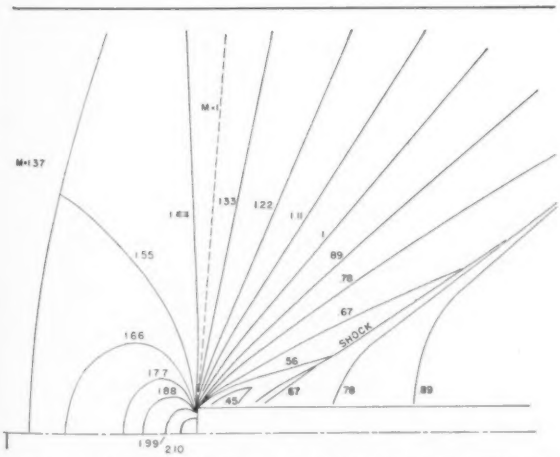

Fig. 6. Density field for wedge of 180° angle in supersonic flow. In Figs. 6–9, the fact that the sonic line reaches the body slightly ahead of the shoulder may be ascribed to the boundary layer.

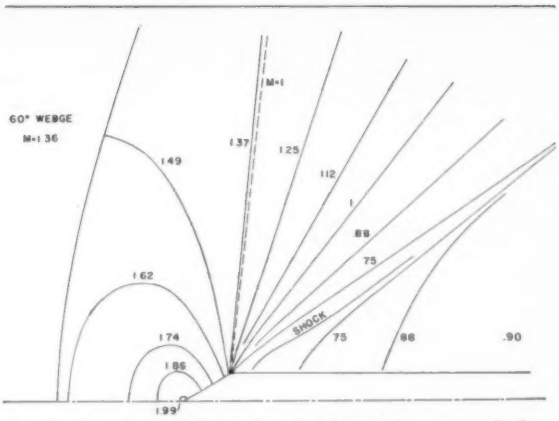

Fig. 7. Density field for wedge of 60° angle in supersonic flow.

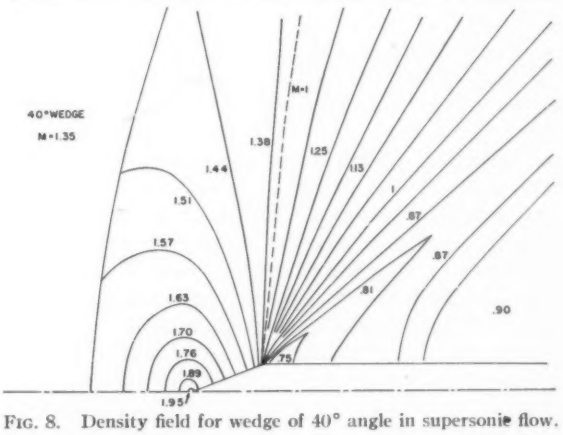

Fig. 8. Density field for wedge of 40° angle in supersonic flow.

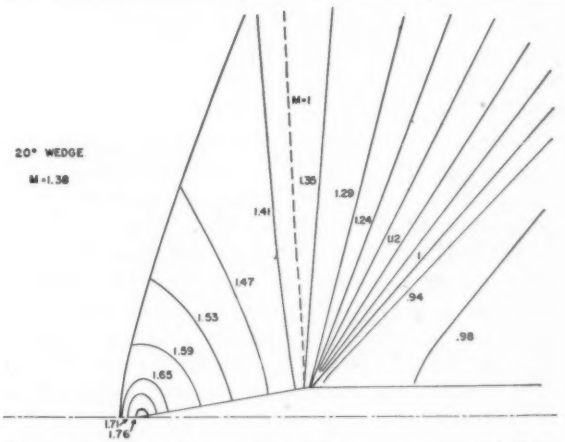

Fig. 9. Density field for wedge of 20° angle in supersonic flow.

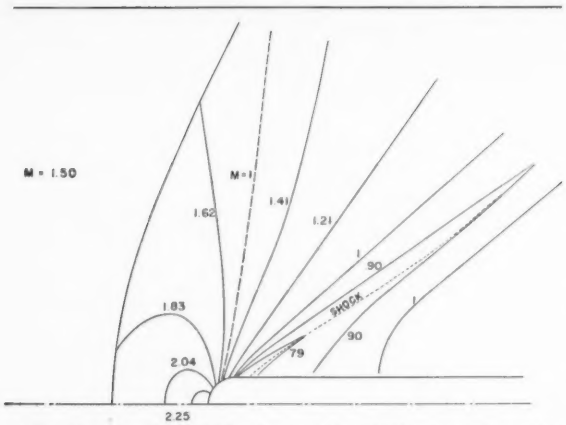

FIG. 10. Density field for flow at $M = 1.50$ past a plate with a half-circular nose. The sonic line meets the surface 59.5° around from the front of the body.

to the shoulder of the wedge. Furthermore, it will be perpendicular to the incline, since the case of a sharp corner will just correspond to a Prandtl-Meyer expansion in a limited region. The figures show that in a real flow these considerations are slightly modified by viscous effects near the surface for the sonic line actually approaches the wedge a little ahead of the shoulder. It is important to note that the sonic line is not necessarily normal to stream lines everywhere. Considering each stream tube as a case of one-dimensional flow, sonic velocity will clearly be reached at the minimum cross section, but there is no requirement that these be adjacent.

When there is no sharp corner, the location of the sonic line is considerably harder to predict theoretically but may be computed from experimental results in the manner already described. For a body whose nose is a half-cylinder, the location of the sonic point will probably depend on M. For $M = 1.50$, it is located 59.5° around from the front as shown in Fig. 10.

Maccoll and Codd[2] have computed numerically the density field for flow at $M = 0.7$ and 1.5 past a 40° wedge and at $M = 1.5$ for a square-ended body. Vorticity produced by the shock is shown to have little influence and so is neglected. What appears to be a more serious assumption is that the sonic line is perpendicular to stream lines everywhere. The subsonic region predicted is considerably smaller than observed in experiment but it will be seen in the next section how this has little effect on the accuracy of computed pressures on the wedge.

A more accurate numerical solution, in the sense that no restriction was placed on the angle between the sonic line and stream lines, was worked out by Drebinger[3] for a finite incline of 1:2 (53.2° wedge) at $M = 1.44$. The resulting shock and sonic line are compared with experiment in Fig. 11. Except for the vicinity of the shoulder already discussed and the fact that the bow wave is slightly farther out in the computed case, the two results are taken to be in agreement within the experimental uncertainty.

(6) Pressure Distribution

Pressure distributions on the front surface of the wedges have been computed and are shown in Fig. 12 for the examples presented in Fig. 3. Here the ratio of the pressure to free-stream pressure p/p_1 is plotted as a function of the fractional distance X from the tip to the shoulder. Since there is always zero velocity at the tip and (nearly) sonic velocity at the shoulder with a detached shock, the end points are the same for the same Mach Number. When the bow wave is attached, as for the 14.4° diamond at $M = 1.39$, the high stagnation pressure is not attained at the tip, and the pressure drag is much reduced.

A comparison of the pressure distributions on the same wedge at different Mach Numbers may be made by plotting $p/p,^*$ where p^* is the pressure corresponding to sonic velocity. According to theory p is equal to p^* at the shoulder and $[(1/2)\ (\gamma + 1)]^{\gamma/(\gamma-1)}p^* = 1.8929p^*$ at the tip. In Fig. 13, data for the 60° and 180° wedges at several Mach Numbers have been plotted in this way. The points lie along the same curve within the accuracy of the measurements. The

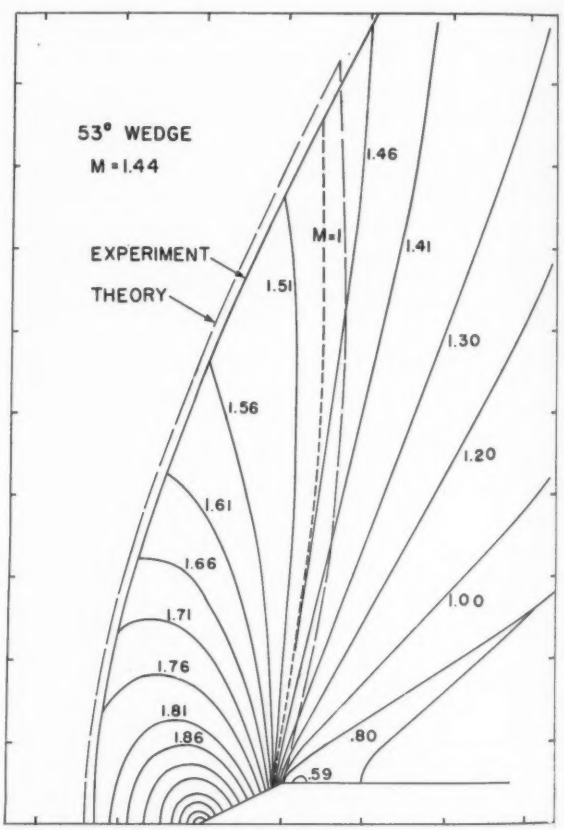

FIG. 11. Comparison of experimental and theoretical shock and sonic line locations for flow at $M = 1.44$ past a 53.2° wedge. The dashed curves are Drebinger's calculated result.

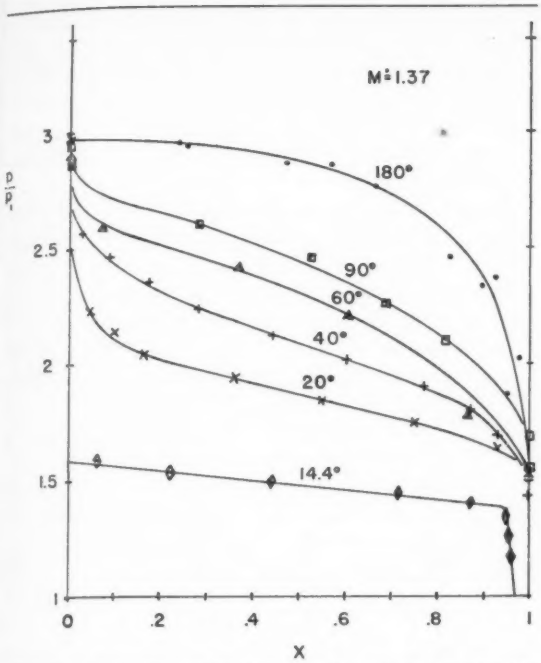

FIG. 12. Pressure distribution from the tip to the shoulder in terms of free-stream pressure for several wedges at Mach Numbers near 1.37 and a 14.4° diamond at $M = 1.39$. The shock is attached to the diamond.

possibility of this was first suggested by Maccoll and Codd, who found that the pressure distribution curve for a 40° wedge had the same shape at $M = 0.7$ and 1.5. Their result for a 180° wedge is indistinguishable from the experimental curve shown in Fig. 13, as is the case with the 40° wedge on a curve not shown. Since the pressure at the tip and shoulder are independent of the computed shock position, it is reasonable that the computed pressure distribution along the incline is relatively insensitive to variations in shock position as long as the shock is at least far enough away to have the standard shape.

Using this result, a drag coefficient for the transonic range may be found as follows:

$$p/p_1 = (p/p^*)\ (p^*/p_{20})\ (p_{20}/p_1) = [2/(\gamma + 1)]^{\gamma/(\gamma-1)}(p/p^*)\ (p_{20}/p_1)$$

The last term is the familiar Rayleigh pressure ratio, which is a function of Mach Number only. The pressure coefficient

$$C_p = (p - p_1)/(1/2)\rho_1 V_1^2 = 2(p/p_1 - 1)/\gamma M_1^2 \quad (2)$$

thus becomes

$$C_p = \frac{2}{\gamma M_1^2}\left[\left(\frac{2}{\gamma + 1}\right)^{\gamma/(\gamma-1)} \frac{p}{p^*}\frac{p_{20}}{p_1} - 1\right] \quad (3)$$

The drag coefficient based on wedge chord as used by Cole, Liepmann, and Vincenti is defined as

$$C_d = D/(1/2)\rho_1 V_1^2 c \quad (4)$$

D is the pressure drag of the half wedge per unit width. In order to obtain a meaningful value for the flat-nosed model (180° wedge) and to facilitate comparison with Maccoll's computed results, a drag coefficient based on the half thickness is defined as

$$C_d(t/2) = D/(1/2)\rho_1 V_1^2(t/2) = \int_0^1 C_p\, dX \quad (5)$$

where X is the fractional distance along the incline from the tip to the shoulder.

For the 60° wedge this gives

$$C_d(t/2) = 1.429(0.773 p_{20}/p_1 - 1)/M_1^2 \quad (6)$$

and for the 180° wedge

$$C_d(t/2) = 1.429(0.917 p_{20}/p_1 - 1)/M_1^2 \quad (7)$$

This is in close agreement with Maccoll's result,

$$C_d(t/2) = 1.429(0.9277 p_{20}/p_1 - 1)/M_1^2$$

From what has been said these formulas should yield the front pressure drag for Mach Numbers in the interval from about 0.7 to at least 1.7.

(7) TRANSONIC SMALL-DISTURBANCE THEORY

The transonic similarity theory is the counterpart of subsonic approximations leading to the Prandtl-Glauert formulas and Ackeret's rule in supersonic flow. Here perturbations from the critical velocity a^* are assumed to be small compared to a^*, so that the x and y velocity components are

$$u = a^* + u', \quad v = v', \quad u', v' << a^* \quad (8)$$

If irrotational flow is assumed so that a potential function Φ may be introduced for the perturbation velocities the equations of gas dynamics reduce to

$$\frac{\partial^2\Phi}{\partial y^2} = \frac{\gamma + 1}{a^*}\frac{\partial\Phi}{\partial x}\frac{\partial^2\Phi}{\partial x^2} + \frac{2}{a^*}\frac{\partial\Phi}{\partial y}\frac{\partial^2\Phi}{\partial x \partial y} \quad (9)$$

By means of an affine transformation, the appropriate similarity parameter is found to be

$$K = (1 - M)/[\delta(\gamma + 1)]^{2/3} \doteq (1 - M^2)/2[\delta(\gamma + 1)]^{2/3} \quad (10)$$

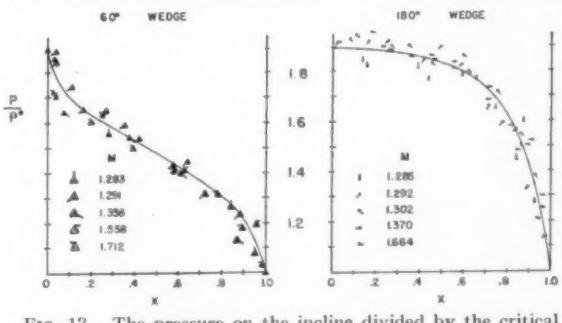

FIG. 13. The pressure on the incline divided by the critical pressure p^* for the 60° and 180° wedges at several Mach Numbers showing that the distribution is independent of Mach Number.

where δ is the wedge half angle. Each solution of the equation therefore provides an infinite number of patterns for similar bodies at appropriate Mach Numbers.

In the hodograph plane, a linear equation is obtained known as the Tricomi equation,

$$\left.\begin{aligned}(\partial^2 y/\partial u_1^2) - u_1(\partial^2 y/\partial u_1^2) = 0 \\ u_1 = (\gamma+1)u'/a^*, \quad v_1 = (\gamma+1)v'/a^*\end{aligned}\right\} \quad (11)$$

It is an equation of this general form for which several solutions have been obtained. Guderley and Yoshihara[18] have computed the flow over a wedge-shaped profile in a free stream at a Mach Number of 1 and obtain for the drag coefficient

$$C_D^* = 1.75\delta^{5/3}/(\gamma+1)^{1/3} \quad (12)$$

which for a 15° wedge in air gives $C_D^* = 0.0441$. Cole[17] uses a doublet to represent the singularity in the hodograph plane corresponding to the flow at infinity and gets a series representation of the drag coefficient for $M \leq 1$. At $M = 1$,

$$C_D^* = 1.67\delta^{5/3}/(\gamma+1)^{1/3} \quad (13)$$

in good agreement with Guderley and Yoshihara. The slope of the drag curve at $M = 1$ is found to be $4\delta/(\gamma+1)$. This has special theoretical significance, which will be discussed later.

Vincenti and Wagoner[16] solved the Tricomi equation by numerical relaxation methods for four values of the similarity parameter chosen to fill in as well as possible the region between $M = 1$ and the pure supersonic régime. In terms of K defined by Eq. (10) the values used were -0.242, -0.352, -0.460, and -0.529. A discussion of the proper way to apply results of this small disturbance theory to real airfoils for Mach Numbers not equal to 1 is included in the next section.

(8) Experimental Results for a 15° Wedge and Comparison with Theory

The 15° wedge used for experiments in the sonic range was made much smaller ($t = 0.080$ in.) than previous shock-tube models in order to increase the relative flow duration and cut down the influence of top and bottom walls of the tube. The incline was followed by a 0.6-in. straight section and was held from the back by a sting extending to the end plate on the shock tube. The model was mounted nearer the top of the tube than the bottom so that any wall interference would cause an unsymmetric flow. No such effect was observed.

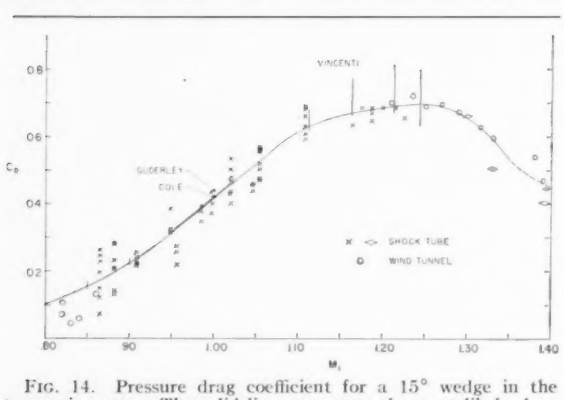

Fig. 14. Pressure drag coefficient for a 15° wedge in the transonic range. The solid line represents the most likely drag curve in terms of experiment and theory.

The fact was mentioned earlier that for Mach Numbers close to 1 sufficient time is not available for the reflected bow wave to reach an equilibrium position. Obviously, in subsonic flow it would never do so but would continue back up the tube indefinitely and become vanishingly weak. As it turns out experimentally, this makes no difference to the establishment of a steady pressure distribution on the wedge for after about 350μ sec. equilibrium is observed, which lasts for 1,600μ sec., until the original shock returns from the end of the tube. The advancing bow wave becomes nearly normal and just replaces the compression extending to infinity by a sudden jump in pressure. Thus it is possible to obtain steady flow patterns in the neighborhood of a model even though conditions are not steady everywhere in the tube.

The drag coefficients on a 15° wedge computed from experiments over the range of times just mentioned for $0.86 < M < 1.11$ are plotted in Fig. 14. Results from measurement of the flow past the 15° wedge and a 14.4° diamond of 3-in. chord with steady bow waves for $1.15 < M < 1.40$ are also plotted. The circles are wind-tunnel data of Liepmann and Bryson.[19]

Within the approximations used in transonic theory, the pressure coefficient may be written alternatively as

$$C_p \equiv (p - p_1)/(1/2)\rho_1 V_1^2 \doteq -2u'/a^* \doteq -2u'/V_1 \doteq 2(M_1^2 - m^2)/(\gamma+1) \quad (14)$$

where m is the local Mach Number. If one uses the last form and applies the conclusions of Section (6) that the local Mach Number distribution is constant in flows near $M = 1$, then necessarily $(\partial m/\partial M_1)_{M_1=1} = 0$ and the slope of the drag curve at $M = 1$ is

$$dC_D/dM_1 = 4\delta/(\gamma+1) \quad (15)$$

This was pointed out by Liepmann and is identical with Cole's theory. From Fig. 14 this is seen to be in excellent agreement with experiment. Fig. 15 shows experimental pressure distributions for Mach Numbers near 1. The vertical marks denote points where $M = 1$ and 0.815 (the Mach Number at mid-chord according to Guderley's calculation).

Vincenti and Liepmann discuss thoroughly the difficulties that arise in applying small perturbation theory to real flows. As they point out, there is no theoretical means of choosing among the various forms for C_p in Eq. (14), since they are all equivalent in the approximation used. Similar uncertainties exist in the value of the Mach Number which should be associated with each value of K for a given wedge. Accordingly, two numbers are computed for C_d corresponding to the

second and third forms for C_p in Eq. (14), and the Mach number is found from the first expression for K in Eq. (10). The results are plotted in Fig. 14. Clearly, the higher values in subsonic flow and the lower ones in supersonic flow correspond to taking $-2u'/V_1$. The experimental data enable us to choose this form as the more reliable one to use.

(9) Conclusion

The flow around wedges in the transonic range has been studied experimentally using a shock tube and Mach-Zehnder interferometer. Detached shocks for wedges of 10°, 15°, 20°, 30°, 40°, 60°, 90°, and 180° total included angle have been observed for $1.16 < M < 1.80$. The shape and location of detached shocks, which are measured appropriately in terms of distances from the shoulder where the sonic line reaches the wedge, are found to be a function of Mach Number only and independent of the wedge angle as long as the shock is not near to attachment. The numerical solution for a 53.2° wedge at $M = 1.44$ obtained by Drebinger is in good agreement with experiment, while the shock and sonic line predicted for a 40° wedge by Maccoll and Codd are somewhat in error, presumably because their assumption that the sonic line crosses stream lines normally everywhere is too severe. A measurement of experimental pressure distributions over the wedge incline shows that Maccoll's values at the surface are correct, however, and that identical distributions exist for a considerable range of supersonic flows. This result and Maccoll's observation that the computed values for a 40° wedge at $M = 0.7$ and 1.50 are the same suggest a simple formula for the drag coefficient for each wedge angle which is expected to hold in most of the transonic range. Such a conclusion extends to wedges of any angle the predictions of transonic small disturbance theory that the pressure distribution on the inclined portion of a thin wedge is constant over a range of Mach Numbers near 1.

For a 15° wedge it has been found that steady conditions may be observed in the neighborhood of the model for all Mach Numbers between 0.860 and 1.16, thus closing for the first time the gap in experimental data around the speed of sound. Measured drag coefficients are found to match wind-tunnel data of Liepmann at either end of this interval and confirm the theoretical predictions of Vincenti, Cole, and Guderley.

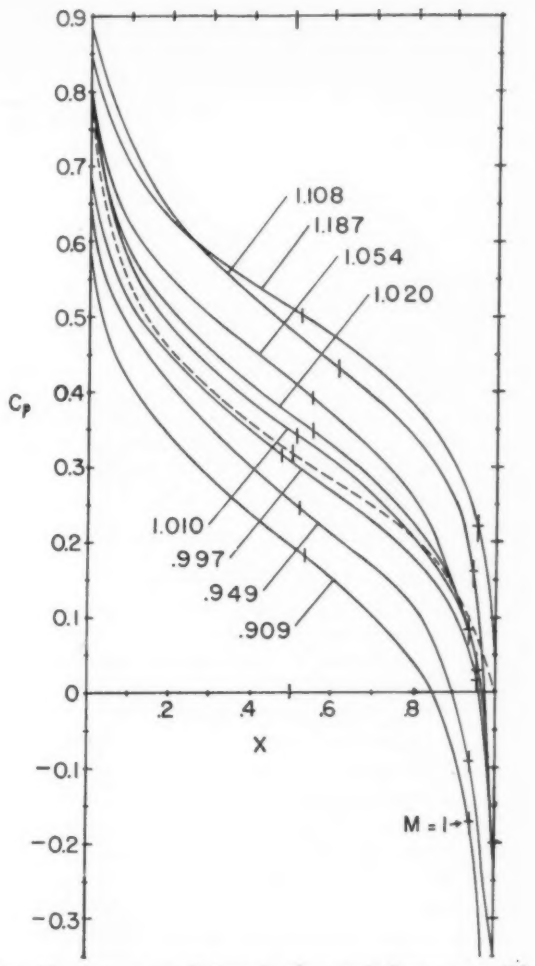

Fig. 15. Pressure coefficients for near sonic flows past a 15° wedge. The locations of points where $M = 1$ and 0.815 (the value at mid-chord according to Guderley's calculation) are marked. The dashed curve is Guderley's theoretical result for $M = 1$.

References

[1] See for instance von Kármán, Th., *The Similarity Law of Transonic Flow*, J. Math. and Phys., Vol. 26, p. 182, 1947.

[2] Maccoll, J. W., and Codd, J., *Theoretical Investigations of the Flow Around Various Bodies in the Sonic Range of Velocities*, T.R.R. 17/45, Armament Res. Dept., B.M.O.S., 1949.

[3] Drebinger, J., *Detached Shock Waves*, Ph.D. Thesis, Harvard University, Cambridge, Mass., 1950.

[4] Pack, D. C., and Groth, E., *Investigations of the Flow Past Finite Wedges of 20 Degree and 40 Degree Apex Angle at Subsonic and Supersonic Speeds, Using a Mach-Zehnder Interferometer*, R. and M. 2321, A.R.C. Tech. Rep., B.M.O.S., 1949.

[5] Laitone, E. V., *An Experimental Investigation of Transonic and Accelerated Supersonic Flow by the Hydraulic Analogy*, Inst. Eng. Res. Rep., Series 3, Issue No. 315, University of California at Berkeley, 1950.

[6] Laitone, E. V., and Pardee, O. O., *Location of Detached Shock Waves in Front of a Body Moving at Supersonic Speed*, N.A.C.A. R.M. A7B10, 1947.

[7] Moeckel, W. E., *Approximate Method for Predicting Form and Location of Detached Shock Waves Ahead of Plane or Axially Symmetric Bodies*, N.A.C.A. T.N. No. 1921, 1949.

[8] Dugundji, J., *An Investigation of the Detached Shock in Front of a Body of Revolution*, Journal of the Aeronautical Sciences, Vol. 15, p. 699, 1948.

[9] Laitone, E. V., *A Note on Detached Shock Waves*, Journal of the Aeronautical Sciences, Vol. 16, p. 441, 1949.

[10] Ladenburg, R., van Voorhis, C. C., and Winkler, J., *The Gas Flow Around Various Objects in a Free Homogeneous Supersonic Air Stream*, NAVORD Rep. 93-46, 1946.

(*Continued on page 264*)

Remarks on Dynamic Loads in Landing

ADAM ZAHORSKI*

North American Aviation, Inc.†

SUMMARY

Engineering aspects of the solution of the equation of motion for the inertia forces on an aircraft wing during the impact of landing are presented. A new and simplified, yet rigorous, approach to the analysis of dynamic loads which can be easily applied to an arbitrary forcing function is described. Working limits are established for the number of modes of vibration which are effective in contributing to the dynamic responses. Examples are given to show how the inertia forces are affected by different modes of vibration, by variation in mass distribution, and by shapes of the forcing function.

STATIC AND DYNAMIC LOADS

ONE of the more difficult problems of structural engineering is to determine the magnitude of the external loads acting on a structure. Most loads fixed by higher authorities or codes are usually specified as static loads, subdivided into dead and live loads. However, live loads are basically static loads—i.e., for analysis purposes, live loads may be considered to be static loads that are varying relatively slowly in a prescribed sequence. Static loads as such are usually not difficult to evaluate and can be checked experimentally with relative ease. But, on the other hand, it has been known for a long time that structures must be able to sustain considerably higher loads than those calculated from the principles of statics. In many cases these higher loads are caused by forces moving over the structures and producing dynamic effects. Dynamic forces are much more difficult to calculate, much harder to interpret physically, and, because they act for only a short time, are difficult to measure. Only recently have reliable instruments been developed which can record transient forces for engineering analysis. An airplane is subjected to dynamic loading by flight through gusts, by rapid maneuvers, by the firing of guns, and by the impact of landing. This paper considers the dynamic loads developed over a wing structure during and just after the impact of landing.

BASIC EQUATIONS

Fundamentally, the problem is similar to the case of a bar that vibrates when struck with a sharp blow. Vibration implies that part of the vibrating body is undergoing accelerated motion and that inertia forces are opposing the acceleration. These inertia forces are the dynamic forces that must be determined in the problem.

There are two kinds of the inertia forces: (1) those that are associated with linear accelerations and are expressed by formulas of the type $F = ma$, and (2) those that are associated with angular accelerations and are expressed by $T = I\alpha$. The former force usually causes the bending or flexure of a wing; the latter, the torsions or twisting of a wing.

The problem is so broad in scope and so complex mathematically that it is necessary to establish certain reasonable limitations. The first limitation is that only the dynamic loads that produce bending of the wing will be considered. (However, many statements also could be extended to include torsional loads.) The second limitation is that the analysis is confined to landing in which the main gear wheels touch the ground simultaneously, thereby producing identical force vs. time relationships at each wheel and only symmetrical modes of vibration in the wing.

The mathematical tools are well developed for handling the response of an elastic system to transient forces. Physicists have derived mathematical equations that represent the natural laws; mathematicians have developed many ways of solving these equations. The engineering task is threefold: (1) to choose mathematical constants that appear in the equations so that they realistically represent the physical system; (2) to select and to simplify the mathematical methods for the problem in hand so that a solution can be obtained in the shortest possible time with a sufficient degree of accuracy; and (3) to present the final results in such a manner that additional facts may be deduced concerning the laws of nature.

The wing is represented mathematically by a line possessing certain elastic properties, known as EI. For each element of the line an equation of motion is set up as follows:

$$\frac{\partial^2}{\partial x^2}\left(EI\frac{\partial^2 y}{\partial x^2}\right) + m\frac{\partial^2 y}{\partial t^2} = f(x, t) \qquad (1)$$

This partial fourth-order differential equation represents the summation of forces in the vertical plane: elastic forces of deformation, inertia forces, and externally applied forces. The equation is similar to the one used by electrical engineers where they desire to find the response of a circuit to suddenly applied voltage. We are obliged to them for various methods of solution

Presented at Specialist's Meeting, Institute of Aeronautical Sciences, in Los Angeles, February 1, 1951; received August 15, 1951.

* Design Specialist, Aerophysics Laboratory.

† Many ideas presented in this article were developed while the author was associated with Northrop Aircraft, Inc.[1]

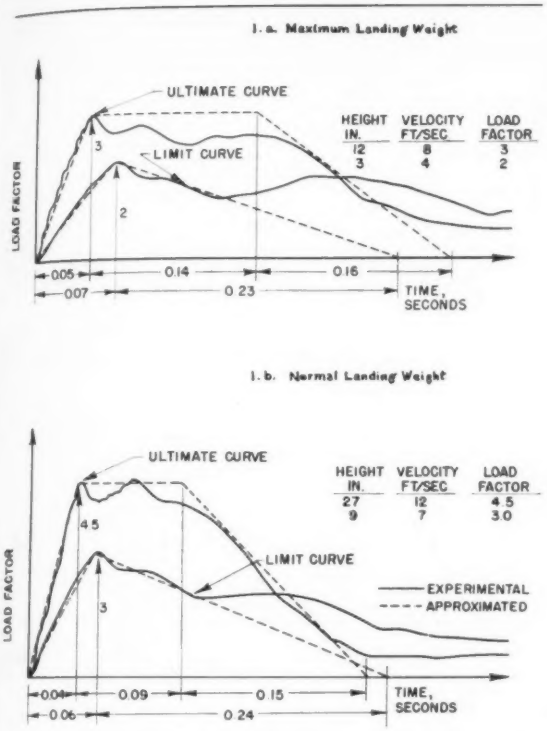

FIG. 1. Actual and approximated drop curves showing the forcing functions for maximum and normal landing weights.

of those types of equations known as "boundary problems."

The method of solution adopted in this paper is that of the natural modes of vibration, sometimes called the "method of characteristic or eigen-functions."

External Transient Forces

External transient forces, which cause vibration in the wing, are represented in Eq. (1) by $f(x, t)$ and are assumed to be known. Actually, they are not known and thus must be determined as a separate problem. Several attempts have been made to determine these forces analytically, showing the variation of force vs. time graphically. Some methods proposed are too difficult to be of practical value, since they involve the solution of nonlinear differential equations for any particular case. Others, such as those proposed by Wright Air Development Center,[2] are simple in calculation but are based on arbitrary assumptions and seldom agree with the experimental results. However, one W.A.D.C. assumption can be adopted without serious error—i.e., the trapezoidal shape of the forcing function—which considerably simplifies the lengthy calculations for dynamic response.

Many dynamic analyses have been made on the basis of forcing functions that were obtained from drop testing of the whole gear assembly. Results of such analyses may be extremely misleading. The technique of drop testing was developed primarily for testing the landing gear at ultimate load and not for obtaining dynamic load data for design of the wing. Because the dynamic response, both in magnitude and shape, is not linearly proportional to the maximum of the applied load, information obtained from an arbitrary free drop (e.g., 27 in.) of the landing gear is practically useless so far as the dynamic loads are concerned.

The four drop curves shown in Figs. 1a and 1b were obtained experimentally for the same landing gear at two different weights and at two different drop heights. They are supposed to represent conditions of maximum weight and normal weight landings at limit and ultimate landing-gear load factors. Dynamic responses are calculated for each condition, thus showing the effects of variation of two parameters. For the purpose of simplifying computations, each drop curve was approximated by a trapezoid or a triangle, as shown by the dotted lines.

Solution of Equation of Motion

The solution of equation of motion [Eq. (1)] by the method of characteristic values assumes that the deflection $y(x, t)$ can be represented by a sum of two functions, such as

$$y(x, t) = \sum_{j=0}^{\infty} Y_j(x) p_j(t) \tag{2}$$

where $Y_j(x)$ is the function of the span coordinate (x) only and is known as the shape of the jth natural mode of vibration and where $p_j(t)$ is the generalized time coordinate associated with the jth mode.

It can be shown[3] that for all natural modes of vibration the following relations are valid:

$$\frac{d^2}{dx^2}\left[EI\frac{d^2Y_j}{dx^2}\right] = \omega_j^2 m Y_j \tag{3}$$

$$\int_0^b m Y_j Y_k \, dx = \begin{cases} 0 \text{ for } j \neq k \\ N_j \text{ for } j = k \end{cases} \tag{4}$$

where ω_j is the frequency of the jth natural mode and N_j is a constant.

It will suffice here to state that Eq. (3) can be solved for Y_j, the shape of natural modes, and that, without loss of generality, Y_j at the wing tip can be set equal to unity. In that case, $p_j(t)$ in Eq. (2) can be interpreted also as the tip deflection of the wing caused by the external disturbing forces $f(x, t)$.

If Eq. (2) is substituted into Eq. (1) and modes of vibration Y_j eliminated by Eqs. (3) and (4) then the differential equation of motion Eq. (1) will be transformed into

$$\ddot{p}_j(t) + \omega_j^2 p_j(t) = A_j F(t) \tag{5}$$

where

$$A_j = R Y_j(L)/N_j \tag{6}$$

R = the maximum vertical force exerted by the landing gear on the wing
$Y_j(L)$ = the ordinate of jth mode at landing gear
N_j = defined by Eq. (4)
$F(t)$ = the forcing function, a nondimensional quantity that describes the variation of transient forces applied to the wing

The maximum value of the forcing function is taken as unity. Thus, the product $RF(t)$ is the history of the transient.

The solution of Eq. (5) is known in the form[4]

$$p_j(t) = (A_j/\omega_j)D_j(t) \tag{7}$$

where $D_j(t)$ is Duhamel's integral

$$D_j(t) = \int_0^t F(\tau) \sin \omega_j(t - \tau)\, d\tau \tag{8}$$

Integration of Eq. (8) is usually difficult. If $F(\tau)$ is an experimental curve and is given by a set of ordinates, then the numerical integration becomes tedious and must be done by a modern high-speed computing machine. Even when high-speed machines are available, a prohibitive length of time is usually required to determine the dynamic response of the wing for many different forcing functions that may arise for various landing conditions.

It is possible to simplify calculations if we note (1) that for the dynamic analysis the chief interest is in the distribution of accelerations along the wing and not in the distribution of deflections and (2) that certain types of superposition are permissible in calculation of Duhamel's integrals and one simple integration will be sufficient to cover vast varieties of forcing functions.

First, note from Eq. (2) that the acceleration at any point along the wing is

$$\ddot{y}(x, t) = \sum_{j=0}^{\infty} Y_j(x)\, \ddot{p}_j(t) \tag{9}$$

and from Eqs. (5) and (7) that the wing tip acceleration is

$$\ddot{p}_j(t) = A_j[F(t) - \omega_j D_j(t)] \tag{10}$$

Gradient Forcing Functions

Let $F_i(t)$ be a forcing function that starts at $t_i = 0$ and uniformly increases with time. This function can be represented by a straight line passing through the origin. Since the slope is constant, we have

$$F_i(t) = F_i'(t) \cdot t_i \tag{11}$$

where $F_i'(t)$ is a constant and subscript i indicates that time t_i is measured at the origin of F_i. The function represented by Eq. (11) will be called a "gradient forcing function." Resolution of landing force vs. time history into four components, each of which is a linear function of time, was proposed by Midwest Research Institute.[6]

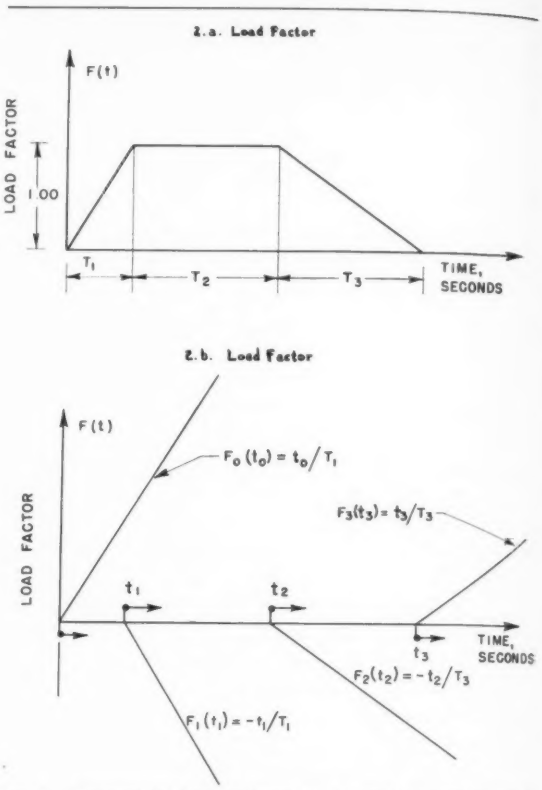

FIG. 2. Trapezoidal forcing function (a) and its equivalent in straight line functions (b).

Substituting Eq. (11) into Eq. (8) and integrating, we get Duhamel's integral for the gradient functions

$$D_{ij}(t) = F_i'[(t_i/\omega_j) - (1/\omega_j^2) \sin \omega_j t_i] \tag{12}$$

and, substituting the above into Eq. (10), we get

$$\ddot{p}_{ij}(t) = A_j(F_i'/\omega_j) \sin \omega_j t_i \tag{13}$$

In general, the forcing functions of any shape $F(t)$ can be approximated by a number of straight lines forming a polygon, and the integration of Duhamel's integral may be performed along several broken lines. However, this integration can be greatly simplified by superposition of Eq. (13), which will be demonstrated on a trapezoidal forcing function.

Let $F(t)$ be a trapezoidal forcing function whose shape is defined by three time intervals: T_1, T_2, and T_3 (Fig. 2a). This function is replaced by one, two, three, or four straight-line functions F_0, F_1, F_2, and F_3 (Fig. 2b), with slope so adjusted that the summation of all forces at any time t is equal to $F(t)$. Thus,

$$F(t) = \sum F_i\,(t_i)$$

Because the superposition of forces is permissible in calculations of responses (reference 4, page 405) and if the time coordinates are measured from the proper origins at intersections of F_0, F_1, F_2, and F_3 with the

abscissa as shown on Fig. 2b, then

$$D_j(t) = D(t_0) + D_j(t_1) + \text{etc.} = \sum D_{ji}(t_i)$$

and, consequently, from Eq. (7),

$$p_j(t) = p_j(t_0) + p(t_1) + \text{etc.} = \sum p_{ji}(t_i)$$

and

$$\ddot{p}_j(t) = \ddot{p}_j(t_0) + \ddot{p}_j(t_1) + \text{etc.} = \sum \ddot{p}_{ji}(t_i)$$

where $\ddot{p}_{ji}(t_i)$ is given by Eq. (13).

For example, by superposition of response, we can say that the acceleration in the region between T_1 and T_2 (Fig. 2a) is

$$\ddot{p}_j(t) = A_j \left[\left(\frac{1}{\omega_j T_1} \right) \sin \omega_j t_0 - \left(\frac{1}{\omega_j T_1} \right) \sin \omega_j t_1 \right]$$

or, since $t = t_0$ and $t_1 = t - T_1$,

$$\ddot{p}_j(t) = A_j \left[\left(\frac{1}{\omega_j T_1} \right) \sin \omega_j t - \left(\frac{1}{\omega_j T_1} \right) \sin \omega_j (t - T_1) \right]$$

This can be written

$$\ddot{p}_j(t) = A_j \frac{\sin (1/2)\omega_j T_i}{(1/2)\omega_j T_i} \cos \omega_j [t - (1/2)T_1] \quad (14)$$

This equation is of a particular interest. The form of the equation is very similar to that derived by Wasserman.[5] However, it is much more general and reveals that both the lag angle and the amplitude of the acceleration are functions of the frequency of natural vibration and of the slope of forcing function. In fact, the amplitude of $\ddot{p}_j(t)$ is an oscillatory function of the product $\omega_j T_1$. If $(1/2)\omega_i T_1 = \pi, 2\pi, 3\pi$, etc., the amplitude of acceleration will be zero and therefore there will be no dynamic response in that particular mode in this region.

Fig. 3 shows the results of calculation of the dynamic response in one mode only due to three different forcing functions that vary only in the initial rate (slope) of the application of the disturbing force. For computation of these curves, Eq. (14) was modified somewhat, as it will be shown later, by introduction of the structural damping that changed a simple harmonic motion to a motion with an exponential decay of amplitude after the break in the forcing function. The dynamic magnification factor in that figure is defined as a number by which the design load factor must be multiplied to obtain vertical acceleration at the wing tip in units of gravity due to dynamic response of the elastic mode only. However, a precise definition is of no importance here, since the curves are presented only as an illustration that the initial slope of the forcing functions may be an important parameter in the calculation of dynamic responses and that an arbitrary drawn line may give misleading results. The figure shows that, if the force attains its maximum in 0.04 sec., then the magnification factor for wing tip acceleration will be 2.12 but that, if the same force attains the same maximum in 0.07 sec., then the magnification factor will be only 0.34.

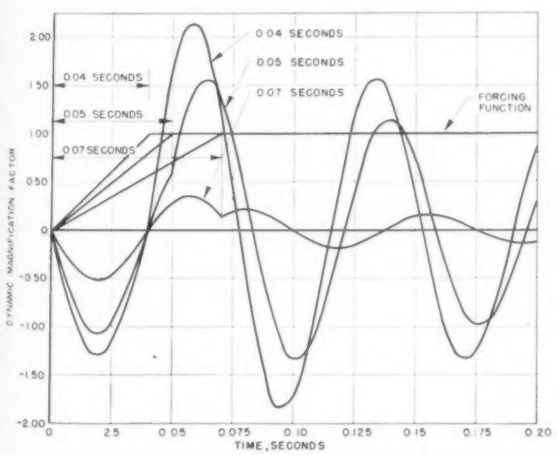

FIG. 3. Dynamic response variation due to change in initial slope of forcing function.

NUMBER OF EFFECTIVE MODES

How many natural modes of vibration should be used in the dynamic analysis is the question of practical importance. Too few or too many modes may lead to erroneous conclusions.

Two different criteria may be simultaneously used in order to limit the number of effective modes. The first criterion is based on the consideration of the magnitude of wing tip deflections of various modes in relation to overall dimensions of the wing; the second considers the effects of the structural damping on the amplitudes of deflection and of acceleration.

TIP DEFLECTIONS

The amplitude of the wing tip acceleration $\ddot{p}_j(t)$ will be, in general, proportional to the ratio $Y_j(L)/N_j\omega_j$. In this ratio, only ω_j increases for higher modes, but there is no prescribed pattern of values for both $Y_j(L)$ and N_j. Therefore, it might be expected that high acclerations may occur at some higher frequencies than were considered in the analysis. On the other hand, it can be seen from Eq. (5) that the ratio $p_j/\ddot{p}_j$ is in all cases inversely proportional to ω_j^2. This means that deflection amplitudes will in all cases diminish rapidly for higher modes in contrast to the case for accelerations.

To arrive at a rational conclusion as to how many modes are necessary in an analysis, the order of magnitude of the wing tip deflection of each consecutive mode must be considered in relation to the overall dimensions of the wing. For the wing of large size, the tip deflection of a few hundredths of an inch, which was theoretically derived for a line beam with uniformly distributed masses and stiffnesses, is not realistic. It can never be detected experimentally and, in fact,

does not exist on the actual wing. If the computed deflections are not realistic, then it is reasonable to deduce that the accelerations derived from those deflections also are not realistic.

Figs. 4a and 4b show wing tip deflections calculated for the first three elastic modes at two different load conditions. These deflections demonstrate that for a particular airplane the modes of beyond the third should not be considered in the dynamic analysis.

Structural Damping

The second approach to limiting the number of modes is the consideration of the effects of structural damping upon deflection and acceleration amplitudes.

There are some questions as to what the properties of structural damping are, how damping should be used in the differential equations, and if the mode of vibration still remains orthogonal. But, if the damping coefficient is small, say of the order of 5 per cent, then there should be no objection to using basically the same method as in the case when damping is neglected.

If it is assumed that the modes of vibration are damped out proportionally to $\exp(-\mu\omega t)$, then a simple diagram showing the variation of amplitude with different frequencies will be helpful in deciding how many modes should be included in the analysis.

If damping is introduced into the equation of motion, then Duhamel's integral will be, instead of Eq. (8),

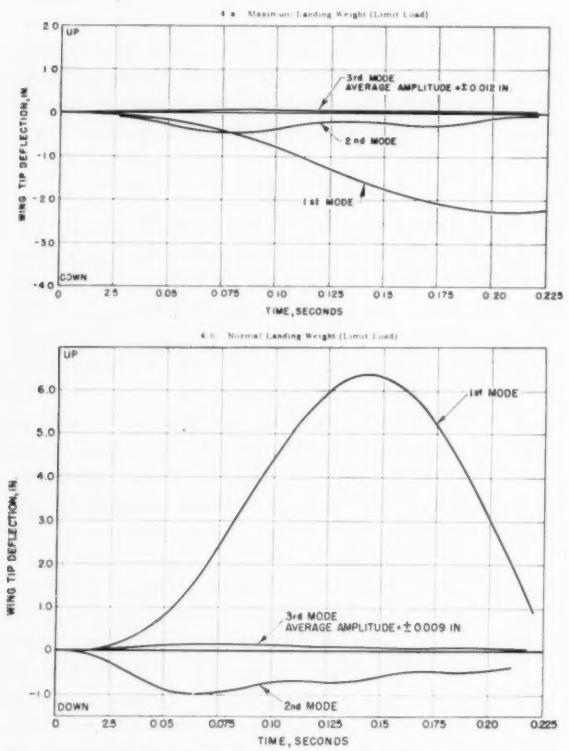

Fig. 4. Wing tip deflections calculated for the first three elastic modes at two different load conditions.

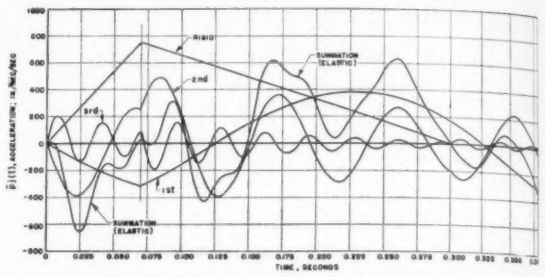

Fig. 5. Calculated wing tip accelerations due to bending at maximum landing weight (limit drop curve).

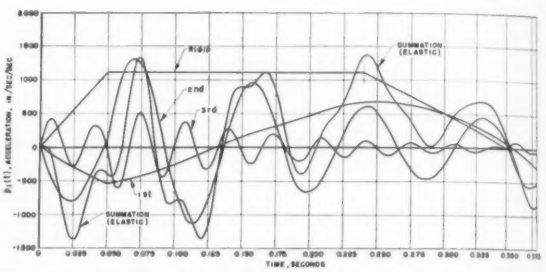

Fig. 6. Calculated wing tip accelerations due to bending at maximum landing weight (ultimate drop curve).

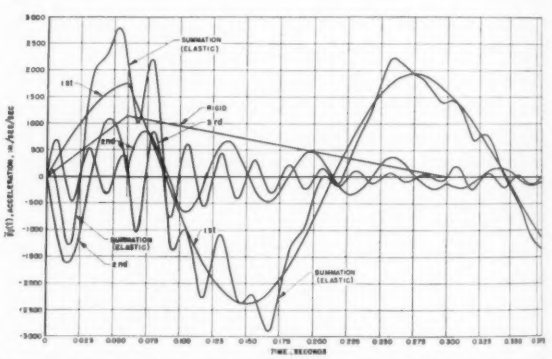

Fig. 7. Calculated wing tip acceleration due to bending at normal landing weight (limit drop curve).

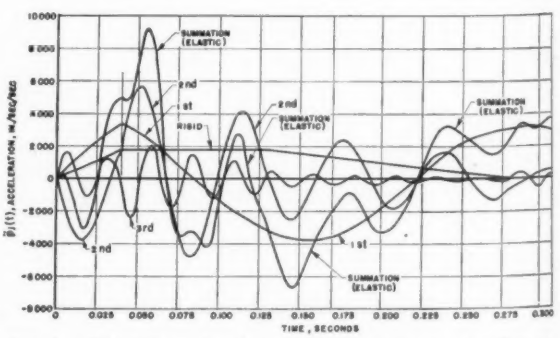

Fig. 8. Calculated wing tip accelerations due to bending at normal landing weight (ultimate drop curve).

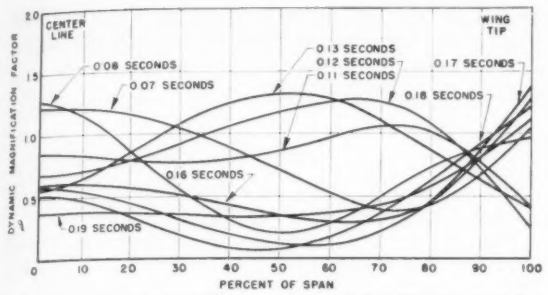

FIG. 9. Dynamic magnification factor in bending vs. span for various times for maximum landing weight (limit drop curve) condition.

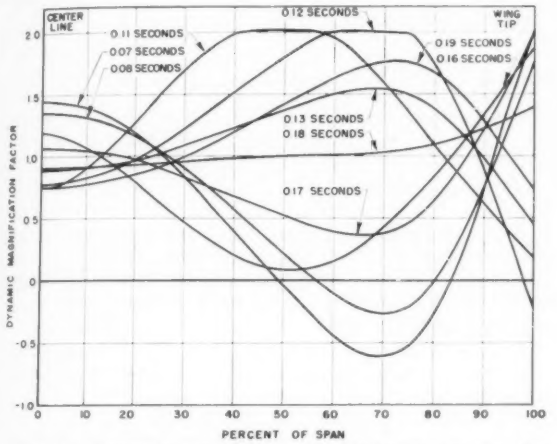

FIG. 10. Dynamic magnification factor in bending vs. span for various times for maximum landing weight (ultimate drop curve) condition.

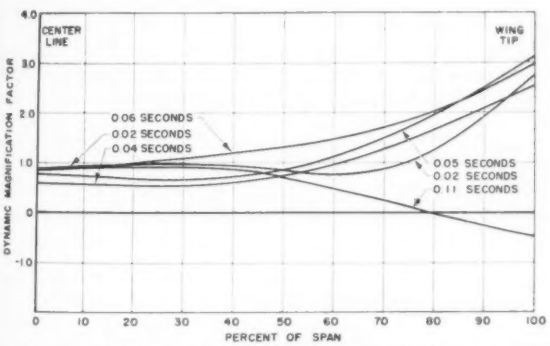

FIG. 11. Dynamic magnification factor in bending vs. span for various times for normal landing weight condition (limit drop curve).

$$D_j(t) = \int_0^t F(\tau)e^{-\mu\omega_j(t-\tau)} \sin \omega_j(t-\tau)\, d\tau \quad (15)$$

This will be integrated for a damping coefficient $\mu = 0.05$ (assuming that $\mu << 1$) and a gradient forcing function $F(\tau) = F'(\tau)\tau$, where $F'(\tau)$ is a constant.

$$D_j(t) = \frac{F'}{\omega_j{}^2}\left[(\omega_j t - 0.10) - e^{-0.05\,\omega_j t} \sin (\omega_j t - 0.10)\right] \quad (16)$$

Substituting the above into Eq. (10), we get

$$\ddot{p}_{ij}(t) = A_j(F_i'/\omega_j)d_{ij} \quad (17)$$

where

$$d_{ij} = 0.10 + e^{-0.05\,\omega_j t} \sin (\omega_j t_i - 0.10) \quad (18)$$

A new function d_i is introduced because of its usefulness in the calculation of the dynamic response and, in addition, because it can be generated quickly (about 35 per min.) on IBM equipment. The dynamic response to any arbitrary forcing function which can be approximated by a number of straight lines need be obtained by the generating function d_i only once for any given frequency ω. At this stage, proper application of superposition means only automatic counting and stacking the cards by the machines.

When $\ddot{p}_j(t)$ has been determined by the above method, all that remains is to substitute its value into Eq. (9) to obtain the spanwise distribution of acceleration in the form of a family of curves for various values of time.

Comparative Results

The method outlined above for the solution of the dynamic loads is simple in application and may be handled by relatively inexperienced engineers.

Thus, it is practicable to calculate the wing tip accelerations ($\ddot{p}_j$) due to four different forcing functions (Fig. 1) from $t = 0$ to $t = 0.500$ sec. after the impact for each 0.001-sec. interval (Figs. 5 to 8).

It is entirely possible that in many engineering offices only one dynamic analysis is made on the bases of only one drop curve and one weight condition. Any one of the diagrams of Figs. 5 to 8 could be accepted as typical for what could be expected in the behavior of the wing during the impact of landing. These four diagrams show that the variations in $\ddot{p}_j(t)$ are very large, and any conclusions derived from any one diagram may be erroneous if projected on any other landing conditions.

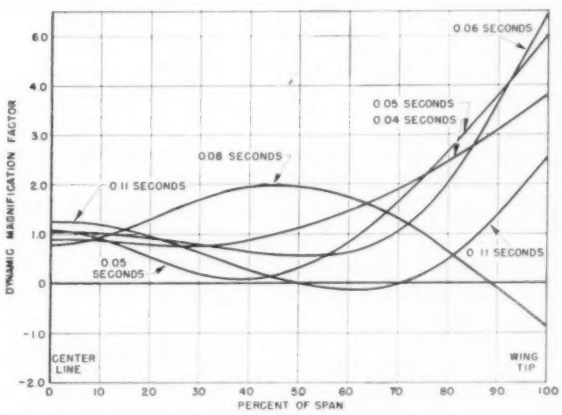

FIG. 12. Dynamic magnification factor in bending vs. span for various times for normal landing weight (ultimate drop curve) condition.

This possibility of error can be further emphasized by showing, through the application of Eq. (9), the spanwise distribution of the dynamic load factors (Figs. 9 to 12).

Load factor or, in this case, the dynamic magnification factor (d.m.f.) is defined as the acceleration in gravity units per unit landing load factor at the gear. This permits comparison of all curves on the basis of one common denominator that is the unit of the maximum reaction at the wheel during landing and permits extrapolation of the effects on dynamic loading due to small changes in weights and intensity of landing. It is the author's contention that inasmuch as accelerations due to dynamic responses are not linear functions of landing load factors, it is much more realistic to use for all design purposes only those forcing functions that *actually* can occur in landing and to apply the desired safety factor to the dynamic accelerations only after the calculations are computed.

References

[1] Northrop Aircraft, Inc., Report No. STR-55.

[2] A.M.C. Report MCREXA-4595-8-A.

[3] Zahorski, A. T., *Free Vibrations of Sweptback Wing*, Journal of the Aeronatuical Sciences, Vol. 14, No. 12, pp. 683-692, December, 1947.

[4] von Kármán, Th., and Biot, M., *Mathematical Methods in Engineering;* McGraw-Hill Company, Inc., New York, 1940.

[5] A.F. Tech. Ref. 5815, p. 58.

[6] Proceedings of the Seventh International Congress of Applied Mechanics, Vol. 4, 1948.

Shock-Tube Studies of Transonic Flow over Wedge Profiles

(*Continued from page 257*)

[11] Heberle, J. W., Wood, G. P., and Gooderum, P. B., *Data on Shape and Location of Detached Shock Waves on Cones and Spheres*, N.A.C.A. T.N. No. 2000, 1950.

[12] Lin, C. C., and Rubinov, S. I., *On the Flow Behind Curved Shocks*, Jour. Math. and Phys. Vol. 27, p. 105, 1948.

[13] Busemann, A., *A Review of Analytical Methods for Treatment of Flows with Detached Shock Waves*, N.A.C.A. T.N. No. 1858, 1949.

[14] Guderley, K. G., *Considerations of the Structure of Mixed Subsonic and Supersonic Flow Patterns*, Tech. Rep. No. F-TR-2168-ND, and *Singularities at the Sonic Velocity*, Tech. No. F-TR-1171-ND, A.A.F., Air Materiel Command, Wright Field, 1947, 1948.

[15] Tsien, H. S., and Baron, J. R., *Airfoils in Slightly Supersonic Flow*, Journal of the Aeronautical Sciences, Vol. 16, p. 55, 1947.

[16] Vincenti, W. G., and Wagoner, C. B., *Transonic Flow Past a Wedge Profile with Detached Bow Wave*, N.A.C.A. T.N. No. 2339, 1951.

[17] Cole, J. D., *Drag of a Finite Wedge at High Subsonic Speeds* Jour. Math. and Phys., Vol. 30, p. 79, 1951.

[18] Guderley, K. G., and Yoshihara, H., *The Flow over a Wedge Profile at Mach Number 1*, Journal of the Aeronautical Sciences, vol. 17, p. 723, 1950.

[19] Liepmann, H. W., and Bryson, A. E., Jr., *Transonic Flow Past Wedge Sections*, Journal of the Aeronautical Sciences, Vol. 17, p. 745, 1950.

[20] Bleakney, W., Weimer, D. K., and Fletcher, C. H., *The Shock Tube, A Facility for Investigations in Fluid Dynamics*, Rev. Sci. Instr., Vol. 20, p. 807, 1949.

[21] Bleakney, W., and Taub, A. H., *Interaction of Shock Waves*, Rev. Mod. Phys., Vol. 21, p. 584, 1949.

[22] Weimer, D. K., *Supersonic Flow in a Shock Tube*, Phys. Rev., Vol. 79, p. 546A, 1950.

[23] Geiger, F. W., and Mautz, C. W., *The Shock Tube as an Instrument for the Investigation of Transonic and Supersonic Flow Patterns*, Eng. Res. Inst. Rep., University of Michigan, 1949.

Navy Symposium on Aeroballistics

A Navy Symposium on Aeroballistics, under the sponsorship of the Bureau of Ordnance, will be held at the Huntington Hotel in Pasadena, Calif., on May 13 and 14, 1952. The meeting will be followed by a visit to the Naval Ordnance Test Station at Inyokern on May 15. The meeting will be closed, and a confidential clearance is required for attendance. The subjects to be discussed include: Aeroelasticity, Aircraft Missile Interaction, Heat Transfer, Hypersonics, Scaling Effects, Relaxation Phenomena, and studies conducted in the Pressurized Ballistic Range and the Shock Tube.

Those wishing to attend should address their requests to the Chairman, Bureau of Ordnance Aeroballistics Committee (Code Rexd-2), Department of the Navy, Washington 25, D.C.

A Study of Transonic Gas Dynamics by the Hydraulic Analogy

E. V. LAITONE*

University of California at Berkeley

SUMMARY

The theory governing the propagation of surface water waves is analyzed to show that an analogy with the two-dimensional flow of a perfect gas exists only if the water depth is approximately 1/4 in., the model is fairly large, and the shock waves or hydraulic jumps present are of the weak type having a negligible increase in entropy.

Photographs of the water surface waves corresponding to shock waves in front of simple wedges and circular cylinders are presented to illustrate these restrictions. It is pointed out that the surface-wave group velocity, which could be considerably less than the so-called wave velocity, provided the only correct analogy to the speed of sound in two-dimensional gas flow over a closed body.

Motion pictures were taken in order to study the effect of constant acceleration on bow shock waves. It was found that at high rates of acceleration the location of a detached shock wave was dependent mainly on a nondimensional acceleration parameter and was practically independent of the instantaneous Mach Number.

Analysis of the Analogy and the Effect of the Group Velocity

If one assumes that surface waves are propagated across the free surface of a large body of shallow water over a horizontal plane bottom in such a manner that the vertical accelerations are negligible, then the horizontal motion is the same at all depths. In this case all infinitesimal disturbances move at a constant velocity of propagation given by $\sqrt{gh}$, where h is the water depth.

This motion is directly analogous to a two-dimensional compressible gas flow where $\sqrt{gh}$ corresponds directly to the speed of sound, a, and the infinitesimal change in h is directly proportional to the isentropic variation of either density (ρ), or temperature (T), in a perfect gas having a specific heat ratio of $\gamma = 2$ (see reference 1) so that

$$\left.\begin{aligned} \frac{h}{h_0} = \frac{\rho}{\rho_0} = \left(\frac{T}{T_0}\right)^{1/(\gamma-1)} = \left(\frac{p}{p_0}\right)^{1/\gamma} \\ \sqrt{gh} = a = \sqrt{\gamma g R T} = \sqrt{\gamma p/\rho} \end{aligned}\right\} \qquad (1)$$

for $\gamma = 2$ only.

This analogy is valid for either stationary or nonstationary isentropic flow. However, the analogy is an approximation that is valid only so long as the vertical acceleration is negligible and Eqs. (1) are true for all surface waves of any wave length.

The first difficulty in the analogy between the shallow-water surface waves and the two-dimensional isentropic gas flow is the fact that the actual velocity of the surface-wave propagation is not given exactly in Eqs. (1), which are only approximations, but is given more nearly by (see reference 2)

$$c = \sqrt{\left(\frac{g\lambda}{2\pi} + \frac{2\pi T}{\rho\lambda}\right) \tanh \frac{2\pi h}{\lambda}} = \sqrt{gh}\left[1 + 2\,\frac{\pi^2 T}{g\rho\lambda^2} + 0\left(\frac{h^2}{\lambda^2}\right)\right] \qquad (2)$$

This indicates that the vertical acceleration is not negligible, even when the frictional drag on the bottom is neglected, unless the wave length $\lambda \gg h$ or unless $h \to 0$ when λ finite. In the latter case, as $h \to 0$, the second term containing the surface tension T becomes predominant for small λ. These shorter wave lengths correspond to the so-called capillary ripples that are entirely a surface phenomena and do not follow the analogy defined in Eq. (1).

Fig. 1 is a plot of c vs. λ for ordinary tap water with a surface tension $T = 0.005$ lbs. per ft. and various water depths. It is seen that

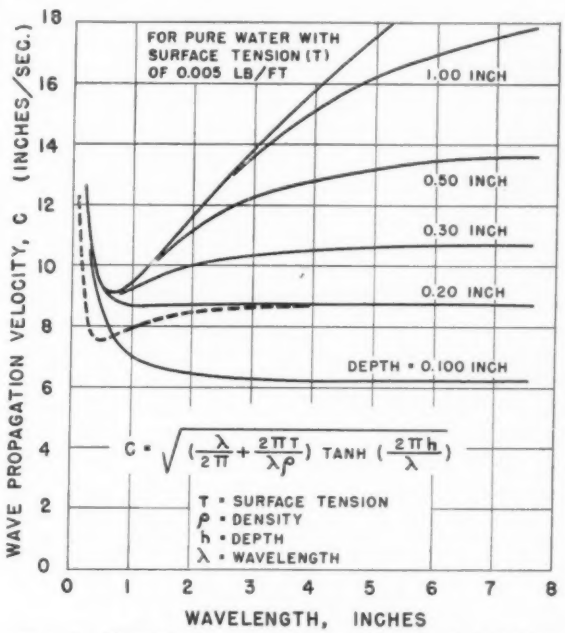

Fig. 1. Variation of wave velocity with wave length from Eq. (2). Dotted line shows effect of decreasing T by 50 per cent.

Presented at the Annual Summer Meeting, I.A.S., Los Angeles, June 27–28, 1951.

* Associate Professor.

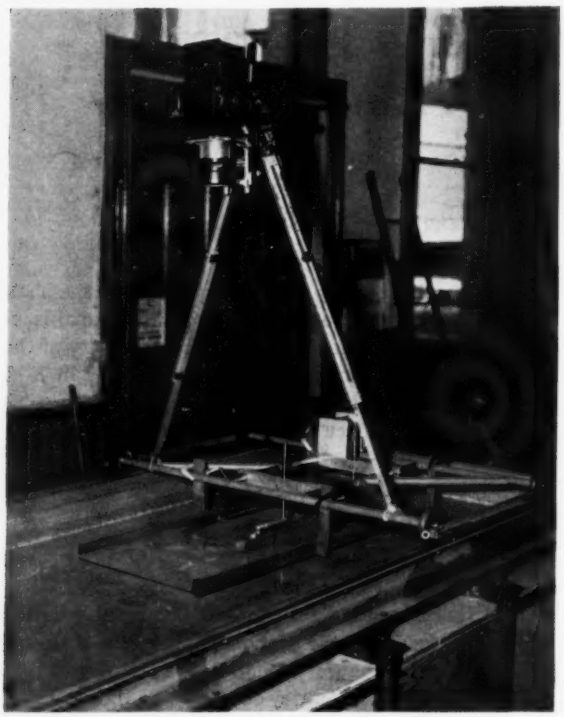

FIG. 2. Hydraulic tank and towing carriage.

$$c \to a = \sqrt{gh}$$

independent of λ, only for small water depths of the order of $^1/_4$ in. and even then only for $\lambda \geq 1$ in. The waves corresponding to λ values smaller than this are entirely capillary ripples that are always unavoidably present in the analogy. Their effect is almost negligible on the formation of the hydraulic jump, analogous to shock waves, but they do appear in the photographs of the surface waves, although their relative effect may be practically eliminated by using a large model.

If the ratio of h/λ is not sufficiently small, then the analogy fails, since there is no constant corresponding to the speed of sound in isentropic gas flow. As a matter of fact, if c varies with λ, not only does the analogy break down but even the concept of the wave velocity c, Eq. (2), itself loses all physical significance. In this case c should actually be termed a phase velocity rather than a wave velocity (see reference 2), since it is neither the rate of propagation of the energy nor the wave form. Then, no given wave form can be propagated without a continuous change in shape, although the overall motion proceeds at a constant velocity called the group velocity. From a physical point of view, this so-called group velocity is always more important than the wave velocity, since the group velocity is directly related to the rate of propagation of the energy itself. The wave velocity is only of importance when it coincides with the group velocity. The individual waves of a given wave length forming a grouped disturbance move more rapidly than the group velocity of the disturbance itself, but these individual waves die out as they approach the front of the group, their energy being continually transferred to the disturbance itself. It is only when the group velocity coincides with the wave velocity that a given disturbance can be propagated without a change in form, as in two-dimensional supersonic flow, at a constant velocity.

It is shown in reference 2 that the group velocity is given by

$$[c - \lambda(dc/d\lambda)]$$

Therefore, the group velocity for any finite combination of waves with the same wave length λ is given by the intercept, on the c axis of Fig. 1, made by the tangent to the curve of c vs. λ at the given λ. It is then obvious from Fig. 1 that the capillary ripples, having a small λ, travel with a group velocity greater than the wave velocity c. On the other hand, gravity waves, having a larger λ, must have a group velocity less than c. Their group velocity is exactly one-half of the wave velocity in deep water ($h \gg \lambda$) no matter how large the model itself may be. Only as the water becomes more shallow does the group velocity approach c, which in turn approaches the constant value, $a = \sqrt{gh}$, which is independent of wave length for all λ except those corresponding to the extremely small capillary ripples.

It is also seen from Fig. 1 that decreasing the water depth below 0.2 in. will make matters worse, at least for the standard value of surface tension for pure water. Likewise, a 50 per cent decrease in the surface tension, as shown by the dotted line in Fig. 1, adversely affects the analogy for $h = 0.2$ in.

The second important restriction on the analogy arises in the investigation of shock waves. The local water depth directly corresponds to the local value of the enthalpy or temperature in the two-dimensional compressible gas flow. In a gas flow there is no change in the stagnation enthalpy (or stagnation temperature) across an ordinary shock wave, since the flow is adiabatic (although nonisentropic). However, for the hydraulic jump or surge formed in water, there exists an actual loss in the stagnation water depth due to the formation of eddies that eventually increase the water temperature. This is an additional loss of available energy or increase of entropy which has no counterpart in the analogous ordinary shock wave in gas flow. Consequently, the shock-wave analogy is limited to that range of Mach Numbers and flow deflections wherein this loss in stagnation depth is negligible. It is obvious that this range must include the shock waves wherein the change in entropy can be neglected, as defined by $(M_0^2 - 1)^3 \to 0$ for normal shock waves or by the flow deflection $\theta^3 \to 0$ for oblique shock waves (see reference 3). Therefore, the shock-wave analogy is valid in the limiting case either as $M_0 \to 1$ or as the wedge angle $\theta \to 0$. However, a comparison of the

computed values for the pressure changes through a normal shock show that the analogy is well within 1 per cent if $M_0 < 1.5$. This range is, of course, satisfactory for the transonic investigation of any normal or oblique shock. This has been verified experimentally in reference 4, where it is shown that for the shock-wave analogy the water depth, as would be expected, must be of the order of $^1/_4$ in.

Table 1 gives the two-dimensional oblique shock-wave relations for the maximum flow deflection ($\theta_{max.}$) which can be produced at a given free-stream Mach Number M_0 in a perfect gas for $\gamma = 2$, while Table 2 gives the same relations for $\gamma = 1.4$ corresponding to air (Table 2 is taken directly from reference 3, and Table 1 is computed in the same manner).

It is immediately noted that the increase in γ produces a large increase in the strength of the shock wave, especially at the higher Mach Numbers. It is important to note that the values given in Table 1 do not correspond to the hydraulic relations for the hydraulic jump or surge actually occurring in the water channel. The hydraulic-jump relations approach the perfect gas relation for $\gamma = 2$ (Table 1) as $M_0 \rightarrow 1$ and give nearly the same values for $M_0 < 1.5$. However, for $M_0 > 1.5$, some of the hydraulic-jump relations depart considerably from the perfect gas relations for $\gamma = 2$, and the analogy therefore cannot be used for any finite model beyond this range, since all of the isentropic flow regions are still governed by Eq. (1) with $\gamma = 2$. This limitation, of course, does not restrict investigation in the transonic range wherein $M < \sqrt{2}$.

The oblique shock-wave analogy may, of course, be carried to higher values of M_0 by limiting the values of θ so that the entropy change, which varies as θ^3, is negligible. In all cases, however, the analogy is valid only for $\gamma = 2$, since all the flow expansion and isentropic compression regions are governed by Eq. (2) and not by the hydraulic-jump relations. The hydraulic-jump relations may be used alone, ignoring Eq. (2) and $\gamma = 2$, only for the trivial case of an infinite wedge in an infinite stream.

Although no real gas has $\gamma = 2$, still the analogy is useful as an experimental verification of any theoretical equation developed from a study of two-dimensional gas flow. Attempts have been made to use other than rectangular water channels in order to obtain different values of γ. For example, an equilateral triangular cross section gives a γ value of 1.5. However, this is based on the *a priori* assumption that the hydrostatic pressure relation may be used or that the vertical acceleration is zero. Fig. 1 shows that this is true for ordinary model sizes only for water depths of the order of $^1/_4$ in., even in an unrestricted infinite body of water of uniform depth; consequently, the analogy must fail for the deeper water depth required in such a channel.

This restriction to small water depths also makes the use of a flowing water channel difficult, since the flow over the fixed bottom cannot be sufficiently uniform when the optimum depth is only $^1/_4$ in. Therefore, the following investigation was made in a rectangular channel 4 ft. wide and 20 ft. long, where the model was towed by means of a carriage. The section of the tank bottom where the pictures were taken was made of glass. A description of the apparatus used, as shown in Fig. 2, is given in references 5 and 6. The photographs were taken by having the light source below the glass bottom of the tank and the camera above the water surface. The camera was focused on a ground-glass screen supported above the model and 1 in. above the water surface.

Fig. 3 was obtained by using a high-intensity carbon arc-light source, while Figs. 4, 5, and 6 were obtained by using a Kodatron speed lamp. In Fig. 3 the grid was below the glass bottom, while in the later pictures the grid was marked on the ground-glass screen, which was above the water.

The present tests were taken for steady transonic flow near $M_0 = 1$ and for accelerated flow, since these are the most difficult to test experimentally in ordinary wind tunnels but present no difficulty with a towing carriage in a still water channel.

It is again stressed that these cannot be considered as model tests but only as an experimental check of any theoretical compressible gas-flow equation wherein the numerical value of γ is taken as 2. There is no necessity of attempting to correlate any parameter other than the Mach Number for steady flow, since there is none in this analogy. For example, correlating the Reynolds Number would have no physical significance because the boundary conditions are entirely different. The only logical basis of comparison is the one available from neglecting all viscosity effects.

TABLE 1
Detachment Angle for Perfect Gas Relations ($\gamma = 2$)

$\theta_{max.}$ (Deg.)	M_0	M	$\frac{p}{p_0}$	$\frac{\rho}{\rho_0}$	$\frac{H}{H_0}$	θ_W (Deg.)
0	1	1	1	1	1	90
$2^1/_2$	1.17	0.957	1.34	1.156	1.000	72.7
5	1.30	0.943	1.61	1.27	0.987	68.9
10	1.56	0.925	2.33	1.50	0.970	64.8
15	1.90	0.932	3.44	1.76	0.900	62.3
20	2.42	0.941	5.70	2.08	0.755	61.0
25	3.51	0.965	12.4	2.48	0.521	60.2
30	∞	1	∞	3	0	60

TABLE 2
Detachment Angle for Perfect Gas Relations ($\gamma = 1.40$)

$\theta_{max.}$ (Deg.)	M_0	M	$\frac{p}{p_0}$	$\frac{\rho}{\rho_0}$	$\frac{H}{H_0}$	θ_W (Deg.)
0	1	1	1	1	1	90
$2^1/_2$	1.14	0.961	1.24	1.17	0.999	74.1
5	1.24	0.944	1.43	1.29	0.995	70.8
10	1.42	0.925	1.84	1.54	0.972	67.5
15	1.61	0.919	2.36	1.81	0.939	65.7
20	1.84	0.920	3.07	2.14	0.870	64.9
25	2.13	0.928	4.13	2.55	0.758	64.6
30	2.52	0.941	5.90	3.06	0.591	64.8
45.6	∞	1	∞	6	0	67.8

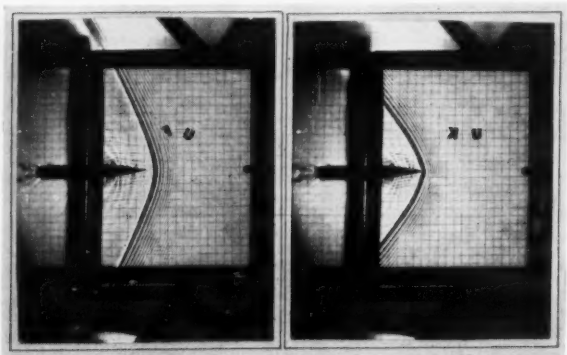

FIG. 3a: $\theta = 10°$, $M_0 = 1.29$ FIG. 3b: $\theta = 10°$, $M_0 = 1.48$

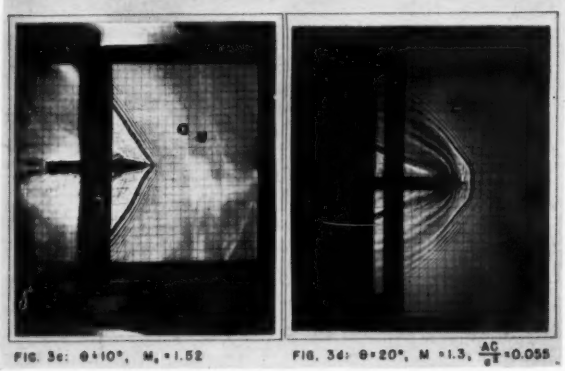

FIG. 3c: $\theta = 10°$, $M_0 = 1.52$ FIG. 3d: $\theta = 20°$, $M = 1.3$, $\frac{AC}{a^2} = 0.055$

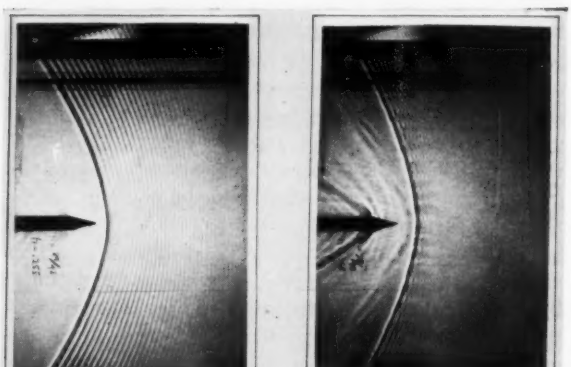

FIG. 4a: $h = 0.255$ FIG. 4b: $h = 0.368$

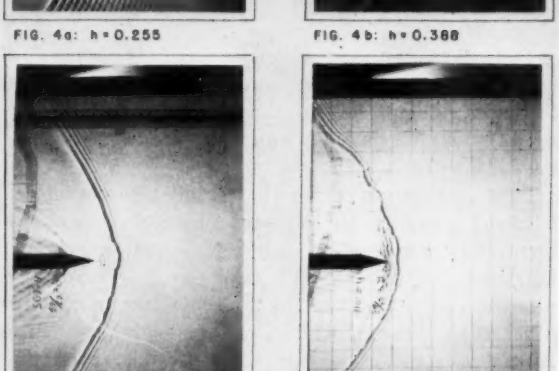

FIG. 4c: $h = 0.695$ FIG. 4d: $h = 1.018$

$\theta = 15°$, $M_0 = 1.20$, $t = 0.75$ in.

Discussion of the Experimental Results

Fig. 3 shows the supersonic flow pattern about a $^3/_4$ in. thick wedge having a nose angle of 20° ($\theta = 10°$) in a still-water depth of 0.33 in. The equivalent to the free-stream Mach Number (M_0) is defined by the carriage speed (V) and the still-water depth (h) as

$$M_0 = V/\sqrt{gh}$$

The theoretical minimum value of M_0 necessary for an attached shock wave to exist at the nose of a 20° wedge is 1.56 for a compressible gas having $\gamma = 2$ (Table 2), while the theory for a hydraulic jump or surge requires $M_0 = 1.51$.

Fig. 3a shows the equivalent of a detached shock wave in steady flow for $M_0 = 1.29$, while Fig. 3b shows the shock wave already at the nose but still curved, proving that it has just become attached (see reference 3) at $M_0 = 1.48$. As would be expected, this result agrees more closely with the hydraulic-jump theory than it does with the compressible gas theory ($\gamma = 2$). However, this difference does not exist in the transonic range defined by $M_0 < \sqrt{2}$. For example, a 10° wedge has the same minimum M_0 of 1.30 for an attached shock to exist either in a compressible gas ($\gamma = 2$) or as a hydraulic jump. The experimental results for a wedge having $\theta = 5°$ closely checked this value (see references 6 or 7).

Fig. 3c presents a completely supersonic attached shock wave at $M_0 = 1.52$ and points out a further difficulty in the analogy—namely, the relatively large thickness of the hydraulic jump or surge as compared to that of the ordinary shock wave in air. This thickness effect invalidates the analogy unless the shock-front radius of curvature is always large. Fortunately, this is generally the case in transonic flow, especially with a detached shock wave.

Fig. 3d illustrates the effect of acceleration on the shape of the detached shock wave, which now continually varies in shape. The nondimensional acceleration parameter is defined by the acceleration (A) multiplied by the nose length (C) and divided by the speed of sound (a) squared, where

$$(AC/a^2) = M_0^2(AC/V^2)$$

The larger this parameter, the more the distortion of the flow pattern (see reference 7).

Fig. 4 demonstrates the effect of water depth upon the wave formation and the group velocity. The pictures were all taken at $M_0 = 1.2$ with a $^3/_4$-in. thick wedge having a nose angle of 30° ($\theta = 15°$). It is seen that for water depths greater than the optimum of $^1/_4$ in., the main surge front representing the detached shock wave is pushed further from the nose and loses the original smooth curvature. Fig. 4b indicates the formation of the secondary wave fronts that alter the shape and location of the detached shock analog. These secondary wave fronts correspond to shock waves

formed at an equivalent free-stream Mach Number that is actually greater than that given by $M_0 = V/\sqrt{gh}$. The expression for M_0 only applies to the wave lengths that have a horizontal tangent ($dc/d\lambda = 0$) in Fig. 1, so that the wave velocity is equal to the more important group velocity. For the other wave lengths the wave velocity itself has no direct effect, and, as previously discussed, the group velocity must be used. Therefore, the equivalent free-stream Mach Number for any group of these wave lengths would be given by

$$M_\lambda = V/[c - \lambda(dc/d\lambda)]$$

which is greater than M_0 for the shorter wave-length gravity waves and less than M_0 for the capillary ripples. As previously pointed out the group velocity for any given wave length is obtained by the intercept on the vertical c axis of the tangent to the curve in Fig. 1. Consequently, different wave lengths, all having different wave velocities, would still have the identical group velocity if they had a common tangent. Then, if a whole series of wave lengths had approximately the same group velocity, any small disturbance composed of them would move at this constant group velocity, which would be equivalent to the speed of sound, although the shape of the disturbance would vary with time unless the wave velocities were also equal, as previously explained. A strong wave front or surge, corresponding to a steady-state shock wave, could be formed only if a considerable portion of the curve of c vs. λ (Fig. 1) formed a nearly straight line. This is so because any finite body essentially produces an infinite number of infinitesimal disturbances, all traveling with their particular group velocity. These infinitesimal disturbances can produce a finite surge moving at the constant speed $V > \sqrt{gh}$ and corresponding to a steady-state shock wave only if a finite range of wave lengths have approximately the same group velocity. If the water depth is greater than $^1/_4$ in., it is therefore possible to have several common group velocities, corresponding to several different speeds of sound. If the capillary ripples are neglected, then the longer gravity waves would have the highest equivalent speed of sound given by $\sqrt{gh}$, while the shorter gravity wave lengths would have an equivalent speed of sound considerably less than the minimum wave velocity. Previous analyses of the analogy (e.g., reference 8) have been in error because they did not realize the importance of the group velocity and because they did not stress the fact that a surge is a finite disturbance that travels at a constant speed much greater than that of an infinitesimal disturbance.

As the depth is increased above $^1/_2$ in., the main surge becomes more distorted until, finally, because of the large variations in the group velocities, no steady-state surge can be maintained. This unsteady state was evident when Figs. 4c and 4d were taken.

Fig. 5 depicts the effect of model size and surface tension. The same geometric shape is used at the same M_0 as in Fig. 4, the wedge now being 3 in. thick. It is seen that the larger model size has produced a relative decrease in the appearance of the capillary ripples, since they correspond to extremely small values of λ. Similarly, the water depth must now be slightly greater before the secondary wave fronts become as strong.

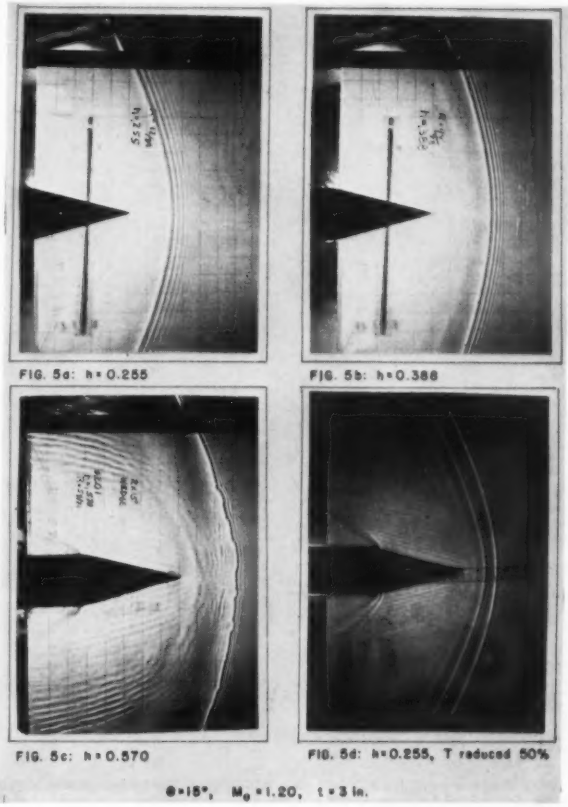
FIG. 5a: h = 0.255

FIG. 5b: h = 0.388

FIG. 5c: h = 0.570

FIG. 5d: h = 0.255, T reduced 50%

θ = 15°, M_0 = 1.20, t = 3 in.

Fig. 5d shows the effect of decreasing the surface tension from 0.005 to 0.0025 lbs. per ft. by adding a wetting agent (Oronite). Strong secondary wave fronts are again formed, even though the water depth remained at its previous optimum value. This is explained by referring to the dotted line in Fig. 1 which corresponds to the 50 per cent decrease in surface tension for a water depth of 0.2 in. The dotted line shows that all λ from approximately $^1/_2$ to 1 in. and from 1 to 2 in. have almost a set of common group velocities and could produce a fairly strong secondary surge.

Fig. 6 shows exactly the same effect of water depth, model size, and surface tension on a circular cylinder. The conclusion is that the optimum water depth for pure water is about $^1/_4$ in. and that the model size should be as large as possible in order to have the larger wave lengths predominate and thereby decrease the relative effect of the shortest gravity waves and the capillary ripples. However, the model size is limited by the width of the tank. For example, a $7^1/_2$-in. diameter cylinder was found to "choke" this 4-ft. wide

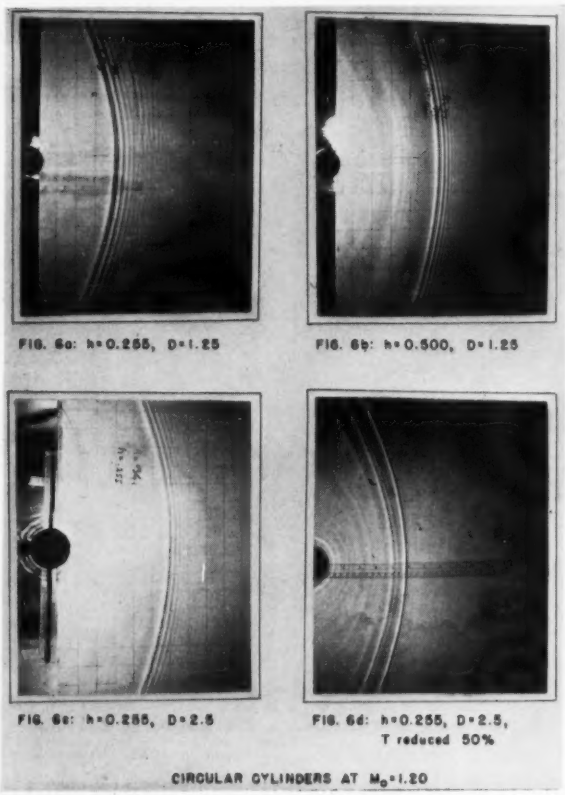

tank for all $M_0 < 1.5$ (see reference 5). This choking phenomena was easily observed as the cylinder started moving. First, the detached shock wave became strong enough to form a Mach reflection at the walls. Then the normal shock portion of the Mach reflection increased in length until it completely spanned the channel moving upstream, ahead of the cylinders.

Comparison of Detached Shock Wave Location with Theory

Because the detached shock wave is in the transonic region and especially because it does not have a sharp radius of curvature, it should provide the most reliable data to test the analogy to a perfect gas with $\gamma = 2$. Figs. 7 and 8 present the experimental measurements of the detachment distance along the line of symmetry for the wedges and the cylinder at various values of M_0. It was found in every case that increasing the still-water depth moved the detached shock considerably further out. In the transonic range there was no noticeable effect of model size on the detached shock location, at least for water depths near $^1/_4$ in. However, the 50 per cent decrease in surface tension seemed to move the detached shock slightly nearer to the circular cylinder (see reference 5).

Unfortunately, there is no satisfactory theory yet available for predicting the detached shock location. Two approximate theories, given in references 9 and 10, are included for comparison. The simplest approximation is the so-called geometric method of Moeckel,[9] which is based on the assumption that

$$y_s/L = \tan \theta_{max.} \tag{3}$$

where $\theta_{max.}$ is the maximum stream-tube deflection that can occur at a given M_0 (Table 1 or 2). y_s is the vertical distance from the sonic point on the body surface to the axis of symmetry of the body. The normal shock or nose of the detached shock wave is then at the distance L from the location of y_s. For a wedge the sonic line appears at the shoulder, so y_s is one-half the thickness (see Fig. 7). For an arbitrary body the sonic line can be assumed to occur at the point where the surface slope is equal to $\theta_{max.}$; consequently, for a circular cylinder the distance L_1 from the centerline to the detached shock is given by

$$(D/2)/L_1 = \sin \theta_{max.} \tag{4}$$

The predicted distances given by Eq. (4) are presented in Fig. 8, using the values of $\theta_{max.}$ for a compressible gas with $\gamma = 2$ (Table 1) and those corresponding to the hydraulic-jump theory. As would be expected, the two curves approach one another for $M_0 < 1.5$ but diverge considerably at the higher Mach Numbers. As previously mentioned, the values of $\theta_{max.}$ for a hydraulic jump exactly approach those of Table 1 for $M_0 < 1.5$ but are more closely approximated by those of Table 2 for slightly higher M_0.

As pointed out by Moeckel,[9] Eq. (3) is more nearly valid for blunt bodies and for transonic Mach Numbers not too near unity. This seems to be the case in Figs. 7 and 8. However, the theory of reference 9 predicts

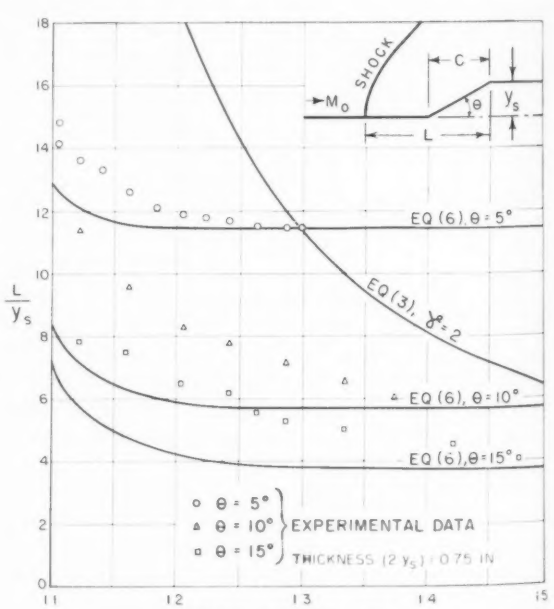

FIG. 7. Comparison of detached shock location for simple wedges.

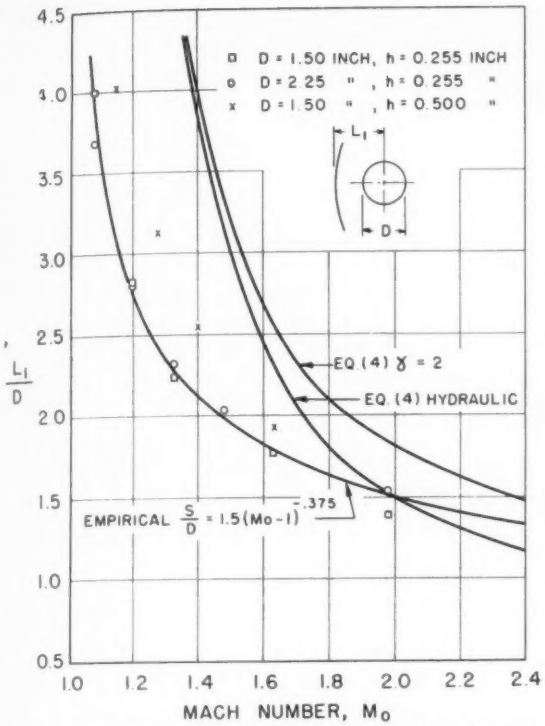

FIG. 8. Effect of water depth and model size on the shock detachment for circular cylinders.

no effect of the nose shape forward of the sonic line, or wedge shoulder, and Fig. 7 proves there is a considerable effect for slender wedges near a Mach Number of unity. The theory presented by the author in reference 10 is more applicable in this case, since it is an approximate first-order solution that is valid for extremely slender wedges near a Mach Number of unity. This theory (see reference 7 or 10) yields the expression

$$1 + \frac{y_s}{(L - C)\theta} = \exp\left[\frac{4\sqrt{2}}{\gamma + 1}(M_0 - 1)^{3/2}\frac{\pi}{\theta}\right] \quad (5)$$

for the wedge shown in Fig. 7. Then, for the analogy with a compressible gas having $\gamma = 2$,

$$\frac{L}{y_s} = \frac{1}{\theta}\left(1 + \frac{1}{\exp\{5.92\,[(M_0 - 1)^{3/2}/\theta]\} - 1}\right) \quad (6)$$

As would be expected, Fig. 7 shows that Eq. (6) is in better agreement with the experimental data nearer a Mach Number of unity, especially for the slenderest wedge.

The Effect of Constant Acceleration on the Detached Shock Wave

The main effect of acceleration, as indicated in Fig. 3d, was to produce a nonsteady detached shock-wave shape that seemed to vary almost periodically from a rounded nose to a flattened, normal shock nose. In order to study this phenomena, a series of photographs was taken of the strong detached shock wave existing in front of a rectangular block 2 in. wide (Fig. 9). The model was started from rest at constant acceleration. The pictures were obtained by mounting a motion-picture camera on the towing carriage itself.

Fig. 9 shows a sequence of photographs at intervals of approximately 0.078 sec. The complete series of six pictures was approximately the cycle representing the periodical change in shape of the detached shock. As the Mach Number increased, at constant acceleration, periodic secondary wave fronts formed between the body and the detached shock. These secondary surges gradually overtook the detached shock, flattening its nose and keeping it at almost a constant distance ahead of the body, independent of the increasing M_0. As seen in Figs. 7 and 8, the detached two-dimensional shock wave, in steady flow at a constant velocity, is nearer the nose at the higher Mach Numbers. On the other hand, it is known that for the one-dimensional flow ahead of a moving piston the shock waves are further ahead of the piston at the higher speeds and still further with a finite constant acceleration. In the present tests it was found that the detached shock wave ahead of a two-dimensional rectangular block, starting from rest at a constant acceleration, approxi-

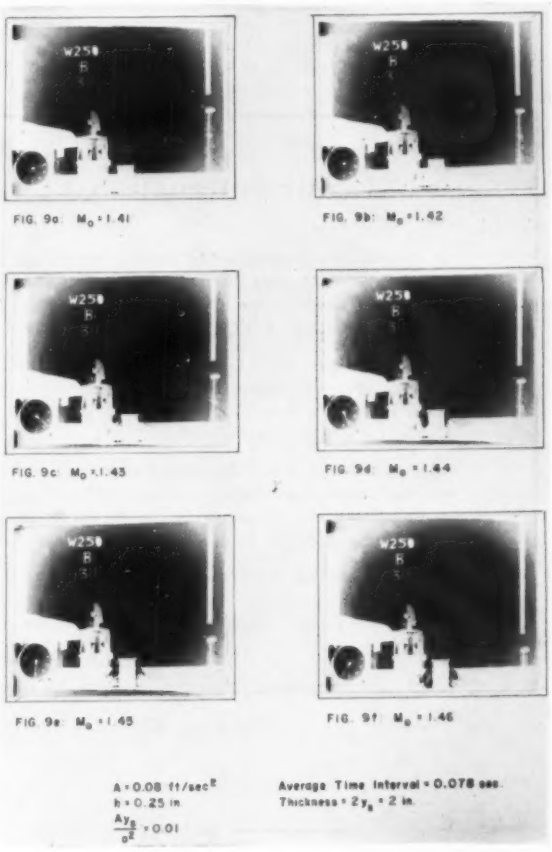
FIG. 9a: Mo = 1.41
FIG. 9b: Mo = 1.42
FIG. 9c: Mo = 1.43
FIG. 9d: Mo = 1.44
FIG. 9e: Mo = 1.45
FIG. 9f: Mo = 1.46
A = 0.08 ft/sec²
h = 0.25 in.
Ay/a² = 0.01
Average Time Interval = 0.078 sec.
Thickness = 2ys = 2 in.

FIG. 9. Constant acceleration.

mately followed the steady-state detachment distance for small values (less than 0.01) of the nondimensional acceleration parameter Ay_s/a^2. However, as the magnitude of this parameter was increased, the detachment distance became more nearly a constant, practically independent of the instantaneous Mach Number. The tendency of the detached shock wave to move toward the body as the Mach Number increased seemed to be counteracted by the energy supplied to it by the periodic formation of the secondary surges formed downstream and continually overtaking and joining the main detached shock front.

Further studies are now in progress to determine the reason for the apparently periodic fluctuation and to extend the validity of the analogy to other nonsteady flow problems. This seems to be the most useful service of the analogy, if valid, since it is a field that is difficult to investigate in ordinary two-dimensional gas flow.

References

[1] Preiswerk, Ernst, *Application of the Methods of Gas Dynamics to Water Flows with Free Surface*, N.A.C.A. T.M. Nos. 934 and 935, March, 1940.

[2] Lamb, H., *Hydrodynamics*, 6th Ed., pp. 381 and 457; Dover Publications, New York, 1945.

[3] Laitone, E. V., *Exact and Approximate Solutions of Two-Dimensional Oblique Shock Flow*, Journal of the Aeronautical Sciences, Vol. 14, No. 1, pp. 32–34, January, 1947.

[4] Bruman, J. R., *Application of the Water Channel-Compressible Gas Analogy*, North American Aviation, Inc., Report No. NA-47-87, March 3, 1947.

[5] Flowers, J. V., *The Development of Experimental Techniques for the Study of Compressible Flow by the Hydraulic Analogy*, Master of Science Thesis, University of California, Berkeley, June, 1951.

[6] Hedgecock, J. L., *A Study of Detached Shock Waves by the Water Channel-Compressible Gas Analogy*, Master of Science Thesis, University of California, Berkeley, September, 1950.

[7] Laitone, E. V., *An Experimental Investigation of Transonic and Accelerated Supersonic Flow by the Hydraulic Analogy*, University of California, Institute of Engineering Research, Series 3, No. 315, July 3, 1950.

[8] Shapiro, A. H., *An Appraisal of the Hydraulic Analogue to Gas Dynamics*, M.I.T. Guided Missiles Program, Meteor Report No. 34, April, 1949.

[9] Moeckel, W. E., *Approximate Method for Predicting Form and Location of Detached Shock Waves Ahead of Plane or Axially Symmetric Bodies*, N.A.C.A. T.N. No. 1921, July, 1949.

[10] Laitone, E. V., *A Note on Detached Shock Waves*, Journal of the Aeronautical Sciences, Vol. 16, No. 7, pp. 441–442, July, 1949.

Eighth International Congress for Applied Mechanics

The Eighth International Congress for Applied Mechanics is to be held at the University of Istanbul, Istanbul, Turkey, on August 20 to 28, 1952. American participation in the Congress is being organized by the U.S. National Committee on Theoretical and Applied Mechanics, which is a Joint Committee of the A.S.M.E., A.I.Ch.E., S.E.S.A., A.S.C.E., I.A.S., A.M.S., and A.P.S.

Five sessions are to be held, as follows: (1) Elasticity, Plasticity, and Rheology; (2) Fluid Mechanics (Aerodynamics and Hydrodynamics); (3) Mechanics of Solids (Ballistics, Vibrations, Friction, and Lubrication); (4) Statistical Mechanics, Thermodynamics, and Heat Transfer; (5) Mathematics of Physics and Mechanics—Methods of Computation.

Membership in the Congress is open to all individuals interested in Applied Mechanics. Each member may present two 15-minute papers. Abstracts (not to exceed 400 words) must be submitted not later than June 1, 1952, on forms that may be secured from the Secretary of the Congress (**Sekizinci Enternasyonal Teorik ve Tatbiki Mekanik Kongresi, P. K. 245, Istanbul, Turkey**).

The American Express Company is the official travel agency for the Congress. For details of the groups tours being planned, write to: **American Express Company, 624 Fourteenth St., N.W., Washington, D.C.** Individual tours to meet special requirements may also be arranged through this agency.

Analysis of Nonuniform Columns and Beams by a Simple D.C. Network Analyzer

GEORGE W. SWENSON, JR.*
Washington University

SUMMARY

The analysis of beams, columns, and beam-columns whose flexural rigidities and/or lateral loadings are arbitrary functions of position can be solved with the aid of a simple electrical network analyzer. In the case of the column, the lowest critical load can be determined with considerable accuracy. The electrical network is of ladder configuration, with displacement represented by node-pair voltages and moments by currents. The column problem requires the use of a number of "negative resistors," which are simulated by subnetworks of positive resistors and adjustable voltage sources.

Problems are discussed which illustrate the application of the analyzer. In the case of a column with a single abrupt transition in rigidity, the value of the critical load is determined to within 0.5 per cent of the analytically calculated value.

INTRODUCTION

THE DETERMINATION OF THE DEFLECTION of a nonuniform beam or beam-column or of the critical load of a nonuniform column can be simplified and expedited by the use of an electrical network analyzer. The general method of attack is to replace the differential equation of bending by a set of approximately equivalent finite-difference equations, a set of linear algebraic equations that must then be solved simultaneously to yield the deflections at a number of equally spaced stations along the member. For acceptable accuracy, one must write a relatively large number of equations; therefore, the computational labor involved in their solution is great enough to warrant the use of some mechanical aid. The similarity in form of the difference equations to the current equations for a lumped-parameter electrical network suggests that such a network be used as an analog to the problem at hand and that the solution be obtained by measurement of the electrical quantities. When such a possibility is further investigated, it is found that both positive and negative network parameters are required. This suggests, in turn, the use of alternating currents, with inductive reactances as the positive parameters and capacitive reactances as the negative parameters or vice versa. However, for reasons of accuracy and economy, it seems desirable to use an all-resistance, direct-current network, if possible, and it has proved feasible to synthesize the required "negative resistors" from positive resistors and voltage or current sources.

Received August 10, 1951.

* Associate Professor of Electrical Engineering. Formerly, Project Associate, Engineering Experiment Station, University of Wisconsin.

The result is a network analyzer capable of solving the general slender beam-column problem rapidly and accurately by an iterative process of adjustment of the network. The saving in labor over conventional numerical techniques is considerable, and the device is useful either for synthesis or analysis

NOMENCLATURE

The following symbols are used:

E	=	Young's modulus, in general, a function of x
h	=	length of finite-difference interval
I	=	second moment of area, in general, a function of x
i_n	=	forcing current inserted at nth node
l	=	length of beam or column
M	=	bending moment, in general, a function of x
P	=	axial load (force) on a column
$P_{cr.}$	=	critical load of a column
R	=	base resistance of network analyzer
R_{nn}	=	resistance connected between nth node and ground
V_n	=	node-to-ground voltage at nth node
x	=	space variable in direction along member
y	=	lateral deflection of member
β_n	=	$Ph^2/(EI)_n - 2$, coefficient of y_n in the nth difference equation
ϕ_n	=	$(M/EI)_n$, normalized bending moment in the nth difference equation

THE DIFFERENCE EQUATIONS AND THEIR ELECTRICAL ANALOG

The differential equation of bending of a slender beam-column is

$$(d^2y/dx^2) + (P/EI)y = M/EI \qquad (1)$$

where the coefficient of y and the term on the right-hand side may vary with x. Referring to Fig. 1, the approximation to the second derivative at point 0, taken from the calculus of finite differences,[1] is

$$(d^2y/dx^2)_0 \approx (y_a + y_b - 2y_0)/h^2 \qquad (2)$$

Thus, at point 0, Eq. (1) is approximated by

$$y_a + y_b + y_0[h^2P/(EI)_0 - 2] = h^2(M/EI)_0 \qquad (3)$$

A similar equation can be written at each of the equally

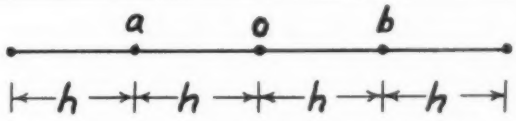

FIG. 1. The finite-difference lattice

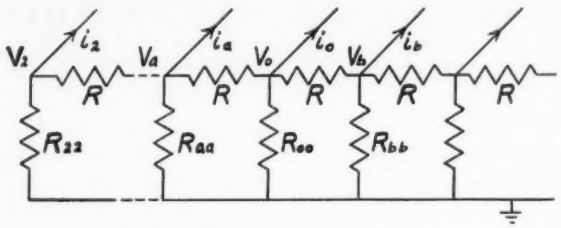

FIG. 2. The d.c. network analyzer.

spaced stations on the member. As h becomes vanishingly small, these equations become exact. After a few trial problems have been solved, experience indicates the number of intervals necessary to assure the desired accuracy. As an example of the complete setup of a problem, the following matrix equation represents a member divided into four intervals, with both ends (stations 1 and 5) assumed to be fixed:

$$\begin{bmatrix} \beta_2 & 1 & 0 \\ 1 & \beta_3 & 1 \\ 0 & 1 & \beta_4 \end{bmatrix} \begin{bmatrix} y_2 \\ y_3 \\ y_4 \end{bmatrix} = \begin{bmatrix} \phi_2 \\ \phi_3 \\ \phi_4 \end{bmatrix} \tag{4}$$

The electrical analog of this system is most easily set up on the basis of Kirchhoff's current law, which states that the sum of the currents entering a junction point, or node, must be zero. Fig. 2 illustrates the network with the desired properties. The current-law equation that applies at node 0 is

$$\frac{V_a - V_0}{R} + \frac{V_b - V_0}{R} - \frac{V_0}{R_{00}} = i_0 \tag{5}$$

or

$$V_a + V_b - V_0(R/R_{00} + 2) = i_0 R$$

Thus, $V_n = y_n$, provided that

$$R_{nn} = -R(EI)_n/(h^2 P) \tag{6}$$

and

$$i_n = h^2(M/EI)_n/R \tag{7}$$

An exception to Eq. (6) occurs at the station adjacent to a station whose displacement is assumed to be zero. In this case, the network at the "adjacent" node has the configuration of node 2 in Fig. 2, corresponding to the first row of the matrix in Eq. (4), and

$$R_{22} = R/[1 - h^2 P/(EI)_2] \tag{8}$$

The Network Analyzer

In Eq. (8), R_{22} is positive for values of h which give reasonable accuracy. R_{nn}, however, representing the node-to-ground resistance at a point in the *interior* of the network, is negative for any value of h. Such a negative resistor can be simulated by the circuit of Fig. 3, in which R_n is a resistance whose value is equal to the magnitude of the desired negative resistance, R_{nn}, and in which the resistors R' have arbitrary but equal values. With the circuit in place in the analyzer, the rheostat R_s is adjusted manually until the voltmeter V reads zero. Under this condition, a current V_n/R_n flows *out* of the circuit, *into* the node of the analyzer, so that the circuit simulates the desired negative resistor.

In the present analyzer, the resistors R_n are arranged to be plugged into jacks on the analyzer panel. Inexpensive volume control potentiometers are used, their values being adjusted on a Wheatstone bridge during the setting-up process. Though 15 or 20 junction points would probably be sufficient for most problems, the present analyzer has provisions for solving 100 simultaneous equations, having been constructed originally for application to the two-dimensional wave equation.[2] Because adjustment of one of the resistors R_s affects the balance of each of the other negative resistance circuits, an iterative adjustment process must be applied until all the voltages V are zero. The process converges for all axial loads less than, and also for a small range just above, critical load.

The results described below could be duplicated on a nine-equation analyzer whose fixed resistors are of 1 per cent tolerance. For measuring the voltages, an electronic d.c. voltmeter is needed, capable of indicating one millivolt. A value of R of about 100 ohms is convenient. Because all the negative-resistance voltage supplies have one common terminal, they can be derived from the same source, which should preferably be a battery of storage cells for constancy of voltage. About 30 volts is adequate. It is estimated that such an analyzer could be built at a cost for materials of less than $100, exclusive of battery, voltmeter, and Wheatstone bridge.

Determination of Critical Load

The difference equations of a slender column with no lateral loads are those of Eq. (4) with the ϕ's equal to zero. Such a system has a nontrivial solution only if its determinant vanishes, and this condition might be used for finding the critical load. However, the numerical labor is great when the number of stations

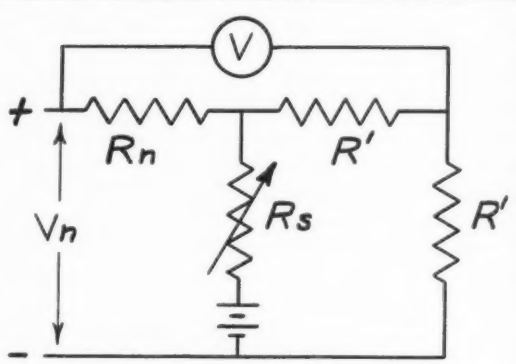

FIG. 3. The negative resistor circuit.

is large enough to yield acceptable accuracy, so that it is preferable to get the results from the analyzer.

When the analyzer is set up to represent such a column, the value of P being arbitrary, and when the negative resistances are systematically adjusted, it is found that a trivial solution is obtained. The remedy is to apply a battery between some one node and ground to force the network to assume a solution at that point conforming to the applied voltage. When the adjustment process is completed, it is found that a current exists in the battery circuit. This current represents the lateral load at that point required to cause a deflection corresponding to the battery voltage. This is true for P either less than or greater than $P_{cr.}$; the analyzer does not concern itself with the fact that the deflection is unstable in the latter case. The current is positive (toward the node) for P less than $P_{cr.}$ and negative for P greater than $P_{cr.}$ For P equal to $P_{cr.}$, a finite deflection requires no lateral force, so that the battery current is zero. Thus, the critical load is determined by graphing the current required to produce a certain node-to-ground voltage at an arbitrary station in the network and by interpolating to the value of P which corresponds to zero current.

Example I. Critical Load of a Tapered Column

A pin-ended column whose flexural rigidity has the form

$$EI = (EI)_0(1 + x/l) \tag{9}$$

was investigated by the above method, using $h = l/10$, and the critical load was found to be

$$P_{cr.} = 14.3(EI)_0/l^2 \tag{10}$$

This is 3.4 per cent lower than that of a uniform column with the same *average* flexural rigidity. The time required for this solution, including calculation of coefficients, setting up the network, and measurement of deflections for several different lateral loads, was approximately two hours.

Example II. Critical Load of a Stepped Column

This pin-ended column has a flexural rigidity described by the equations

$$\left.\begin{aligned} EI &= (EI)_0, & 0 \leqslant x < l/2 \\ EI &= 1/8(EI)_0, & l/2 < x \leqslant l \end{aligned}\right\} \tag{11}$$

Because one station was located at the point of transition, the rigidity at this point was arbitrarily made equal to the average of the other two values. Again, using ten finite-difference intervals (nine equations), the critical load was determined to be

$$P_{cr.} = 0.196(EI)_0/l^2 \tag{12}$$

This value checks within 0.5 per cent of the previously published analytical solution,[3] obtained with the aid of the Laplace transformation, and within 1.7 per cent of an experimental value[3] for a Douglass fir column.

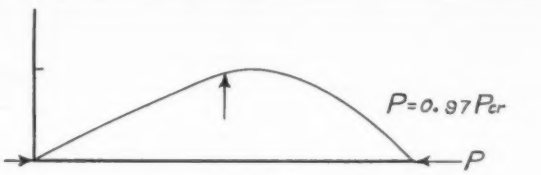

Fig. 4. Deflection of the stepped column.

Higher Modes of Buckling

Should it be desired to know the critical loads for higher modes of buckling, they can be determined by a trial-and-error process. The column is divided into sections corresponding to an initial estimate of the locations of the points of zero displacement. Then the critical loads of the individual sections are determined by means of the analyzer, and the locations of the zero points adjusted to make the respective critical loads more nearly equal. This process is continued until the desired accuracy is attained. The critical load for the mode in question is then equal to the critical load of any one of the sections.

This scheme, and indeed the entire technique of the analyzer herein described, can be applied equally well to problems in the oscillations of nonuniform strings, plane-wave acoustical resonators, coaxial electromagnetic resonators, and so on.

Beam-Columns and Beams

It is necessary to apply a simulated lateral load in determining the critical load of a column; thus the solution of such a problem also includes the solutions of one or more beam-column problems. For example, Fig. 4 illustrates the deflection of the stepped column under the influence of a lateral load applied at the center and an axial load of slightly less than the critical value. Deflections produced by arbitrary distributions of lateral loading are easily determined by inserting currents at the several node points of the network, according to Eq. (7).

The beam problem in the absence of axial load is particularly simple. In this case the term in y of Eq. (1) is absent, so that no node-to-ground resistors, either positive or negative, are required. The solution is available immediately when the appropriate currents, as determined from Eq. (7), are inserted into the appropriate nodes. These currents are most conveniently obtained from a common high-voltage power supply through dropping resistors whose values are high compared with the base resistance of the network.

(*Continued on page 278*)

Reply to Discussions of the Wright Brothers Lecture*

P. B. WALKER†

Royal Aircraft Establishment

THE DISCUSSIONS FOLLOWING the Wright Brothers Lecture have added much valuable material to the original paper. Though there are minor differences of opinion on some matters, the discussions as a whole are remarkable for the general measure of agreement on fundamentals. The comments which follow are mainly directed towards answering specific questions or in response to requests for further information.

Mr. A. B. Callender asks how the fatigue test criterion —an alternating load of $7^1/_2$ per cent of the design ultimate, applied two million times—was obtained. It is, of course, difficult to trace all the tentative processes leading to an empirical criterion, but there are a few points which may be of interest.

The single fatigue test has to represent a wide range of loading conditions, corresponding to an extensive working portion of the endurance (*SN*) curve. From this standpoint, the $7^1/_2$ per cent alternating load is chosen as being well placed in a sensitive region of the typical curve and as not calling for undue length of testing time. In addition, the criterion has to cover in a somewhat indefinable way the cumulative effect of mixed cycles. In this connection it is of interest to record that recent British calculations indicate that $7^1/_2$ per cent for the alternating load is a little on the high side theoretically, but not more so in practice than is required to give a reasonable working margin of fatigue strength. This conclusion is at variance with Mr. Callender's figures, though it is endorsed by a later speaker (Mr. Hitchcock).

It is intended that the complete criterion be modified as necessary with increasing experience or to meet special conditions. In general, it is simpler to alter the required number of cycles than the alternating load. The two million cycles stipulated is regarded as corresponding roughly to a life of 30,000 flying hours or about 10 years. Within reasonable limits, however, proportionate reduction is permissible when a shorter life is expected for reasons not concerned with fatigue. Adjustments are also to be expected when fatigue loading data are available for particular aircraft operating over particular routes. The original criterion was intended to set a conservative standard at which designers were advised to aim. Later experience, obtained since the lecture, indicates that the criterion may not always err on the side of safety.

Professor N. J. Hoff's comments are most encouraging. In a deliberate presentation of a case for greater recognition of experimental work in the structural field, there was a danger of appearing to minimise the value of mathematical and theoretical work. There is, of course, no conflict between the two branches of structural research, but it is good to have this view endorsed by an outstanding leader in theory of structures.

Mr. Paul Kuhn, whilst recognising the value of small-scale work, expresses doubts as to its accuracy. I do not share these doubts. As stated in the original paper, the model work is not regarded as a method for absolute prediction of stresses in real structures, but British experience leads to the conclusion that it is reliable for comparative work such as the examples given in the paper.

On the question of comparison between "aerodynamic" and "structural" ribs, Mr. Kuhn gives N.A.C.A. results conflicting with those of R.A.E., and suggests that this discrepancy is an indication of the margin of experimental error. I would suggest some other explanation, though I cannot speak with certainty in the absence of detailed knowledge of the N.A.C.A. tests. The R.A.E. models had ribs designed to represent typical ribs as used on actual aircraft. Heavier ribs, especially ribs with heavy flanges, might behave differently; but in this event a direct comparison becomes difficult and results are open to different interpretations. According to R.A.E. calculations, moreover, the participation stresses mentioned by Mr. Kuhn are not significant for ordinary light ribs, and for heavy ribs become significant only at angles of sweepback exceeding 60°. The R.A.E. tests, incidentally, did not go beyond 45°.

Mr. Kuhn's suggestion that the engine loading effect could have been predicted from theoretical work already published in England is not strictly correct. The relevant portion of this work dealt only with a change of torque. The effect of the offset engine load is not so simple, and it is much greater than could have been accounted for by the then existing theory.

In reply to Mr. Kuhn's query about the future use of the counting accelerometer, it can be stated that this will be installed on as many aircraft as operators will tolerate. With increasing realisation of the fatigue danger, it may well be on the way to becoming a piece

* Walker, P. B., *The Experimental Approach to Aircraft Structural Research*, Journal of the Aeronautical Sciences, Vol. 19, No. 3, p. 145, March, 1952.

† Head, Structures Department.

of standard equipment for fitting to all civil and transport aircraft. The point about speed being significant as well as acceleration is fully appreciated, and is covered in my reply to Mr. Hitchcock.

Mr. Walter Ramberg raises some vital points about design and test interpretation which unfortunately cannot be treated adequately in brief comments. As I understand the term, "general instability" did not occur in any of the tests analysed. Nevertheless, it does not follow that the only alternative was local weakness which "could and should have been caught before the test of the complete structure." Stress diffusion, as mentioned in the paper, and other allied effects often lead to premature failure of a structure whose components would have been regarded as satisfactory when treated individually.

As regards Mr. Ramberg's next point, it is not generally possible to make a clear-cut distinction between failures which could have been prevented by careful design and construction and those which could not have been predicted. In the first place, the economics of design comes into the picture. The prospects of predicting any form of failure depend upon the time, money, and effort that can be expended in design research and theoretical study. Without setting precise limits to these, it is impossible to divide premature failures generally into predictable and unpredictable classes. In the second place, it has to be borne in mind that the designer normally makes every endeavour to produce a satisfactory structure, and does not hesitate to make laborious calculations when these are thought to be necessary. The result is that—apart from the few unqualified mistakes—premature failure, when it occurs, frequently admits of no simple explanation and is attributable to a complexity of causes. Faced with such a situation, it becomes difficult for the structural specialist to say exactly what it is that the designer is supposed to have predicted.

Professor E. E. Sechler does a great service in giving a warning against unrestrained enthusiasm for analog and digital computing machines. Development in this field is extremely important, but must not be allowed to reduce interest in the direct experimental approach. The two approaches are not alternatives, and both increase in value when they are followed in parallel. Incidentally, in applying the Xylonite-model technique there are times when a model can almost be regarded as an analog machine rather than as a physical representation of a structure.

Mr. J. F. McBrearty appears to be seriously concerned at what he regards as the over-ready acceptance of the design philosophy by which structures are tested, broken, modified and re-tested as a matter of deliberate policy. I entirely agree with him in pointing out the dangers of unrestrained use of the principle which underlies this philosophy. As stated in my paper, it is possible to produce a structure that is altogether too weak, and beyond remedial action, whilst the time expended in repairs and re-tests might well become intolerable. I do not agree, however, that the principle is being misused to any appreciable extent. In Britain, the evidence indicates that a good practical compromise is being achieved, and I would have thought that much the same applies in America.

I entirely agree with Mr. McBrearty that testing is no substitute for a proper stress analysis. In my view, testing of a structure that has not been fully investigated theoretically is largely a waste of time, money, and effort. Testing is a safeguard against direct mistakes remaining undetected, but this is only part of its purpose. It should be regarded as a check on theory, of a kind which will benefit not ony the particular aircraft tested but many others which follow.

Mr. L. M. Hitchcock's remarks on ordinary static strength testing are of great interest, and a welcome additon to my own records. There is only one point on which comment appears appropriate, and that concerns the advisability of having a central testing unit available to the whole country. The situation in U.S.A. is different from that in England owing to the much greater distances involved. Even in Britain, however, it is considered that the central unit should not operate in competition with industry, and that its contribution must be additional and complementary to industry's own effort. It is considered that there is a purpose to be served by a central advisory body in the strength testing field, but that such a body cannot function realistically without first-hand testing experience. Furthermore, there are long-term and uneconomic research projects which industry cannot normally be expected to undertake.

On the question of testing pressure cabins in water, I think Mr. Hitchcock overestimates the difficulties. Pressure testing equipment, whether permanent or improvised, is much more easily produced than might at first sight be expected. It is, moreover, not at all difficult to arrange fatigue tests to reproduce the raising and lowering of cabin pressure as occuring on aircraft in operational use. Successful fatigue experiments, in fact, have been made in the water tank illustrated in the paper.

The value of information additional to that given by the counting accelerometer is appreciated. There is a more elaborate version which records photographically speed, time, and altitude, as well as acceleration counts. This is necessarily heavier and more expensive than the simple one, but does not need to be fitted so frequently. It should be understood that, as Mr. Paul Kuhn stated, this additional information is required for the benefit of subsequent designs or for the same aircraft operating under different conditions. The simple version covers adequately the normal fatigue hazards of the particular aircraft on which it is fitted.

There are a number of direct queries put by Mr. Hitchcock on fatigue which can be answered briefly.

(a) It is intended eventually to cover a range of both high and low temperatures in the testing programme for the Meteor tail plane. (b) As to the choice of materials, I prefer not to comment on the particular materials mentioned, but feel justified in saying that in future more consideration will have to be given to the fatigue properties of materials and less to ultimate static strength—at least for civil and transport aircraft. (c) There is a nickel-chromium steel (British Specification D.T.D.247) which has about the same coefficient of expansion as aluminium alloy. It appears to have been used at one time for dealing with a similar problem for engines, but is probably unsuitable for bolt manufacture. Research to discover a suitable steel might well be justified. (d) The interference fit found necessary to produce increased life of joints having steel bolts loaded in shear is approximately three thousandths of an inch for $^1/_2$-in. and $^3/_4$-in. diameter steel bolts. It is interesting to remark that as the negative tolerance is progressively increased from zero there is at first no significant change in fatigue life, but then the life increases rapidly to something of the order of 100 times.

Dr. Karl Arnstein's comments reached me later than the others, and there is only one specific point on which I would like to comment. It is true that scale-model work, just as mathematical analysis, cannot when directly applied be more accurate than the simplifying assumptions. The main object in using the models for comparative work as described in my paper, however, was to nullify most of the errors introduced by simplifications. With reasonable care these can usually be made to affect equally the two models that are being compared, and so bring out the differences relating to the one particular phenomenon or structural principle that is being studied.

I am grateful to Dr. Arnstein for his useful summary of the whole situation for present-day structural work. It is true that "many roads lead to Rome," and, while we should all study the methods of others, success is possible only with those methods in which we have gained confidence through direct experience.

Analysis of Nonuniform Columns and Beams by a Simple D.C. Network Analyzer

(*Continued from page 275*)

Conclusions

The network analyzer technique for nonuniform beams and columns compares favorably with conventional techniques of numerical analysis, especially with regard to time consumption, mental effort, and accuracy. As compared with other types of analog computing equipment, the d.c. analyzer offers outstanding advantages in economy and accuracy.

Although the examples presented involve only pin-ended members, any other boundary conditions can be accommodated as well. The analyzer is therefore adaptable to any statically determinate problem involving a slender beam or column.

References

[1] Southwell, R. V., *Relaxation Methods in Theoretical Physics*, 1st Ed., p. 19; Oxford University Press, London, 1946.

[2] Swenson, G. W., Jr., *A Direct-Current Network Analyzer for Solving Wave-Equation Boundary-Value Problems*, Ph.D. Thesis, University of Wisconsin, 1951.

[3] Thomson, W. T., *Critical Load of Columns of Varying Cross Section*, Journal of Applied Mechanics, Vol. 2, No. 2, pp. 132–134, June, 1950.

Readers' Forum

BRIEF REPORTS of investigations in the aeronautical sciences and discussions of papers published in the JOURNAL are presented in this special department. The publication will be completed approximately 8 to 10 weeks after receipt of the material. The Editoral Committee does not hold itself responsible for the opinions expressed by the correspondents. Contributions sohuld not exceed 800 words in length.

Secondary Flow in Cascades

Hsuan Yeh
Department of Mechanical Engineering, The Johns Hopkins University, Baltimore
December 20, 1951

THE PROBLEM OF SECONDARY FLOW IN CASCADES received much attention recently because of its close relationship with the flow in a turbomachinery. In a recent article[1] in the Readers' Forum of this JOURNAL an attempt was made to derive the secondary flow in cascades from the principle of conservation of circulation. The interpretation of this principle (and, hence, the conclusion reached in reference 1), however, needs some clarification.

An approximate solution to this problem has been obtained by Squire and Winter[2] and Hawthorne.[3] However, the following shows that essentially the same results can be obtained in a much more direct manner.

For incompressible nonviscous steady flows, the principle of permanence of vorticity can be expressed by[4]

$$d\bar{\Omega}/dt = (\bar{V}\cdot\nabla)\bar{\Omega} = (\bar{\Omega}\cdot\nabla)\bar{V} \tag{1}$$

where $\bar{\Omega}$ is the vorticity vector and $\bar{V}$ is the velocity vector.

If our interest is to find the variation along a stream line of the vorticity component which is parallel to the stream line (this vorticity component gives rise to the so-called secondary flow), we seek to find the value of $\bar{V}\cdot\nabla(\bar{\Omega}\cdot\bar{V})$. Now,

$$\nabla(\bar{\Omega}\cdot\bar{V}) = (\bar{V}\cdot\nabla)\bar{\Omega} + (\bar{\Omega}\cdot\nabla)\bar{V} + \bar{V}\times(\nabla\times\bar{\Omega}) + \bar{\Omega}\times(\nabla\times\bar{V})$$

is a vector identity. Therefore, the dot product of $\bar{V}$ with the above gives

$$\bar{V}\cdot\nabla(\bar{\Omega}\cdot\bar{V}) = \bar{V}\cdot[(\bar{V}\cdot\nabla)\bar{\Omega} + (\bar{\Omega}\cdot\nabla)\bar{V}] \tag{2}$$

Let ξ be the vorticity component parallel to the stream line, q be the absolute magnitude of the velocity vector $\bar{V}$(i.e., $q = |V|$), then $\xi = (\Omega\cdot\bar{V})/q$. Hence, Eq. (2) can be written, with the help of Eq. (1), as

$$\bar{V}\cdot\nabla(\xi q) = 2\bar{V}\cdot[(\bar{\Omega}\cdot\nabla)\bar{V}] \tag{3}$$

Integrating along a stream line, we obtain,

$$(\xi q)_2 - (\xi q)_1 = 2\int_1^2 \frac{\bar{V}\cdot[(\bar{\Omega}\cdot\nabla)\bar{V}]}{q}\,ds \tag{4}$$

where ds is an elementary distance along the stream line. A similar expression appears as Eq. (10) of reference 3. However, in evaluating the integral of Eq. (10) of reference 3, one experiences some difficulty when there is a stagnation point along the stream line. This difficulty seems to have been removed when the above equation [Eq. (4)] is used instead, since the integrand of Eq. (4) remains finite when q goes to zero. Although this shows that ξ, contrary to some earlier theories, does not become infinite *downstream* of a stagnation point, the calculation is not made any easier because the linearization process (below) fails when ξ is not very small.

To obtain a solution to Eq. (4), it is desirable that some approximation be made. The most common one is the assumption that the value of ξ is so small that the main $\bar{V}$ and $\bar{\Omega}$ are not affected by it. This is essentially a process of linearization. Applying this to a cascade and approximating the passage between any two blades by a curved channel as shown by Fig. 1, it is seen that $(\bar{\Omega}\cdot\nabla)\bar{V}$ or the variation along the direction of $\bar{\Omega}$ (in this case along r) of the velocity vector is

$$(\bar{\Omega}\cdot\nabla)\bar{V} = |\Omega|(d\bar{V}/dr)$$

If we further assume that the turning is made in a passage of a circular arc with an arc angle of ϵ, that the flow in the circular passage is that of a free vortex, and that the channel is so narrow compared with the radius of turn that the latter is essentially the same (r_0) for all stream lines, then,

$$\frac{d\bar{V}}{dr} = \frac{d}{dr}\left(\frac{V_0 r_0}{r}\right) = -\frac{V_0}{r_0}$$

Furthermore, since $(\bar{\Omega}\cdot\nabla)\bar{V}$ is a vector along the direction of $\bar{V}$,

$$\bar{V}\cdot[(\bar{\Omega}\cdot\nabla)\bar{V}] = -q^2\Omega/r_0$$

In Eq. (4) and for this case, $(\xi q)_1 = 0$ and $ds = r_0 d\theta$. Also, by this approximation, q and Ω are both constant. Hence,

$$\xi_2 = -2\epsilon\Omega \tag{5}$$

which is also obtained in references, 2 and 3.

Physically, it is interesting to note in connection with Eq. (5) that one-half of the secondary vorticity ξ is caused by the turning of the streamline by an angle ϵ, assuming $\bar{\Omega}$ remains *exactly* constant (the component of $\bar{\Omega}$ along the new velocity direction is

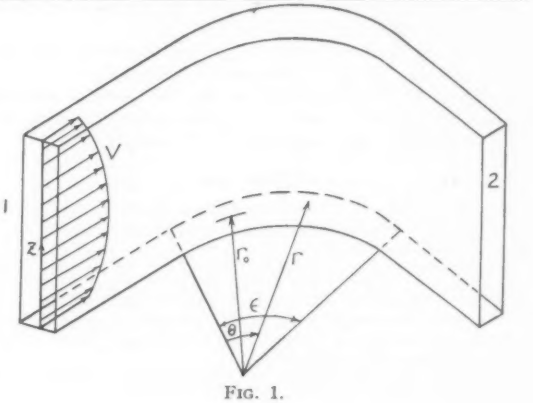

FIG. 1.

therefore $\xi\Omega$). However, we also have the other half of ξ caused by the continuous reorientation of original vorticity, as clearly indicated by Eq. (1). Since reference 1 ignores this second half of ξ, the result therefore appears to be less representative. There is also some doubt as to the justification of any refinements based on the actual cascade geometry, unless more refined application of the exact Eq. (4) is made at the same time.

Apart from the secondary vorticity discussed above, there is the additional secondary vorticity due to the shedding of trailing vortices behind the cascade blade, when the circulation along the blade span is nonuniform. The total induced flow is therefore the sum of two flows induced by the two kinds of vorticity. The two kinds of vorticity, however, are at different locations relative to the cascade. A simple algebraic addition of the two vorticities, disregarding their variation from point to point, appears inadequate to prove that induced velocity is a minimum when the exit velocity is axial, as is claimed in reference 1.

References

[1] Stephenson, J. M., *Secondary Flow in Cascades*, Readers' Forum, Journal of the Aeronautical Sciences, Vol. 18, No. 10, p. 699, October, 1951.

[2] Squire, H. B., and Winter, K. G., *The Secondary Flow in a Cascade of Airfoils in a Nonuniform Stream*, Journal of the Aeronautical Sciences, Vol. 18, No. 4, p. 271, April, 1951.

[3] Hawthorne, W. R., *Secondary Circulation in Fluid Flow*, Gas Turbine Laboratory, Massachusetts Institute of Technology, May, 1950.

[4] Milne-Thomson, L. M., *Theoretical Hydrodynamics*, 2nd Ed., p. 78; Macmillan & Co., London, 1949.

Sweptback Wing Stress Analysis

L. A. Goran
McDonnell Aircraft Corporation, St. Louis, Mo.

November 19, 1951

TWO RECENT PAPERS[1, 2] have reviewed the theoretical and experimental literature on the sweptback wing stress-analysis problem. On this subject, two McDonnell Aircraft Corporation reports,[3, 4] not discussed in these references, should be of general interest.

In reference 3, test results and a minimum strain energy method of analysis are presented for a sweptback box beam having ribs parallel to the air stream.

A summary of the work presented in reference 4 is given below:

A minimum energy method of analysis is presented for the problem of the four-element sweptback box beam. The solution consists of a set of self-equilibrating "correcting" loads that are added to the loads calculated by ordinary bending theory.

The solution is extended to apply to the case of a multicelement sweptback wing by assuming that the correcting loads have a linear stress distribution across the top and bottom cover plates.

An approximate "two-bay" method of analysis is presented. In this method the structure outboard of the root rib is considered to be of constant section, having an infinite number of closely spaced ribs, and a differential equation is solved to determine the stress distribution in this bay. It is shown that good agreement exists at the root between the approximate method of analysis and the more laborious "exact" method.

References

[1] Lang, A. L., and Bisplinghoff, R. L., *Some Results of Sweptback Wing Structural Studies*, Journal of the Aeronautical Sciences, Vol. 18, No. 11, p. 705, November, 1951.

[2] Heldenfels, Richard R., Zender, George W., and Libove, Charles, *Stress and Distortion Analysis of a Swept Box Beam Having Bulkheads Perpendicular to the Spars*, N A C.A. T.N. No. 2232, November, 1950.

[3] Islinger, J. S., *Stress Analysis and Stress Measurements for a Swept-Back Wing Having Ribs Parallel to the Air Stream*, McDonnell Aircraft Corporation Report No. 1127, April 8 1949.

[4] Goran, L. A., and Goetsch, G. F., *Stress Analysis of Swept-Back Box Beams Having Ribs Perpendicular to the Spars*, McDonnell Aircraft Corporation Report No. 1128. July 15, 1949.

Slender Body Theory for Supersonic Unsteady Flow

John W. Miles*
Fulbright Lecturer, Auckland University College, Auckland, New Zealand

November 12, 1951

PRESENTED HERE ARE THE RESULTS of extending Ward's slender body theory[1] to the case of unsteady flow, a question treated heuristically in a previous paper.[2] The complete analysis is to be presented in a forthcoming N.O.T.S. report,[3] representing work supported by the Office of Naval Research.

In the following the body length (l) has been chosen as the characteristic linear dimension and the free-stream velocity at time zero as the characteristic velocity (U). All subsequent quantities are dimensionless, and the characteristic, dimensionless parameters of the problem are δ, the larger of the transverse body dimension or amplitude of transverse motion; M_0, the free-stream Mach Number; and k, the measure of time rate of change, which for harmonic motion reduces to the well-known reduced frequency. As coordinates, the Cartesian set s and $z = x + iy$ were chosen, where s is measured downstream from the body nose.

The restrictions on body shape are identical with those given by Ward. To investigate the extent of the linearized régime, we follow the procedure applied by Lin, Reissner, and Tsien[4] to the two-dimensional problem and find the essential restrictions ensuring small perturbations to be

$$k = 0(1): \quad \delta \ll 1 \text{ and } (M_0\delta)^2 \ll 1 \tag{1a}$$

$$k \gg 1: \quad k\delta \ll 1 \text{ and } (kM_0\delta)^2 \ll 1 \tag{1b}$$

It is found that the velocity potential satisfies Laplace's equation in planes transverse to the flow and is given by the real part of the complex potential

$$w(s, z, t) = a_0(s, t) \ln z + b_0(s, t) + \sum_{m=1}^{\infty} a_m(s, t) z^{-m} + 0\left[\left(\frac{1}{k^2}\right) M_0^2\delta^4 \ln \delta\right] \tag{2}$$

subject to the linearized boundary condition

$$\phi_n = \frac{Dn}{Dt} + 0\left[\left(\frac{1}{k}\right)\delta^2 \ln \delta\right] \tag{3}$$

where n denotes the normal to the body contour in a transverse plane, (D/Dt) implies

$$\frac{D(\ \ )}{Dt} = [1 + u(t)]\frac{\partial(\ \ )}{\partial s} + \frac{\partial(\ \ )}{\partial t} \tag{4}$$

and $u(t)$ is the increment of flight velocity acquired in the interval t. It suffices to invoke this boundary condition at the mean position of the body. The pressure is given by

$$\left(\frac{p - p_0}{q_0}\right) = -2\frac{D\phi}{Dt} + 4|\phi_z|^2 + 0\left[\left(\frac{1}{k^4}\right) M_0^2\delta^4 \ln^2 \delta\right] \tag{5}$$

where p_0 and q_0 are the static and dynamic pressures in the undisturbed flow. In each of the error terms, the larger of the factors 1 or k^n is implied.

By an analysis similar to that given by Ward, it is found that

$$a_0(s, t) = \frac{1}{2\pi}\frac{D}{Dt} S(s, t) \tag{6}$$

* On leave from University of California, Los Angeles; formerly Consultant, U.S. Naval Ordnance Test Station, Invokern, Calif.

$$b_0(s,t) = \ln (M_0/2)a_0(s,t) - \frac{1}{2}\int_0^t \ln (t-\tau)\cdot \frac{\partial}{\partial \tau}\left\{a_0\left[s - \left(\frac{M_0+1}{M_0}\right)(t-\tau) - \int_\tau^t u(\xi)d\xi,\ \tau\right] + a_0\left[s - \left(\frac{M_0-1}{M_0}\right)(t-\tau) - \int_\tau^t u(\xi)d\xi,\ \tau\right]\right\} d\tau \quad (7)$$

where $S(s,t)$ is the transverse cross section, the results being valid for both time and spatial variations thereof. The nonbase drag is given by

$$\left(\frac{D-D_B}{q_0}\right) = 4\pi\int_0^1 b_0\frac{\partial a_0}{\partial s}ds - 2\pi(a_0b_0)_{s=1} - \left(\oint \phi\phi_n dl\right)_{s=1} - 2\int_0^1\left(\oint \phi_t n_s dl\right)ds + 0\left[\left(\frac{1}{k^4}\right)M_0^2\delta^6\ln^2\delta\right] \quad (8)$$

where the line integrals are taken around the body contour at station s. For the transverse force and rolling moment per unit length, we find

$$\frac{\partial}{\partial s}\left(\frac{X+iY}{q_0}\right) = 4\pi\frac{D}{Dt}a_1 + 2\frac{D^2}{Dt^2}(z_g S) + 0\left[\left(\frac{1}{k^4}\right)M_0^2\delta^4\ln^2\delta\right] \quad (9)$$

$$\frac{1}{q_0}\frac{\partial N}{\partial s} = -2\frac{D}{Dt}\left[\oint \phi\cdot(x\,dx + y\,dy)\right] + 0\left[\left(\frac{1}{k^4}\right)M_0^2\delta^6\ln^2\delta\right] \quad (10)$$

where z_g denotes the centroid of the cross section at s. We remark that the contribution of the terms $a_0 \ln z$ and b_0 to the last integral are null.

The foregoing results have been applied to the questions of the acceleration and transverse motion of winged bodies of revolution. In the latter case we find

$$\frac{\partial}{\partial s}\left(\frac{X+iY}{q_0}\right) = -2\pi\frac{D}{Dt}\left\{[b^2 - a^2 + (a^4/b^2)]\frac{D}{Dt}z_g\right\} \quad (11)$$

$$\frac{1}{q_0}N - \frac{1}{4}\rho[b + (a^2/b)]^4\left[\frac{\varphi^2}{\pi} + \left(1 - \frac{\sin 4\varphi}{2\pi}\right)\varphi + \left(\frac{\pi}{4}\right)(1-\cos^4\varphi) - \frac{1}{4}\sin 4\varphi + \frac{1}{4\pi}\sin^2 2\varphi\right] \quad (12)$$

$$\varphi = \cos^{-1}[2ab/(a^2+b^2)] \quad (13)$$

where a is the body radius and $2b$ the total wing span (tip to tip), evaluated at station s in Equation (11) and at the trailing edge in Eq. (12), and p is the angular velocity in roll. These particular results are subject to the restriction

$$b'(s) \geq 0 \quad (14)$$

and, in the case of Eq. (11), to the requirement that the body either terminate at the trailing edge or be of constant cross section thereafter. The restriction (14), which ensures no wake effects, is more severe than that required in steady flow, where $b'(s)$ may be negative provided that the body be of constant cross section aft of the maximum wing span.

REFERENCES

[1] Ward, G. H., *Supersonic Flow Past Slender Pointed Bodies*, Quart. Jour. of Mech. & Appl. Math., Vol. 2, pp. 75–97, 1949.

[2] Miles, J. W., *On Non-Steady Motion of Slender Bodies*, Aero. Quart., Vol. 2, pp. 183–194, 1950.

[3] Miles, J. W., *Unsteady Supersonic Flow Past Slender Pointed Bodies*, Naval Ordnance Test Station, Inyokern, China Lake, Calif., N.O.T.S. (TM-357).

[4] Lin, C. C., Reissner, E., and Tsien, H. S., *On Two Dimensional Non-Steady Motion of a Slender Body in a Compressible Fluid*, J. Math. & Ph., Vol. 27, pp. 220–231, 1949.

Comments on "The Evaluation of Theoretical Critical Compression in Sandwich Plates"

Bernard Budiansky and Charles Libove
Langley Aeronautical Laboratory, N.A.C.A.

November 12, 1951

A FOOTNOTE IN A RECENT PAPER by Goodier and Neou[1] may be misleading. The footnote states that "since a wide strip must *begin* to bend *with* anticlastic curvature . . . the critical load for infinitesimal buckling would appear, therefore, not to require the factor $1/(1-\nu^2)$." It is indeed true, as shown by Ashwell,[2] that in *pure bending* of a wide plate there is a gradual transition due to finite deflections from E to $E/(1-\nu^2)$ in the effective Young's modulus. However, the initial buckling of a plate column of finite width *supported along its loaded edges* always occurs with some inhibition of anticlastic curvature; Houbolt and Stowell[3] have shown that, as the plate width varies from zero to infinity, the *initial* buckling load ranges from the column value (based on E) to a value slightly below the full plate value [based on $E/(1-\nu^2)$]. For a width-height ratio of only 6 the initial buckling load of a simply supported aluminum plate column is already 99 per cent of the full plate value.

After buckling commences at the Houbolt-Stowell load, it is probably true that, for the buckle to grow, the applied load must be increased in order to overcome the stiffening that occurs as the anticlastic curvature is suppressed still more through the finite deflection mechanism discussed by Ashwell. The upper limit to this load would be the full plate value based on $E/(1-\nu^2)$.

REFERENCES

[1] Goodier, J. N., and Neou, I. M., *The Evaluation of Theoretical Critical Compression in Sandwich Plates*, Journal of the Aeronautical Sciences, Vol. 18, No. 10, p. 649, October, 1951.

[2] Ashwell, D. G., *Anticlastic Curvature of Rectangular Beams and Plates*, Journal of The Royal Aeronautical Society, Vol. 54, p. 708, November, 1950.

[3] Houbolt, J. C., and Stowell, E. Z., *Critical Stress of Plate Columns*, N.A.C.A. T.N. No. 2163, August, 1950.

Three-Dimensional Conformal Transformations

Keeve M. Siegel
Willow Run Research Center, University of Michigan, Ypsilanti, Mich.

November 26, 1951

BECAUSE OF THE SUCCESS in the use of conformal transformations in two-space for ideal fluid flow, one would be interested *a priori*, in conformal transformations in three-space. The three-dimensional method of inversion is valid in electrostatics. However, it will be shown that this method is not valid in hydrodynamics.

When one attempts to find an exact three-dimensional solution to a boundary-value problem, he is almost always limited to the contour surfaces of coordinate systems in which the variables in the equation of the motion can be separated. When Laplace's equation is the equation of the motion and a solution is found for such a contour surface (in electrostatics, for example), one usually uses Kelvin's inversion theorem to find solutions for other bodies. Thus, from a known electrostatic solution for a cone, a

contour surface of a coordinate system for which Laplace's equation is separable, a solution was obtained for an ogive[1] by the method of inversion. However, the ogive is not a contour surface of a coordinate system for which Laplace's equation is separable.

Lemma 1. The inversion transformation (sometimes called the reciprocal radii transformation) is the only nontrivial conformal transformation in three-space.[2]

Theorem 1. *There is no nontrivial three-dimensional conformal transformation which is applicable to boundary-value problems in fluid mechanics.*

By Lemma 1, to prove theorem 1, we need only discuss the inversion transformation. Let us consider the equation for an ideal, incompressible, axially symmetric flow in cylindrical coordinates (r, x, θ).

Boundary-Value Problem I

$$\psi = \text{stream function}$$

$$E^2\psi = \frac{\partial^2\psi}{\partial r^2} - \frac{1}{r}\frac{\partial\psi}{\partial r} + \frac{\partial^2\psi}{\partial x^2} = 0$$

$$\psi_{\text{evaluated at body}} = 0$$

Boundary-Value Problem II

$$\phi = \text{velocity potential}$$

$$\nabla^2\phi = \frac{\partial^2\phi}{\partial r^2} + \frac{1}{r}\frac{\partial\phi}{\partial r} + \frac{\partial^2\phi}{\partial x^2} = 0$$

$$\left(\frac{\partial\phi}{\partial\ \text{normal}}\right)_{\text{evaluated at body}} = 0$$

Boundary-value problem I cannot be solved by inversion because the equation of the motion does not remain invariant under the inversion transformation. Boundary value problem II cannot be solved by inversion (even though Laplace's equation would remain invariant) because it has a Neumann boundary condition.[3]

In hydrodynamics, for all nontrivial cases, it can be shown that, when the equation of the motion is not Laplace's, the equation does not remain invariant under the inversion transformation. When the three-dimensional Laplace's equation does occur, it occurs with Neumann boundary conditions.

In two-dimensional theory, the method of inversion becomes applicable in both fields because in two-space the stream-function equation becomes Laplace's equation.

In three-dimensional electrostatics, the method of inversion is valid because the Dirichlet boundary conditions, $\phi = 0$, can exist at the same time as Laplace's equation.

REFERENCES

[1] Macdonald, H. M., *Demonstration of Green's Formula for Electric Density Near the Vertex of a Right Cone*, Camb. Phil. Trans., Vol. XVIII, p. 292, 1900.

[2] Liouville, J., Journal de Math. Pures et appl., Vol. XII, 1847.

[3] Sommerfeld, A., *Partial Differential Equations in Physics*, 1st Ed., Vol. 1, p. 138; Academic Press, Inc., New York, 1949.

Erratum[1]

N. Scholz
Dr.-Ing., Institute of Fluid Mechanics, Technical University, Braunschweig, Germany
January 2, 1952

UNFORTUNATELY, MY REPORT[1] obtains a misprint that makes unintelligible Eq. (10) of this note. This equation should read

$$\Gamma = U_\infty t \times \left[a_0 e^{-i\lambda}\sinh\left(\frac{\pi c}{2t}e^{i\lambda}\right) + e^{-i\lambda}\sum_{n=1}^{\infty}{}^{**}a_n \tan h^n\left(\frac{\pi c}{4t}e^{i\lambda}\right)\right]$$

Σ^{**} means that the summation has to be taken only over the odd terms.

REFERENCE

[1] Scholz, N., *On an Extension of Glauert's Theory of Thin Airfoils to Profiles in Cascade*, Readers' Forum, Journal of the Aeronautical Sciences, Vol. 18, p. 637, September, 1951.

Comments on "Horizontal Tail Loads in Abrupt Pull-Ups from Level Flight"[1]

R. M. Rosenberg
Design Specialist, Boeing Airplane Company
January 9, 1952

DECKER'S PAPER ON TAIL LOADS[1] presents an approach to that subject which will yield correct results of interest to the engineer. Since his results are integrals of the differential equations in hand, they will approximate to nearly the same degree the response of an airplane as his differential equations approximate the behavior of the system.

Before discussing the method used by Decker, it would be well to clear up an unintentional misunderstanding. Decker implies in his "Introduction" that Kelley and Misall[2] have considered the same problem and have developed a method yielding solutions that are "not unique." Certainly, Decker did not intend to say all that is suggested by this statement. Decker, as well as Kelley and Misall, has considered a linear problem of the sort

$$L(x^{(n)}, x^{(n-1)}, \ldots, \dot{x}, x) = F(t) \qquad (1)$$

If such an equation possesses unique solutions in the accepted sense of this term, then it is not possible to construct correct methods yielding solutions that are not unique. Decker's remark on lack of uniqueness is meant to say only that there is no unique $F(t)$ that satisfies the condition that, at a particular time t_i, $\vec{x}(t_i) = \vec{x}_i$ (a constant), but no more. Clearly, this remark refers to the uniqueness of the equation and not to that of solutions.

Decker's mode of attack on the problem is an inverse method. It consists in prescribing for Eq. (1) the solution $x = x^*(t)$ where the * is used to indicate that the solution is picked arbitrarily (within suitable restrictions to be defined later). Assuming that Eq. (1) satisfies the requirements for uniqueness and existence of solutions and that $x^*(t)$ is admissible as a solution, it follows that $x^*(t)$ is the unique solution to Eq. (1) provided

$$F(t) \equiv L(x^{*(n)}, x^{*(n-1)}, \ldots \dot{x}^*, x^*)$$

$F(t)$ is the forcing function in Eq. (1). We also identify it as the "object function," because it is that function in Eq. (1) which is to be so adjusted that a prescribed solution satisfies the equation. On physical grounds, $F(t)$ of Decker's problem must be continuous everywhere. Therefore, in general, any $x^*(t)$ is admissible if it satisfies all prescribed initial and end conditions and if it possesses continuous derivatives up to order n.

Decker's approach is extremely simple and effective when applied to difficult problems because it changes the need for solving a differential equation to one of solving an algebraic equation for an object function. This algebraic equation can always be solved explicitly for any quantity of interest if the original differential equation is linear. Even when that equation is nonlinear, one can often solve the corresponding algebraic equation explicitly for the object function,[3] but at times this may not be possible.

It should be pointed out that only a limited amount of information can be gathered by this method of finding equations that are satisfied by a prescribed solution. This limitation is brought about by the fact that only one particular solution, satisfying one particular set of boundary values of one particular equation, is found. This precludes, for instance, the possibility of answering the following question related to Decker's problem: What are the conditions on the elevator motion $F(t)$ such that a prescribed maximum load will not be exceeded at any time? A solution of the differential equation in terms of $F(t)$ (say, a convolution integral) can provide this answer; such methods as the one used by Decker can also be used at times to provide answers of this type if they are pooled with other phases of analysis.[3]

In the past, the method used by Decker has been applied with good success to linear and nonlinear systems, antonomous or not.[3-6] In autonomous systems the object function is usually a function $f(x)$ of the dependent variable. In these cases, the prescribed solution takes the form $\dot{x} = \dot{x}^*(x)$ rather than $x = x^*(t)$; all other arguments remain unchanged.

In nonlinear problems, the inverse method is particularly powerful because it releases the investigator from the restriction that solutions must lie in the neighborhood of those to a related linear problem; thus, particular solutions to strongly nonlinear equations can be found easily, and solutions neighboring on these may still be found by perturbation methods or iterative procedures. Finally, valuable quantitative information regarding the behavior of a nonlinear system can be gathered from the correspondence between object functions and solutions, obtained when prescribed solutions are varied in a systematic fashion over wide intervals.

References

[1] Decker, James, L., *Horizontal Tail Loads in Abrupt Pull-Ups from Level Flight*, Journal of the Aeronautical Sciences, Vol. 18, No. 12, p. 835, December, 1951.

[2] Kelley, Joseph, Jr., and Misall, John W., *Maneuvering Horizontal Tail Loads*; A.A.F. T.R. 5185.

[3] Rosenberg, R. M., *A Rational Approach to the Design of Metering Pins in Oleo Struts*, presented at the Sixteenth Annual Meeting, I.A.S., New York, January, 1948.

[4] Durand, H. P., and Rosenberg, R. M., *A New Approach to the Design of Metering Pins in Oleo Struts*, University of Washington Engineering Experiment Station Bulletin 118, December, 1950.

[5] Rosenberg, R. M., *A Note on Systems With or Without Nonlinear Elements*, presented at The International Congress of Mathematicians, Harvard University, August, 1950. (To be published in the *Proceedings* of the Congress.)

Bernard Etkin
Assistant Professor of Aeronautical Engineering, University of Toronto, Canada

December 18, 1951

THE PAPER BY DECKER[1] is an application of the inverse method in airplane dynamics. In this method the airplane motion is specified and the required control time histories are determined. It appears to have been used first in reference 2. When properly used, it is a powerful tool and can be applied to nonlinear, as well as linear, problems. It has not in the past received the attention it merits. Several problems, including the subject of the paper, have been, and are being, investigated by this approach at the University of Toronto.[3, 4]

Insofar as tail loads are concerned, the paper is the fourth published solution by the inverse method. The first three are references 5, 6, and 3, the last two of these having appeared within the past year and a half.

In applying the inverse method, it must be remembered that there are infinite numbers of ways in which the airplane may perform a given type of maneuver (e.g., attain a given load factor in a given time). The success or failure of the method hinges entirely upon the choice of function that is to describe the maneuver.

In Decker's paper, Eq. (13) is the chosen function in this case. The function must, above all, represent a physically possible motion of the airplane, consistent with the assumed initial conditions and the limitations imposed by the machine, the pilot, and the control system. It should, in addition, be in accord with the manner in which the maneuver is likely, or may be required, to be done. Thus, the solution obtained must be continuous in all displacements, velocities, and accelerations. (Discontinuous accelerations will involve discontinuous control displacements.) Violation of any of these conditions implies infinite forces, which cannot exist.

In references 5 and 6 this state of affairs has been satisfactorily achieved, with the result that the maneuvers are realistic and check well with flight records.

In the present paper, the choice of Eq. (13) is rather unfortunate in this respect.

(1) The initial rate of displacement of the elevator is not zero, and thus the maneuver is not consistent with an initial state of steady unaccelerated flight. It entails an infinite acceleration of the control system at time zero; this is, of course, impossible.

(2) The negative maximum of $d\delta_e/dt$ is too small compared with the positive maximum. This results in the maximum δ_e occurring too late and in underestimation of the positive $\bar{\theta}$ and negative L_t, which occur in the initial stages. The last effects may be important (see references 6 and 7).

(3) The tail load used by the author as the design value is that occurring at $n_{max.}$, *even though it is still increasing*. This artificial cutting-off of the solution is made necessary by the failure of Eq. (13) to represent this type of maneuver adequately. If the solution were continued in time with that equation, the maximum tail load would exceed that determined by Decker and occur at a time later than $n_{max.}$. Decker correctly notes that this is not in accord with experience.

References

[1] Decker, I. L., *Horizontal Tail Loads in Abrupt Pull-Ups from Level Flight*, Journal of the Aeronautical Sciences, Vol. 18, No. 12, p. 835, December, 1951.

[2] Jones, R. T., and Weick, F. E., *The Effect of Lateral Controls in Producing Motion of an Airplane as Computed from Wind-Tunnel Data*, N.A.C.A. Report No. 570, 1936.

[3] Etkin, Bernard, and Woodward, F. A., *Calculation of Maneuvering Tail Loads by the Inverse Method*, National Research Council of Canada, Report AR-8, 1951.

[4] Etkin, Bernard, *Charts for Evaluating Rolling Performance*, National Research Council of Canada, Report R-13 (soon to be issued).

[5] Dickinson, H. B., *Maneuverability and Control Surface Strength Criteria for Large Airplanes*, Journal of the Aeronautical Sciences, Vol. 7, No. 11, p. 469, September, 1940.

[6] Pearson, H. A., McGowan, W. A., Donegan, J. J., *Horizontal Tail Loads in Maneuvering Flight*, N.A.C.A. T.N. No. 2078, April, 1950.

[7] Matheney, C. E., *Comparison Between Calculated and Measured Loads on Wing and Horizontal Tail in Pull-up Maneuvers*, N.A.C.A. A.R.R. L5H11, 1945.

Erratum

P. P. Bijlaard
Professor, Cornell University, Ithaca, N.Y.

December 18, 1951

IN MY PAPER, "Analysis of the Elastic and Plastic Stability of Sandwich Plates by the Method of Split Rigidities—II," in the December, 1951, issue of the JOURNAL OF THE AERONAUTICAL SCIENCES reference 1 incorrectly referred to Part I in the May,

1951, issue of the JOURNAL. This reference, as given in the original manuscript, should read: [1] Bijlaard, P. P., *Analysis of the Elastic and Plastic Stability of Sandwich Plates by the Method of Split Rigidities*, Preprint No. 259, Institute of the Aeronautical Sciences, pp. 1–45, January, 1950.

On the Flow Around a Rotating Disc in a Uniform Stream*

Arthur N. Tifford and Sheng To Chu
Ohio State University
January 8, 1952

IN REFERENCE 1, Schlichting and Truckenbrodt summarized a "Pohlhausen-type" solution of the boundary layer on a rotating disc in a uniform stream. The existence of exact solutions of the Navier-Stokes equations in two of the cases covered—namely, (1) the case of a negligible stream velocity far from the disc and (2) the case of zero disc rotation is (as stated) well known. The existence of these solutions led us to suspect that all the cases treated are amenable to exact mathematical analysis. And indeed, we have found them so.

The details of our analysis will be given in a later paper.† Some of the numerical results, however, are discussed below.

Table 1 lists the values obtained for the corrected frictional moment coefficient as a function of the relative fluid and disc motions. As a partial check on precision, it may be noted that, in the case of negligible free-stream velocity—i.e., $a/\omega = 0$—the moment coefficient based upon Cochran's calculations,[2] agrees within 0.5 per cent with our value.

In Table 2 are given values of the corrected (surface) radial shearing stress coefficient as a function of the relative fluid and disc motions. Checking again with Cochran's calculations (for the case $a/\omega = 0$), agreement within 1 per cent is found. Homann's analysis[3] of the stationary disc—i.e., $a/\omega = \infty$, provides an addition check. Making use of Hartree's more precise evaluation of Homann's function—available as the case, $\beta = 0.5$, in reference 4—we find agreement with present results within 0.4 per cent.

* Work supported by the Flight Research Laboratory, U.S.A.F. The numerical results of Tables 1 and 2 were obtained by the Computation Section of the Flight Research Laboratory, U.S.A.F.

† It has just been brought to our attention that Batchelor has reported in reference 8 the existence of such an analysis as *British A.R.C. Paper No. 10,482*, 1947, authored by Miss D. M. Hannah.

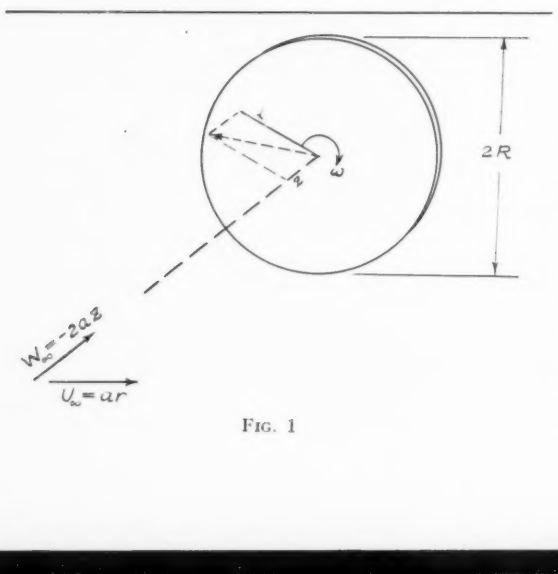

FIG. 1

TABLE 1
Corrected Disc Frictional Moment Coefficient as Function of Relative Disc and Fluid Motions

$\frac{a}{\omega}$	$C_M\sqrt{R_{e_1}}$ or $\frac{M\sqrt{\frac{\omega R^2}{\nu}}}{(1/2)\rho(\omega R)^2R^3}$
0	1.94
0.1	2.03
0.25	2.24
0.5	2.65
1.0	3.21
1.5	4.20
2.0	4.82
4.0	6.67
6.0	8.32

TABLE 2
Local (Corrected) Radial Friction Coefficient as Function of Relative Disc and Fluid Motions

$\frac{a}{\omega}$	$c_f(\text{radial})\sqrt{R_{e_2}}$ or $\frac{\tau_r}{(1/2)\rho(a^2+\omega^2)r^2}\sqrt{\frac{(a^2+\omega^2)r^2}{\nu}}$
0	1.03
0.1	1.05
0.25	1.14
0.5	1.38
1.0	1.83
1.5	2.17
2.0	2.33
4.0	2.52
6.0	2.57
∞	2.61

It appears probable, then, that the frictional coefficients of Tables 1 and 2 are correct to within at least 1 per cent. On the other hand, the frictional moment coefficient values given by Schlichting and Truckenbrodt are about 7 per cent lower than those of Table 1. (Values of the radial shearing stress coefficient were not reported.) These discrepancies are presumably mainly due to the relatively approximate nature of their analysis.

As might be anticipated, the same coordinate system that leads to the exact solution of the Navier-Stokes equations, leads to the exact solution of the energy equation. Thus, the analyses of references 5, 6, and 7‡ may be unified into a single mathematical treatment that simultaneously covers all intermediate flow geometries.

REFERENCES

[1] Schlichting, H., and Truckenbrodt, E., *The Flow Around a Rotating Disc in a Uniform Stream*, Readers' Forum, Journal of the Aeronautical Sciences, Vol. 18, No. 9, pp. 639–640, September, 1951.

[2] Cochran, W. G., *The Flow Due to a Rotating Disc*, Proceedings of the Cambridge Philosophical Society, Vol. 30, pp. 365–375, 1934.

[3] Homann, F., *Der Einfluss grosser Zahigkeit bei der Stromung um den Zylinder und die Kugel*, Zeitschrift fur angewandte Mathematik und Mechanik, Vol. 16, pp. 153–164, 1936.

[4] Hartree, D. R., *On An Equation Occurring in Falkner and Skan's Approximate Treatment of the Equations of the Boundary Layer*, Proceedings of the Cambridge Philosophical Society, Vol. 33, Part 2, pp. 223–239, April, 1937.

[5] Millsaps, K., and Pohlhausen, K., *Heat Transfer by Laminar Flow from a Rotating Plate*, Readers' Forum, Journal of the Aeronautical Sciences, Vol. 18, No. 5, pp. 354–355, May, 1951.

[6] Tifford, A. N., *Note on "Heat Transfer by Laminar Flow from a Rotating Plate,"* Readers' Forum, Journal of the Aeronautical Sciences, Vol. 18, No. 8, pp. 567–568, August, 1951.

[7] Tifford, A. N., *An Exact Thermal Solution in Laminar Viscous Flow*, Proceedings of the First U.S. National Congress of Applied Mechanics, 1951 (to be published).

‡ As applied to the three-dimensional, rotationally symmetric, forward stagnation region.

[1] Batchelor, G. K., *Note on a Class of Solutions of the Navier-Stokes Equations Representing Steady Rotationally-Symmetric Flow*, The Quarterly Journal of Mechanics and Applied Mathematics, Vol. IV, Part 1, pp. 29–41, March, 1951.

Frequency Response of an Airplane from Flight-Test Data

G. M. Andrew and J. H. Polve
Air Force Flight Test Center, Edwards Air Force Base, Muroc, Calif.

December 1, 1951

THE TREND IN MODERN AIRPLANES AND MISSILES toward using autopilots, stabilized gun platforms, automatic landing devices, guidance systems, and all kinds of servomechanisms is becoming increasingly more prevalent.

The dynamic behavior of these complicated systems is described by the transfer functions. As the computations are not too accurate, the transfer functions are often determined experimentally. The transfer function can be determined in the laboratory by putting a component, say the autopilot, on a table oscillating with a known frequency and amplitude and recording the magnification factor and phase lag of the forced oscillation. The result covering a certain frequency range is called the frequency response.

If the autopilot is built into an airplane, the overall transfer function of the system (airplane plus autopilot) is given by the product of the airplane transfer function and the autopilot transfer function. The transfer function of the airplane must be determined from a flight test. Disturbing the steady-state flight by control surface motion (pulse or step) results in a dynamic response (angle, angular velocity, acceleration) of the airplane which is recorded vs. time. Because the experimental transfer function of the autopilot is obtained as a function of frequency, and that of the airplane as a time history, the response of the airplane must be now translated in terms of frequency. When that is done, the product of both transfer functions can be obtained.

The Laplace transformation relates the function $f(t)$ of the time history to its transform $f(s)$ in terms of frequency by the equation

$$f(s) = \int_0^\infty e^{-st} f(t)\, dt \tag{1}$$

where

$$s = \sigma + j\omega \tag{2}$$

Eq. (2) and $\sigma = 0$ give

$$f(j\omega) = \int_0^\infty e^{-j\omega t} f(t)\, dt = \int_0^\infty \cos \omega t f(t)\, dt - j \int_0^\infty \sin \omega t f(t)\, dt \tag{3}$$

Generally, because a considerable number of time histories are recorded in a flight test, some automatic computing machine such as an IBM machine is needed to obtain results (say from a 90 ordinate scheme) in a reasonable time. Where only slide rules and desk computers are available, the method of trapezoidal approximation, which requires a small number of ordinates, can be successfully used as a timesaving method. This method is used in reference 1 for the solution of the converse problem of getting time history from the frequency response. The derivation of the method and the technique of computation are as follows: Fig. 1 represents the time history of the airplane response $f(t)$. The function $f(t)$ is approximated by a few straight lines (f,a,b,c,d,e). Point e corresponds to $t = T$, where $f(t)$ assumes a constant value $f(T)$. Each trapezoid must be extended to the

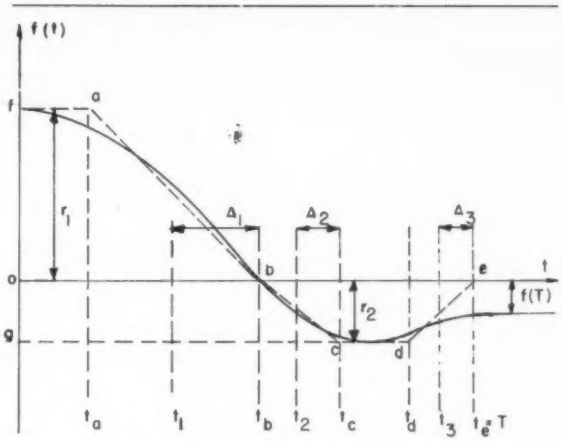

FIG. 1.

$f(t)$ axis, like $(f,a,b,0)$, $(0,b,c,g)$, $(0,e,d,g)$. Let the areas above the t axis have the plus sign; areas below, minus. If the area of the trapezoid does not contribute to the area between the curve and the t axis, the sign must be reversed. Thus, the minus sign for $(0,b,c,g)$ has to be reversed to plus for this reason. From the notation given in Fig. 1, it can be seen that

$$t_1 = (t_a + t_b)/2$$
$$\Delta_1 = (t_b - t_a)/2$$
$$A_1 = r_1 t_1$$

In order to illustrate the evaluation of Eq. (3), consider the trapezoid $(f,a,b,0)$ for which the imaginary part becomes

$$Im_{(f,a,b,0)} = -j \int_0^{t_1-\Delta_1} \sin(\omega t) r_1\, dt - j \int_{t_1-\Delta_1}^{t_1+\Delta_1} \sin(\omega t) r_1 \left(\frac{t_1 + \Delta_1 - t}{2\Delta_1}\right) dt$$

Proceeding similarly with the real part and summing all the trapezoids, it can be demonstrated[2] that the transformation Eq. (3) yields

$$f(j\omega) = \sum_{n=1}^{k} A_n \left[\frac{\sin t_n\omega}{t_n\omega}\right]\left[\frac{\sin \Delta_n\omega}{\Delta_n\omega}\right] - j \sum_{n=1}^{k} \frac{r_n}{\omega} \times \left[1 - \left(\frac{\sin \Delta_n\omega}{\Delta_n\omega}\right)\cos t_n\omega\right] \tag{4}$$

The tables of the function $\sin x/x$ are given in reference 1, p. 357. When at time $t = T$, the function $f(t)$ has a constant final value $f(T)$ (Fig. 1), the end correction must be applied

$$\Delta f(j\omega) = -\frac{f(T)\sin \omega T}{\omega} - j\frac{f(T)\cos \omega T}{\omega} \tag{5}$$

The real part of this correction is to be added to the real part (and the imaginary added to the imaginary part) of Eq. (4).

For a satisfactory frequency response plot, it is enough to select from six to ten values of ω for use in Eqs. (4) and (5).

Comparing the results of this short method with the laborious one using, say, 90 ordinates, it will be found that the approximation is surprisingly satisfactory.

REFERENCES

[1] Brown, G. S., and Campbell, D. P., *Principles of Servomechanisms;* John Wily & Sons, Inc., New York, 1948.

[2] Andrew, G. M., and Polve, J. H., *Trapezoidal Approximation of Transient Flight Data to Obtain Aircraft Frequency Response*, Memorandum Report No. 51-24, Air Force Flight Test Center, Edwards Air Force Base, Calif., 1951.

On the Speed of Sound in Gases

Irvine I. Glass
Research Associate, Institute of Aerophysics, University of Toronto, Toronto, Canada
November 4, 1951

A KEEN DISCUSSION of the speed of sound in fluids was conducted recently in these pages by Professors Truesdell, Murdochow, Morkovin, Millikan, and Munk.[1]

In the case of one-dimensional nonlinear unsteady and inviscid flow such as through a rarefaction wave, the local speed of sound may be defined as the rate of propagation into the gas of a characteristic line (Mach wave) with respect to the flow velocity at the point under consideration.[2] This definition follows as a consequence of the solution of the nonlinear differential equations and does not depend on the linearized equations used in acoustics.

This definition was tested experimentally in a wave interaction tube (shock tube)[3] by taking schlieren photographs with a wave speed camera of the rarefaction wave that is therein produced. In the theory of the shock tube[4] it is assumed that, when a diaphragm, which separates a gas at high pressure from a gas at low pressure in a tube of uniform cross section, is suddenly ruptured, a shock wave and a contact surface are propagated into the low-pressure chamber (expansion chamber) and a centered rarefaction wave is propagated into the high-pressure chamber (compression chamber). The waves are assumed to form instantaneously. It is also assumed that the waves are plane and travel at uniform velocities and separate regions of constant state.

The theoretical (x, t)-plane of this wave model is shown in Fig. 1. Along with this model are shown two schlieren photographs of the flow in the wave interaction tube, which were taken with the wave speed camera. The tube[3] has a 2.25 in. O.D. and a 1.00-in. I.D. The flow is viewed through a lucite window 24 in. long and of a $^3/_{16}$-in. tee cross section. The wave speed camera has a rotating drum 12 in. in diameter. Seventy-millimeter film is used, and it attains a peripheral speed of 215 ft. per sec. The longitudinal striations on the photographic records are in main due to the lucite windows.

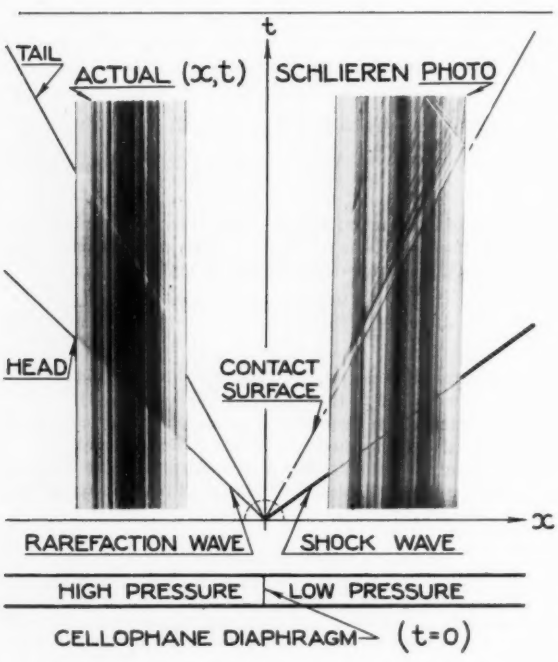

FIG. 1. The wave system generated in a shock tube.

The experimental results for the shock wave and contact surface are reported in reference 3.

The present note deals with the rarefaction wave. For a centered rarefaction wave moving to the left (Fig. 1), the following relations may be used:

$$x/t = u - a \tag{1}$$

$$u + [2a/(\gamma - 1)] = 2a_0/(\gamma - 1) \tag{2}$$

$$\left(\frac{\partial \rho}{\partial x}\right)_t = -\frac{2\rho_0}{(\gamma+1)\,a_0 t}\left[1 - \frac{\gamma-1}{\gamma+1}\left(\frac{x}{a_0 t}+1\right)\right]^{(3-\gamma)/(\gamma-1)} \tag{3}$$

where

a = local speed of sound
a_0 = speed of sound in the rest state into which the rarefaction wave is advancing
t = time
x = distance
u = flow velocity at a point (x, t)
γ = ratio of the specific heats C_p/C_v
ρ_0 = density of the rest state

Since the rarefaction wave separates two constant states, the density derivative $(\partial\rho/\partial x)_t$ is discontinuous at the head and at the tail of the rarefaction wave. As a result, these two border Mach lines should show up in a schlieren photograph of the (x, t)-plane.

At the head of the wave $u_0 = 0$ and therefore $x/t = -a_0$, the speed of sound of the gas in the rest state (the minus sign is consistent with Fig. 1). At the tail of the wave $x/t = u_1 - a_1$, and, if u_1 is known, this relation would give a means of measuring the speed of sound in gases at extremely low temperatures and pressures.

The speed of sound in the rest state is directly determined from the trace of the head of the rarefaction wave on the schlieren record, when the film speed and the optical magnification factor are known.

Experimental results were obtained for the speeds of sound in air, argon, and carbon dioxide by direct measurement of the traces of the head of the rarefaction wave from a large number of schlieren photographic records, similar to the one that appears in Fig. 1. Distances on the photographic records could be measured to 10^{-4} cm. with a traveling microscope. Timing markers of 10-microsec. duration also appear on the photographic film and give a continuous time scale. This makes it possible to determine the film speed to five significant figures. The effects of film shrinkage must also be taken into account. A diaphragm pressure ratio range of 1.2 to 2,400 was utilized during the experiments. The sound speed in the rest state is independent of the pressure and of the diaphragm pressure ratio.

The following are the values obtained from the head of the rarefaction wave for the speed of sound at 0°C. in air, argon, and carbon dioxide.

Air:	a_0	= 1087 ± 2 ft. per sec.
Argon:	a_0	= 1009 ± 1 ft. per sec.
Carbon dioxide:	a_0	= 844 ± 1 ft. per sec.

The above results are in good agreement with the theoretical sound speed obtained from the isentropic relation $a_0 = \sqrt{\gamma R T_0}$ for a perfect gas, or $a_0 = \sqrt{\gamma R T_0}\,(K)$ for a real gas. K is a small correction factor depending on the equation of state used for the gas. The present results are also in good agreement with the values for a_0 obtained from acoustic methods.[6–8] For further details see reference 5.

In the present experiments the tail of the rarefaction wave did not appear on the schlieren records. Therefore, it was not possible to measure the rate of propagation of this Mach wave. It is likely that the discontinuity in the density gradient tends to be smoothed out by viscous action where the gas is in motion. Comments on this point are invited.

REFERENCES

[1] Truesdell, C., *On the Velocity of Sound in Fluids*, Readers' Forum, Journal of the Aeronautical Sciences, Vol. 18, No. 7, p. 510, July, 1951.

[2] Courant, R., and Friedrichs, K. O., *Supersonic Flow and Shock Waves*; Interscience Publishers, Inc., New York, 1948.

[3] Glass, I. I., *Design of a Wave Interaction Tube*, U.T.I.A. Report No. 6, June, 1950.

[4] Patterson, G. N., *Theory of the Shock Tube*, U.T.I.A. Report No. 2, 1948.

[5] Glass, I. I., *An Experimental Determination of the Speed of Sound in Gases from the Head of a Rarefaction Wave*, U.T.I.A. Report No. 9, April, 1952.

[6] Hardy, H. C., Telfair, D., and Hielemeier, W. H., *The Velocity of Sound in Air*, Journal of the Acoustical Society of America, pp. 226–233, January, 1942.

[7] Kay, G. W. C., and Sherratt, G. G., *The Velocity of Sound in Gases in Tubes*, Proceedings, Royal Society (London), A141, p. 123, 1933.

[8] Dixon, H. B., Campbell, C., and Parker, A., *On the Velocity of Sound in Gases at High Temperatures, and the Ratio of the Specific Heats*, Proceedings, Royal Society (London), A 100, p. 1, 1921.

On Interference Factors for Finned Bodies

John W. Miles*

Fulbright Lecturer, Auckland University College, Auckland, New Zealand

November 12, 1951

THE QUESTION OF WING-BODY INTERFERENCE for a slender body of revolution carrying a low aspect ratio wing has been treated by Ward.[1] We present here the extension of his results to the case of multiple fins.

The conformal transformation

$$z_1^{n/2} + (a^2/z_1)^{n/2} = \zeta^{n/2} + (c^2/\zeta)^{n/2} \tag{1}$$

maps the profile of the circle $|z_1| = a$ and the n, symmetrically disposed, radial segments bounded by the circles $|z_1| = a$ and $|z_1| = b$ on the circle $|\zeta| = c$, where

$$2c^{n/2} = b^{n/2} + (a^2/b)^{n/2} \tag{2}$$

The correct phases of the various radicals involved are ascertained by placing all branch cuts inside of the respective circles $|z_1| = a$ and $|\zeta| = c$ and by requiring the transformation to reduce to $z_1 = \zeta$ at infinity, in order to preserve the flow there.

Following the analysis of Ward, the transformation (1) enables us to determine the flow past a slender pointed body of revolution of radius a on which are mounted n isogonal fins of maximum total envelope $2b$, provided that we impose the restriction that either the body radius be constant aft of the maximum fin span or that both body and fins terminate at maximum fin span. The resulting lift due to an angle of attack α is found to be

$$L = 2\pi q b^2 \alpha \left\{ \xi^2 + 2(1 + \delta_n{}^1 + \delta_n{}^2)\left[\left(\frac{1+\xi^n}{2}\right)^{4/n} - \xi^2\right]\right\} \tag{3}$$

$$\xi = a/b \tag{4}$$

where q is the free-stream dynamic pressure and $\delta_j{}^i$ the Kronecker delta ($= 1$ if $i = j$; $= 0$ if $i \neq j$).

The lift due to the body alone is given by setting $b = a$, whence

$$L_B = 2\pi q a^2 \alpha \tag{5}$$

Further, the lift due to $(1/2)n$ wings of span $2(b - a)$ in the absence of interference is given by

$$L_F = (2\pi b^2 q)(1 - \xi)^2 \cdot \frac{1}{2} n \left[\frac{\alpha}{n} \sum_{m=1}^{n} \cos^2\left(\frac{2\pi m}{n}\right)\right] \tag{6a}$$

$$= (2\pi b^2 q\alpha)(1 - \xi)^2 \cdot \frac{1}{2} n \cdot \left(\frac{1 + \delta_n{}^1 + \delta_n{}^2}{2}\right) \tag{6b}$$

where the quantity in square brackets is the average incidence. We then define the interference factor

$$\eta_n(\xi) = \left(\frac{L - L_B}{L_F}\right) = \left[\frac{2^{3-(4/n)}}{n}\right]\left[\frac{(1+\xi^n)^{4/n} - 2^{4/n}\xi^2}{(1-\xi)^2}\right] \tag{7}$$

The first factor in Eq. (7)—namely, $(2^{3-(4/n)}/n)$, may be thought of as a cascade (mutual fin) interference factor and the second as a fin-body interference factor, albeit this division is rather arbitrary.

For very small wings, we have

$$\lim_{\xi \to 1} \eta_n(\xi) = 4 \tag{8}$$

which is a generalization of the result obtained by Ward. Thus, as might be expected, the extremely small fins act independently of one another and effectively have their aspect ratios doubled as a result of reflection in the body.

A question of particular interest is the effectiveness of increasing the number of fins. For practical rockets the cases $n = 1$ and 2 are of no interest, since they provide forces that are dependent on the angle of roll. Moreover, the cruciform ($n = 4$) may be taken as a standard configuration, and we are led to define the aerodynamic effectiveness factor

$$\epsilon_n(\xi) = \left(\frac{L_n - L_B}{L_4 - L_B}\right) = 2(1 - \xi^2)^{-2}\left[\left(\frac{1+\xi^n}{2}\right)^{4/n} - \xi^2\right], \quad n \geq 3 \tag{9}$$

The limits of interest are

$$\epsilon_n(0) = 2^{1-(4/n)} \tag{10}$$

$$\epsilon_n(1) = n/4 \tag{11}$$

$$\epsilon_n(\xi) = 2(1 - \xi^2)^{-1}\left[1 - \left(\frac{4}{n}\right)\left(\frac{\ln 2 - \xi}{1 - \xi^2}\right)^n + 0(n^{-2})\right], \quad n \gg 1 \tag{12}$$

It would appear that, in virtue of representing a ratio of similar quantities, $\epsilon_n(\xi)$ would have a much wider range of validity than the slender body theory *per se*.

We remark that the result obtained by allowing n to become infinite in Eq. (3), viz.,

$$\lim_{n \to \infty} L_n = 2\pi q b^2 \alpha (2 - \xi^2) \tag{13}$$

does not correspond to a body of revolution of radius b, since the fins have been assumed to have zero cross section.

REFERENCE

[1] Ward, G. N., *Supersonic Flow Past Slender Pointed Bodies*, Quart. Jour. of Mech. & Appl. Math., Vol. 2, pp. 75–97, 1949.

* On leave from University of California, Los Angeles; formerly Consultant, U.S. Naval Ordnance Test Station, Inyokern, Calif.

Comments on "Uniformly Loaded Semiinfinite Wedge-Shaped Plates"

Eric Reissner

Department of Mathematics, Massachusetts Institute of Technology, Cambridge, Mass.

December 19, 1951

THE SOLUTION OF THE PROBLEM considered by Morgan[1] can be obtained a good deal more simply than the author has done

by using polar coordinates instead of cartesian coordinates. The differential equation

$$\nabla^4 w = P(x, y)/D \quad [\text{with } P(x, y) = \text{const.}]$$

is reduced by the assumption $w = r^4 W(\theta)$ to an ordinary differential equation with constant coefficients for $W(\theta)$. Mr. Morgan's solution can be written in the form

$$w = r^4 \cos^4 \theta f(\tan^{-1} \theta)$$

and the function f then follows from a differential equation with variable coefficients. It would be difficult to see how Mr. Morgan recognized the possibility of solving this equation with variable coefficients as simply as it was done were it not for the known fact that the assumption $w = r^n W(\theta)$ reduces the expression $\nabla^4 w$ to an expression $LW(\theta)$, where the operator L has constant coefficients.

Use of polar coordinates appears to remove Mr. Morgan's restriction that wedge angles greater than 180° cannot be considered. It may also be seen that the same procedure is possible for load functions of the form

$$p(x, y) = r^m Q(\theta)$$

for which the proper choice for w is

$$w = r^{m+4} W(\theta)$$

Concerning the problem of *finite* sector plates, reference should be made to a recent paper by Carrier and Shaw in the *Proceedings of Symposia of Applied Mathematics*, Vol. 3, p. 125, McGraw-Hill Book Company, Inc., New York, 1950.

Reference

[1] Morgan, A. J. A., *Uniformly Loaded Semi-Infinite Wedge-Shaped Plates*, Readers' Forum, Journal of the Aeronautical Sciences, Vol. 18, No. 12, p. 845, December, 1951.

The Compressible Boundary Layer

(*Continued from page 236*)

[2] von Kármán, Th., and Tsien, H. S., *Boundary Layer in Compressible Fluids*, Journal of the Aeronautical Sciences, Vol. 5, No. 6, p. 227, April, 1938.

[3] Brainerd, J. G., and Emmons, H. W., *Effect of Variable Viscosity on Boundary Layers, with a Discussion on Drag Measurements*, J. Appl. Mech., Vol. 9, No. 1, March, 1942.

[4] Cope, W. F., and Hartree, D. R., *The Laminar Boundary Layer in Compressible Flow*, Phil. Trans. Roy. Soc. London, Series A, Vol. 241, 1948.

[5] Crocco, L., *The Laminar Boundary Layer in Gases*, Monografie Scientifiche di Aeronautica, No. 3, December, 1946. (Also Translation by North American Aviation, Project Bumblebee, APL/JHU CF-1038, 1948.)

[6] Bush, V., and Caldwell, S. H., *A New Type Differential Analyzer*, Jour. Franklin Inst., Vol. 240, pp. 255–326, 1945.

[7] Janssen, E., *The Differential Analyzer of the University of California;* University of California Press, Berkeley, 1947.

[8] Janssen, E., and Lebell, D., *Application of a Mechanical Differential Analyzer to Electrical Engineering*, Electrical Engineering, Vol. 70, pp. 432–435, May, 1951.

[9] Rubesin, H. W., and Johnson, H. A., *A Critical Review of Skin-Friction and Heat-Transfer Solutions of the Laminar Boundary Layer of a Flat Plate*, Trans. A.S.M.E., Vol. 71, p. 383, May, 1949.

[10] Rubesin, H. W., Maydew, R. C., and Varga, S. A., *An Analytical and Experimental Investigation of the Skin Friction of the Turbulent Boundary Layer on a Flat Plate at Supersonic Speeds*, N.A.C.A. T.N. No. 2305, February, 1951.

[11] Keenan, J. H., and Kaye, J., *Gas Tables;* John Wiley & Sons, Inc., New York, 1948.

[12] Krieger, F. J., and White, W. B., *The Composition and the Thermodynamic Properties of Air at Temperatures from 500 to 8000°K. and Pressures from 0.00001 to 100 Atmospheres*, Project RAND, The RAND Corporation, Report R-149, April 15, 1949.

[13] Fortier, A., *Thèse de Paris;* Publications Scientifiques et Techniques du Ministere de l'Air, No. 111, 1937 (see reference 14).

[14] Vasilesco, V., *Recherches Experimentales sur la Viscosite des Gaz aux Temperatures Elevees*, Annales de Physique, Vol. 20, pp. 292–334, May-June, 1945.

[15] Hirschfelder, J. O., and Curtis, C. F., *Thermodynamic Properties of Air II*, University of Wisconsin CM-518, December 21, 1948.

[16] Tribus, M., and Boelter, L. M. K., *An Investigation of Aircraft Heaters II—Properties of Gases*, N.A.C.A. W-9, October, 1942.

[17] Boelter, L. M. K., and Sharp, W. H., *An Investigation of Aircraft Heaters XXXII—Measurements of Thermal Conductivities of Air and of Exhaust Gases Between 50° and 900° F*, N.A.C.A. T.N. No. 1912, July, 1949.

[18] Stops, D. W., *Effect of Temperature upon the Thermal Conductivity of Gases*, Nature, Vol. 164, No. 4179, p. 966, December, 1949.

[19] Hirschfelder, J. O., Bird, R. B., and Spotz, E. L., *The Transport Properties for Non-polar Gases*, Jour. Chem. Phys., Vol. 16, No. 10, October, 1948.